Distribution Agreement

In presenting this thesis or dissertation as a partial fulfillment of the requirements for an advanced degree from Emory University, I hereby grant to Emory University and its agents the non-exclusive license to archive, make accessible, and display my thesis or dissertation in whole or in part in all forms of media, now or hereafter known, including display on the world wide web. I understand that I may select some access restrictions as part of the online submission of this thesis or dissertation. I retain all ownership rights to the copyright of the thesis or dissertation. I also retain the right to use in future works (such as articles or books) all or part of this thesis or dissertation.

_____ _____

Ana A. Alcaraz Date

Computational Studies of Ligand-Protein Interactions

Part I: The T-Taxol Conformation

Part II: Elucidating Interdependent Binding Sites on Tubulin

By

Ana A. Alcaraz

Doctor of Philosophy

Chemistry

Dennis C. Liotta, Ph.D.
Co-Advisor

James P. Snyder, Ph.D.
Co-Advisor

Fred Menger, Ph.D.
Committee Member

James T. Kindt, Ph.D.
Committee Member

Accepted:

Lisa A. Tedesco, Ph.D.
Dean of the Graduate School

Date

Computational Studies of Ligand-Protein Interactions
Part I: The T-Taxol Conformation
Part II: Elucidating Interdependent Binding Sites on Tubulin

By
Ana A. Alcaraz
B.S., Southwestern University, 2003

Advisors: Dennis C. Liotta, Ph.D.
James P. Snyder, Ph.D.

An abstract of
A dissertation submitted to the Faculty of the Graduate School of Emory University in partial fulfillment of the requirements for the degree of
Doctor of Philosophy

in Chemistry

2009

Abstract

Computational Studies of Ligand-Protein Interactions

Part I: The T-Taxol Conformation

Part II: Elucidating Interdependent Binding Sites on Tubulin

By Ana A. Alcaraz

Part I: T-Taxol is a proposal for the bioactive conformation of paclitaxel (PTX) derived from fitting ligand conformations to the electron crystallography (EC) density of the tubulin-ligand complex. It has been confirmed by independent refinement of the PTX-tubulin structure, the activity of bridged T-Taxol analogs, and mutation studies in the yeast tubulin framework. Nonetheless, some structural ambiguities remain based on an uncritical interpretation of the solid state REDOR measurement of two internuclear ^{13}C---^{19}F distances in a fluorinated derivative of PTX. The issues are evaluated by an analysis of the static and dynamic properties of PTX and the PTX-tubulin complex, torsional force field parameters, and the error assigned to the REDOR distances ($\pm$ 0.5 Å). In addition, a proposed alternative to T-Taxol (PTX-NY) is shown to be incompatible with both the EC density and the activity of a highly active series of bridged taxanes. The development of series of bridged and simplified taxanes using the T-Taxol conformation resulted in analogs of the former that induce microtubule formation more efficiently. NAMFIS analysis, along with molecular dynamics simulations and docking, are used to analyze the compounds, and we propose that the enhanced ability to assemble microtubules by these taxane derivatives is linked to their ability to effectively shape the conformation of the M-loop of tubulin for cross-protofilament interaction.

Part II: A model of colchicine (COL) and 2-methoxyestardiol (2ME2) binding to tubulin was developed using molecular dynamics and docking. Available experimental data, including a number of labeling studies, supports the two-site hypothesis in which conformational changes in the H7—H8 loop open opposing sites with differing binding properties and affinities. The β-Val236Ile mutation that causes resistance to 2ME2 with no cross-resistance to COL is located in the site designated for the former ligand and not near the site for the later one.

Computational Studies of Ligand-Protein Interactions
Part I: The T-Taxol Conformation
Part II: Elucidating Interdependent Binding Sites on Tubulin

By
Ana A. Alcaraz
B.S., Southwestern University, 2003

Advisors: Dennis C. Liotta, Ph.D.
James P. Snyder, Ph.D.

A dissertation submitted to the Faculty of the Graduate School of Emory University in partial fulfillment of the requirements for the degree of
Doctor of Philosophy

in Chemistry

2009

Acknowledgements

I wish to thank my advisors Dr. Dennis Liotta and Dr. Jim Snyder for the guidance and encouragement they have both provided me during my graduate school experience. When I wanted to try and learn something new during rotations, you opened your arms and allowed me to explore a new area of chemistry I had never known existed. Thank you for giving me such a great opportunity. Dr. Snyder, thank you especially for understanding the roller coaster ride that is life.

To the members of my committee, Dr. Fred Menger and Dr. James Kindt: I truly enjoyed our yearly 'chats'. You always encouraged me to think outside my own little box and your advice has always been helpful and most welcome. Thank you especially for the focus you provided this past year. Dr. Stefan Lutz: thank you for your input and insight during the proposal process.

No computational chemist can truly excel without the support and critical assessment of collaborators. I have had some great ones in Dr. David Kingston, Dr. Susan Bane, Dr. Evi Giannakakou, and Dr. Jake Schaefer and their respective groups. I especially thank Dr. Thota Ganesh, Dr. Daniel Escuin and Natasha Shanker for their excellent data, questions and input. Thanks, too, to Dr. Anil Mehta and Scott Johnson for their work detailed in Chapter 2. Anil, thank you too for your friendship, support, advice and that long night we redid my entire presentation. I think it was worth it!

The Liotta/Snyder group is an amazing place to work. It is great to be able to say that so many of the people you work with are also your friends. There have been a lot of people that have come and gone, but I would like to especially thank Itta, my mentor; Marike and Sarah for listening; and Yesim, Rhonda, Ann, Cara, Annette, Kim, Yi, Mark

and everyone else for making it such a great place. I should especially mention Cindy, and now Onix, Dulce and the others that make sure everything runs smoothly and gets done. I'm not sure we would make it without you. In that same vein, thanks to Jan, Ann, the front office and everyone that makes this place run.

To our own little sub-group cramped up on the 4th floor: you are some of the most amazing people to work with. Serdar, Jim, Jaime, Mi-Sun, Haipeng, Jin, Yutao, and now Erik and Pieter: thank you for the support, the informal chats and even for those long group meetings. I have learned so much thanks to you. Andy and Ash, who've been with me through the ups and downs of the past few years: we will all make it. Pahk and Matt, you're not last because you're least. I knew nothing about modeling when I started my rotation. I had never heard of Unix or Linux or workstations, but you two really got me going, answering questions and figuring out the random errors I used to make appear on my screen. I truly believe that most of what I know I have learned from you. My sincerest "Thank you!"

We had a great incoming class in 2003, very competitive, but always very supportive. I wish to especially thank Jennifer Sorrells and Uliana Danilenko for their continual support and friendship. Thanks for all the pep talks, advice and down time. Carolyn, Tom, Brad, Rebecca, Cara, Erika and Amy: thank you for the study nights, happy hours, free dinners, anything and everything to help. Linda, my best friend in the world, your random conversations, support, love and prayers will never be forgotten. Lexi, I know I would not have finished this journey without you. Thank you. I must also thank the owners, staff and friends I made at ChocoLaté Coffee these last few months.

You always made sitting in front of the computer for hours upon hours, day after day, bearable, especially with your fantastic coffee.

To my parents, brothers, sister-in-law, aunt and uncle that I consider my 'immediate' family, as well as to all those aunts, uncles, cousins and family that always had me in their thoughts and prayers, no matter the distance that separated us: Thank you for all your love and support and for always being my greatest cheerleaders. I know it's been difficult to understand what it is I do, or what this process is like, but thank you for supporting me regardless. "La educación es lo unico de valor que les puedo dehar que nadie les puede robar." Ya tengo mi hederencia. Los quiero siempre.

A CHEMIST who can extract from his heart's element compassion, respect, longing, patience, regret, surprise, and forgiveness and compound them into one can create that atom which is called LOVE.

Kahlil Gibran

'Me? Books! And cleverness! There are more important things — friendship and bravery and —'

J. K. Rowling, *Harry Potter and the Sorcerer's Stone*

Table of Contents

List of Figures

List of Tables

List of Abbreviations

1JFF-PTX: 1JFF structure of paclitaxel

2CTC: 2-chloroacetyl-2-demethylthiocolchicine

2-FB-PT: 2-(*p*-fluorobenzoyl)paclitaxel

2ME2: 2-methoxyestradiol

3CTC: 3-chloroacetyl-3-demethylthiocolchicine

BMS: Bristol-Meyers Squibb

$CDCl_3$: deuterated chloroform

COL: colchicine

DMSO: dimethyl sulfoxide

DTX: Taxotere®, docetaxel

EC: electron crystallographic

GBSA: Generalized Born/Solvent-Accessible Surface

GDP: guanosine 5'-diphosphate

GMPCPP: guanylyl-(α,β)-methylene-diphosphonate

GTP: guanosine 5'-triphosphate

LMMC: Low Mode Monte Carlo

MC: Monte Carlo

MD: molecular dynamics

MM3*: molecular mechanics 3* force field

MMFF: Merck molecular force field

NAMFIS: NMR Analysis of Molecular Flexibility in Solution

NMR: Nuclear Magnetic Resonance

NOE: Nuclear Overhauser Effect

NSCLC: non-small cell lung cancer

NTX: nonataxel

PDB: Protein Data Bank

PIPES: piperazine-1,4-bis(2-ethanesulfonic acid)

PTX: Taxol®, paclitaxel

PTX-NY: New York conformation

PTX-TB: paclitaxel-tubulin complex

REDOR: Rotational Echo Double Resonance

RMS/RMSD: root mean square/deviation

SAR: structure-activity relationships

SLD: stathmin-like domain

vdW: van der Waals

PART I

THE T-TAXOL CONFORMATION

It was the best of times, it was the worst of times, it was the age of wisdom, it was the age of foolishness, it was the epoch of belief, it was the epoch of incredulity, it was the season of Light, it was the season of Darkness, it was the spring of hope, it was the winter of despair, we had everything before us, we had nothing before us…in short, the period was so far like the present period…

Charles Dickens, *A Tale of Two Cities*

CHAPTER ONE

> Whatever complexity means, most people agree that biological systems have it.
>
> H. Frauendfelder & P. G. Wolynes

> Carbon is only the fifteenth most common element…what sets the carbon atom apart is that it is shamelessly promiscuous. It is the party animal of the atomic world, latching on to many other atoms (including itself) and holding tight, forming molecular conga lines of hearty robustness—the very trick of nature necessary to build proteins and DNA.
>
> Bill Bryson, *A Short History of Nearly Everything*

Drug Discovery

Humans have been using concoctions from plants and animals to treat disease and illnesses for many centuries. Trial and error led to mixtures that helped relieve pain and fight infections. Still, the mixtures were not systematically prepared, and therefore, different results would occur from treatment to treatment. The isolation of salicin and salicylic acid, precursors to the first synthetically prepared pharmaceutical, aspirin (Figure 1),[1,2] from willow bark in the latter part of the nineteenth century was a major achievement in the understanding of small molecules as therapeutic agents. Aspirin was recognized as a universal pain reliever in the early 1900's and is still used commonly in most of the world today.[3] The purification of biologically active organic molecules then became more common, leading to the isolation of more potent painkillers, such as morphine and codeine from opium poppy, [4] the anti-malarial agent, quinine, from cinchona (china bark), and digitalis from the leaves of the purple foxglove plant to treat heart disease.[5]

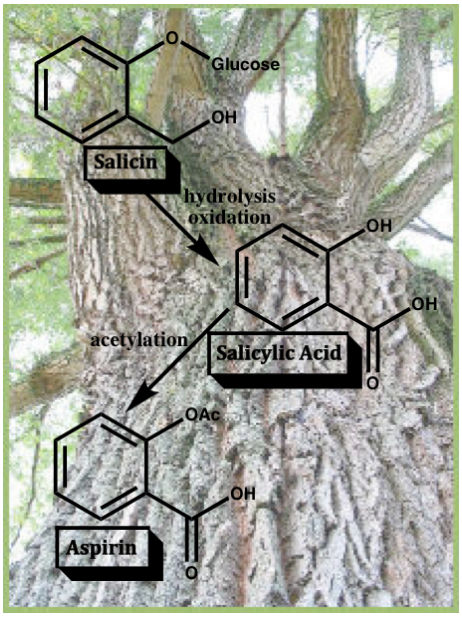

Figure 1. Picture of white willow bark (*Salix alba*) overlaid with the basic transformations of salicin to aspirin.

At the time, Louis Pasteur had already established the germ theory of disease[6] and Paul Ehrlich had introduced "chemoreceptors",[7] receptors as selective

binding sites for chemotherapeutic agents, as the basis of chemotherapy. This opened the door to the more functional concept of receptors by J. N. Langley in 1905.[8] He proposed that receptors work as "switches" that can be blocked by antagonists or activated by agonists as needed or desired. After this, the new era of therapeutic intervention for medicine picked up momentum quickly. Major advances occurred in synthetic organic chemistry, such as the total synthesis of tropinone by Robert Robinson in 1917;[9] as well as in biochemistry and in medical microbiology, including the isolation of microbial agents that cause infectious diseases and the elucidation of their means of transmission.[10] All these breakthroughs and advances culminated in one of the most revolutionary moments in medicine, the discovery of insulin in 1921-22.[5] The introduction of insulin seemed like a miracle at the time, allowing people, especially children with diabetes, to live full and productive lives. Prior to its discovery, a diagnosis of diabetes was a death sentence. Now, over 26.3 million people in the United States alone live with the condition.[11] The pharmaceutical industry was underway, developing new therapeutics and what can be considered the first "biotechnology" (synthesis of insulin).

Over the next two decades, many landmark discoveries were made, including the synthetic sulfa drugs, the natural antibiotic, penicillin, from *Penicillium notatum* by Alexander Fleming,[12] and the anti-tubercular aminoglycoside, streptomycin, from *Streptomyces griseus* by Salman Waksman.[13] The importance of vitamins in health was also being uncovered at the time. Then advances in technologies such as X-ray crystallography, NMR spectroscopy and mass spectrometry contributed to further

discoveries and developments.[5] Chemistry, pharmacology, microbiology and biochemistry came together to identify, characterize and develop new medicines in a vitalized and expanding industry.[5,14]

Rational Drug Design

From the beginning, pharmaceutical companies used a physiology-based approach to drug discovery: compounds were determined to have a physiological effect, i.e. killed cancer cells, and were then optimized and prepared for clinical use. The development of the anticancer agent Taxol® (**1**, Figure 3) is a good example of a stunning success from this approach.[15] Approximately 15 years ago, rational drug design began to complement this approach. Increased screening capacities were also thought to result in increased productivity.[16,17] Rational drug design is a more focused approach to drug discovery, using information about the structure of a target or a natural ligand to screen other ligands or develop de novo candidates. The number of successes has steadily increased, initially in the design of peptide-based HIV protease inhibitors and moving on to other targets (Table 1).[18,19]

Table 1. Examples of successful pharmaceuticals developed by rational or structure-based drug design.

Drug	Target	Pharmaceutical Company
Agenerase	HIV protease	Glaxo Wellcome
Viracept	HIV protease	Agouron
Saquinavir	HIV protease	Roche
Relenza	Neuraminidase	Biota
Tomudex	Thymidylate synthase	Agouron
Dorzolamid	Carbonic anhydrase	Merck Sharp and Dohme
Gilvec	Abityrosine kinase	Novartis
Ro466240	Thrombin	Roche

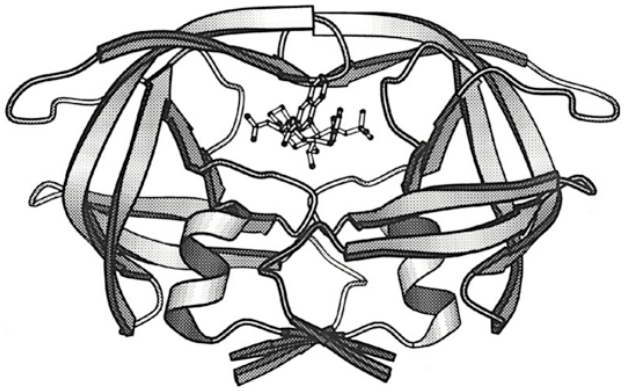

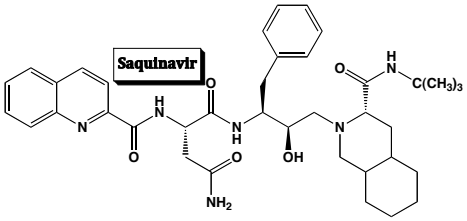

Figure 2. HIV-1 retroviral protease in complex with the inhibitor Saquinavir.[19]

Another name for rational drug design is structure-based design, from the use of three-dimensional structures of drug targets with bound small molecules (Figure 2) as guides to the development of new and "better" drugs, i.e. new compounds with increased activity and selectivity, as well as better bioavailability and that overcome resistance. The structure allows researchers to see how a molecule, or set of molecules, interacts directly with its target; as well as what features of the target could be taken into consideration for de novo design. These

three-dimensional structures are obtained from X-ray and electron diffraction, as well as solution and solid state NMR.[20] Ligand-based and pharmacophore approaches also exist for use in drug design.

Computational Techniques

To analyze these structures, a number of computational and modeling tools exist including pharmacophore development, docking, homology modeling and molecule dynamics.[21] The former two can be especially useful in high-throughput screening of large databases of molecules against a target structure. The later two are more time intensive and time-consuming methods used to study such properties as the function of proteins and mechanisms of action.[22] Using the available tools, modeling can play an important role in the early stages of the drug discovery process by finding leads and optimizing models to help direct the research. The more information known about a target or system, the more these tools can be useful. The structure and active conformation of known ligands, as well as accurate and detailed data about the structural and chemical characteristics of the biological receptor are needed. These include the size, polarity and shape of any binding sites on known 3-D structures; the homology to related targets; and knowledge of the key amino acids modulating selective binding or functional activity. This information is helpful in determining the feasibility of developing a novel small molecule with the desired activity and selectivity profile. Computational chemists then become mediators between medicinal chemistry, biology, physics and mathematics, bringing together ligand information with biological and structural data on the target, and interpreting computational results to influence research.[20,23]

As mentioned above, the development of Taxol® (**1**, Figure 3) is an excellent example of the physiology-based approach to drug discovery.[15] However, even after its use as a chemotherapeutic was common, many questions remained about its nature, including how and where it bound to tubulin. As computational techniques improved and structural data about the drug and protein target became available, many groups addressed the open questions about how and where the drug binds and how to improve the activity of the drug while reducing toxicity and side effects and overcoming resistance. The tools for structure-based design[24-26] were applied to understand binding and structure-activity relationships (SAR). Many groups made analogs, developed binding models and attempted to develop novel scaffolds in a very active area of research that continues to expand and contribute to the drug discovery process.

Taxol® (Paclitaxel)

In the late 1960's a National Cancer Institute (NCI) screening program discovered that the bark extract of the Pacific yew tree (*Taxus brevifolia*) showed significant cytotoxic and antileukemic activity. [27,28] In 1971 Drs. Monroe Wall and Munsakh Wani, along with their colleagues, reported the major active constituent as the novel diterpenoid paclitaxel (Taxol®, PTX, **1**, Figure 3).[29,30] It was a unique structure among the known anticancer drugs, possessing a relatively rigid tetracyclic ring system with four flexible side chains at the 2, 4, 10 and 13 positions. Two serious problems, though, interfered with its use as a drug: (1) it is not very soluble in water, thus making it difficult to formulate for administration as an injection; and (2) an adequate supply would be very difficult to achieve, as its initial

isolation yield was 0.0014% from *T. brevifolia* bark.[28] Depending on the size, it has been estimated that 3 to 10 trees would be needed to treat one patient. Still, additional testing of the natural product showed promising activity against breast cancer and melanoma, so the NCI invested in a full-scale preclinical development of the compound as an anticancer agent in 1977.[15,27]

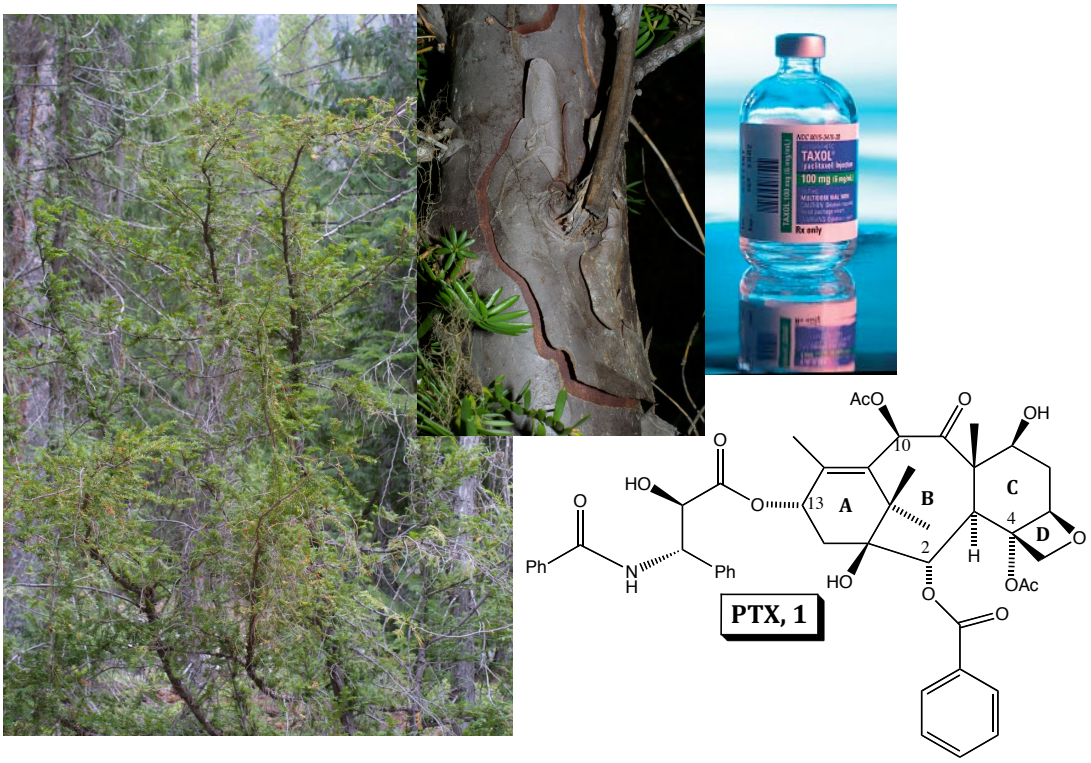

Figure 3. *Clockwise*: Pacific yew tree (*T. brevifolia*); bark close-up; Taxol® preparation for chemotherapy; and the PTX (**1**) 2-D structure.

In 1979, Horwitz reported that PTX acts as a promoter of microtubule assembly (Figure 5),[31] the first compound known to act in such a way. At the time, colchicine was known to prevent assembly of microtubules, but no compound was known to enhance it. In the 1980's, the drug proceeded through Phase I and Phase II clinical trials with the first report of clinical activity against ovarian cancer published in 1989,[32] followed closely by a report of activity against breast cancer.[33]

These reports unambiguously demonstrated that PTX showed significant activity against solid tumors, so Bristol-Myers Squibb (BMS) took over development for commercial use and Taxol® was approved for treatment of drug-resistant ovarian cancer by the U. S. Food and Drug Administration (FDA) in 1992, followed by approval for breast cancer treatment in 1994. Since then, clinical use of the drug has increased steadily and today it is also used for the treatment of non-small-cell lung cancer, small-cell lung cancer, and squamous cancer of the head and neck, among others, as well as for AIDS-related Kaposi's sarcoma.[34] In 2001, Japan became the first country to approve the drug for gastric cancer, based on results from clinical trials performed exclusively in that country. PTX reached its peak of global sales at $1.6 billion in 2000 but has decreased in sales since the introduction of generics.[35]

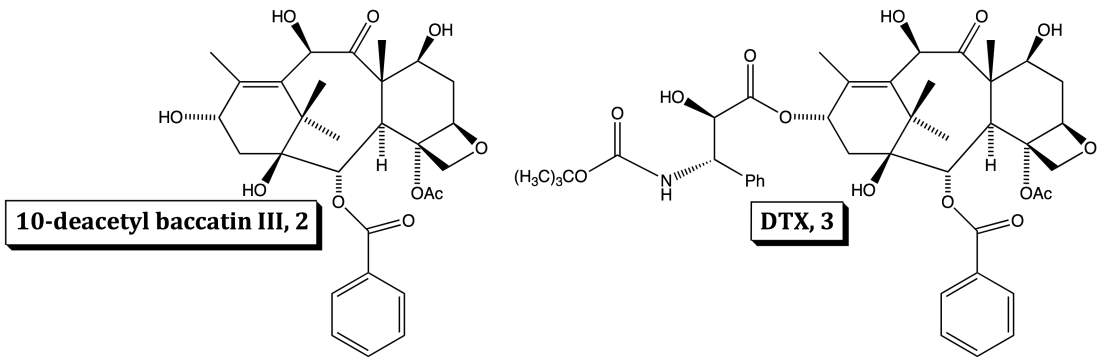

Figure 4. 10-Deacetyl baccatin III (**2**) is the starting structure for the semi-synthesis of PTX (**1**) and DTX (**3**) is a PTX analog also in clinical use.

The supply problem was solved by an efficient semi-synthetic procedure starting from 10-deacetyl baccatin III (**2**, Figure 4),[36] a congener of PTX that can be readily extracted in high yields from the leaves of *Taxus baccata* L. Harvest of the

yew leaves, unlike that of bark, is not lethal to the tree population, if performed prudently, due to their quick regeneration. The availability of such a precursor also allowed for the synthesis of PTX analogs. In 1981, French researchers at the Institut de Chimie des Substances Naturelles and Rhone-Poulenc developed the PTX analog Taxotere® (generic name docetaxel, DTX, **3**, Figure 4),[37,38] a chemotherapeutic agent currently approved by the FDA for the use in the treatment of advanced or metastatic breast cancer, for second-line use in locally advanced or metastatic NSCLC, and for first-line therapy in combination with cisplatin for inoperable, locally advanced, or metastatic NSCLC.[35] It entered clinical practice in the U. S. in 1996.

Though the problems with availability and administration were solved, others have risen as the use of PTX for cancer treatment progressed. PTX has high toxicity[39] and high rates of resistance develop from treatment.[40,41] Research into different aspects of the compound, including its SAR, its mechanism of action, and its binding conformation, has and continues to produce new analogs that address these issues.

Microtubules

As previously mentioned, PTX was found to have a unique mechanism of action some time after its discovery, though many new molecules have been found to act in a like manner, including the epothilones and laulimalide. Taxanes stabilize microtubules by binding to the β monomer of the α,β-tubulin dimers that aggregate to form the long, hollow structures important to the cell's structural stability and movement.[42] Microtubules are an integral part of the cytoskeleton of all eukaryotic cells. They participate in a vast number of cellular functions, including mitosis,

morphogenesis, intracellular transport and secretion. They are the scaffolds upon which motor and structural proteins attach to do their work throughout the cell.

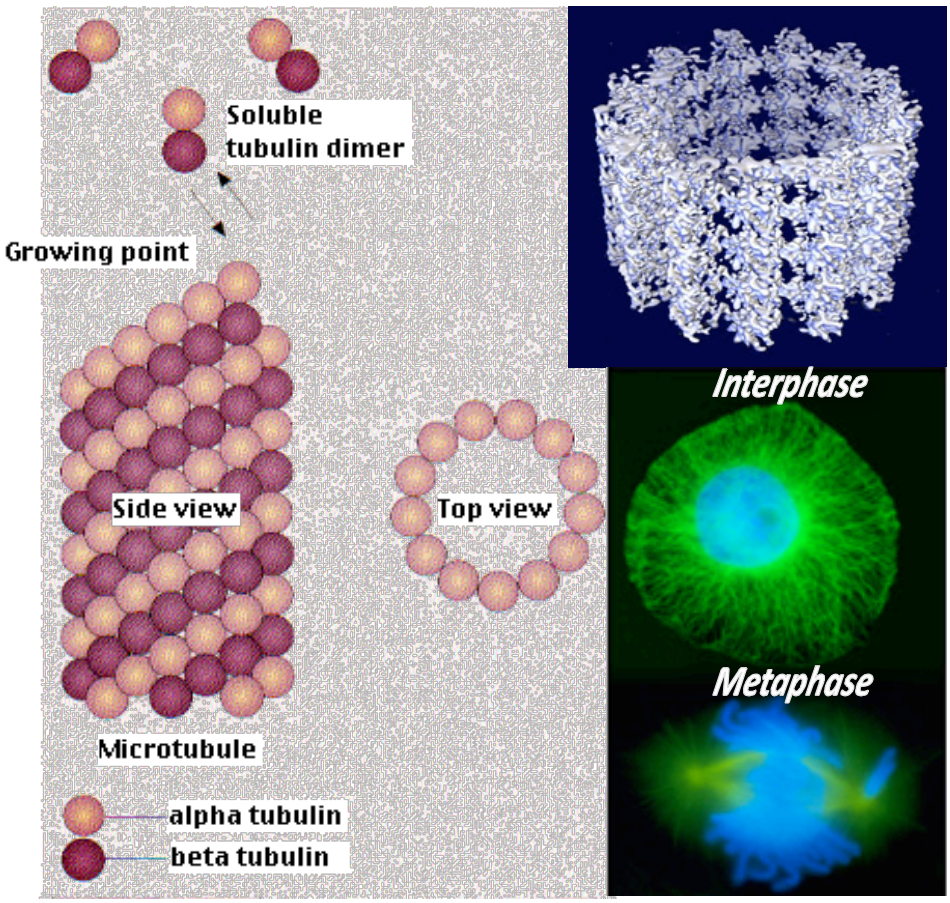

Figure 5. *Left*: Cartoon of α,β-tubulin dimers adding to the plus/growing end of a microtubule with a top view of the formed 13-protofilament cylinder that is more accurately portrayed by the 3-D electron microscopy map at 8 Å resolution (*top right*). *Bottom right*: Dark field fluorescence microscopy of resting (interphase) and dividing (metaphase) cells with microtubules in green and DNA in blue.

Microtubules are composed of tubulin, an 110kD heterodimer protein. The repeating α,β dimers reversibly bind head to tail to form linear protofilaments connected by longitudinal bonds. Lateral bonds primarily connect α-to-α and β-to-β subunits, associating protofilaments in parallel to make the cylindrical microtubule. The final structure is dynamic, with an equilibrium of rapid association and dissociation operating primarily at the plus end, or growing end of the polymer.[42] The delicate equilibrium that exists between polymerization and depolymerization is particularly important during replication. In interphase (non-dividing) cells, the minus ends of microtubules are anchored at a microtubule-organizing center located adjacent to the nucleus. During mitosis, microtubules extend out from the duplicated centrosomes that separate the two poles of the dividing cell, forming the mitotic spindle (green microtubules in metaphase, Figure 5). They spread out to the center of the cell, attaching onto the chromosomes at their kinetochores. When the chromosomes have been aligned and need to be separated into two daughter cells, the microtubules begin to depolymerize, pulling the chromosomes apart.[43] Inhibition of the depolymerization process, as when PTX is bound and stabilizing the microtubules, locks the protein and freezes the cell during mitosis. The cell, then, eventually follows the path to apoptosis, or programmed cell death.[31,44,45] PTX, then, as well as other compounds that disrupt microtubules, are excellent chemotherapeutic agents, attacking cells that are rapidly and uncontrollably dividing; that is, cancer cells.

Cancer

Cancer describes over 100 types of diseases, some more lethal than others, that led to just over half a million deaths in the United States in 2008; this accounts for almost a quarter of all deaths that year.[46] Heart disease is the only condition more lethal. Lung cancer is by far the most deadly form among both men and women, accounting for approximately 30% of cancer deaths, followed by 10% from prostate for men and 15% from breast for women. All cancers have one unifying feature: uncontrolled cellular growth.[47]

The name originates from the similarity the Greek physician Galen noted between the enlarged vein-like sores of a tumor and a crab's legs (Greek: *karkinos* for crab; Latin: *cancer* for crab). Cancer cells have a number of distinctions when compared to normal cells: they are immortal in culture, whereas there is a limit of approximately 50 divisions (Haflick's limit) for normal cells; they produce telomerase; and they resist apoptosis.[47] Three main treatments exist for the treatment of this disease: surgery, radiation, and chemotherapy (*left*).[46]

Surgery is the most effective treatment because it often removes the entire tumor preventing further spreading in the body, but many cancers are inoperable due to their location in the body. At the same time, some surgeries can be traumatic due to the damage of healthy cells and tissue

surrounding the tumor. Radiation treatment does not discriminate between cancerous and noncancerous cells, causing serious side effects. Chemotherapy is the most evolving treatment method for cancer, with drugs on the market that approach the destruction of cancer cells by means of a number of different routes. PTX and other microtubule-targeting agents are popular choices in the field, and extensive research continues to illuminate the intricacies of their mechanisms of action. In some cases, new analogs can overcome the obstacles of side effects and resistance.

CHAPTER TWO

There is one thing even more vital to science than intelligent methods; and that is, the sincere desire to find out the truth, whatever it may be.

Charles Pierce

Facts are the air of scientists. Without them you can never fly.

Linus Pauling

Background

Paclitaxel's (Figure 3; **1**) importance as an anticancer drug has motivated a generation of investigation into its chemistry and mechanism of action. Interest increased in the compound, and its derivative DTX (Figure 4; **3**), as they became the drugs of choice for the treatment of ovarian and breast cancer. Research addressed the many difficulties of the drugs with administration, side effects and acquired resistance. More easily synthesized compounds, as well as novel scaffolds that could be patented, were also of interest to BMS and other groups. Many laboratories made chemical modifications to study the SAR of PTX with tubulin. Virtually every position on the four-ring baccatin core and the side chains has been subjected to structural modification.[27,48-56] The main conclusions of these early studies are summarized in Figure 6: the C-13 side chain, the ester groups at C-2 and C-4, and the oxetane ring were found to all be essential for biological activity.

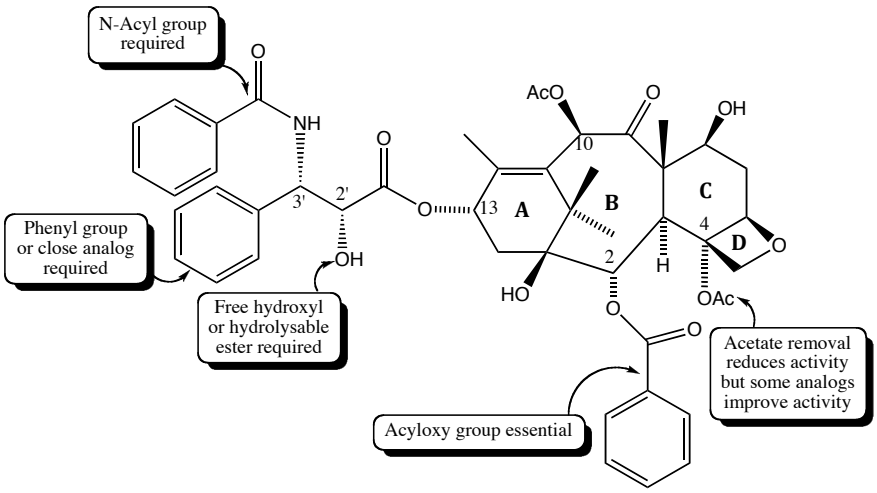

Figure 6. Some structure-activity relationships of PTX (**1**). The groups on carbons 1, 7, 9 and 10 can be removed or reduced without major changes in activity. Adapted from reference 27.

Using the large quantity of published SAR data, many research groups attempted to develop pharmacophores that explained the data and could be used for the prediction of new active analogs.[24-26,57] Though many proposals were put forth, none were predictive for more active compounds. To improve these models and stimulate further research, the bioactive conformation of PTX was needed. Understanding how PTX interacts with its target in detail would better explain the available SAR and lead to intelligent predictions and the design of ligands that overcome resistance.

The Bioactive Conformation of PTX

The bioactive conformation of a drug is considered to be the three-dimensional geometry it achieves when associated with the protein. X-ray crystallography is most often used to obtain structural information,[58] but flexible molecules can be difficult to crystallize, and X-ray data usually only yields a single conformation in the solid state. For proteins, a method for expression must be developed and crystals need to form. NMR spectroscopy has also been applied to obtain both static and dynamic conformational information,[59] but a system size limit exists. Other biophysical techniques such as electron crystallography (EC),[60,61] solid state NMR (REDOR)[62] and fluorescence resonance energy transfer (FRET)[27,54] have all been applied to the PTX binding problem.

Polar and Non-polar Conformations

For many years, most of the work published about PTX, DTX and their analogs proposed one of two clustered forms as the bioactive conformation of

taxanes, with each experiencing hydrophobic collapse between the C-2 benzoyl phenyl and one of the terminal phenyl rings of the C-13 side chain.[63] The prevalence of either one depends on the nature of the solvent: in non-polar solvents, the conformation identified by the close interaction of the C-3' benzamide and C-2 benzoyl groups dominates (Figure 7a);[64-66] the polar conformation (Figure 7b),[58,67,68] characterized by the clustering of the C-2 benzoyl, C-3' phenyl and C-4 acetyl groups, was described by NMR in polar solvents, including D_2O or D_2O/DMSO mixtures.

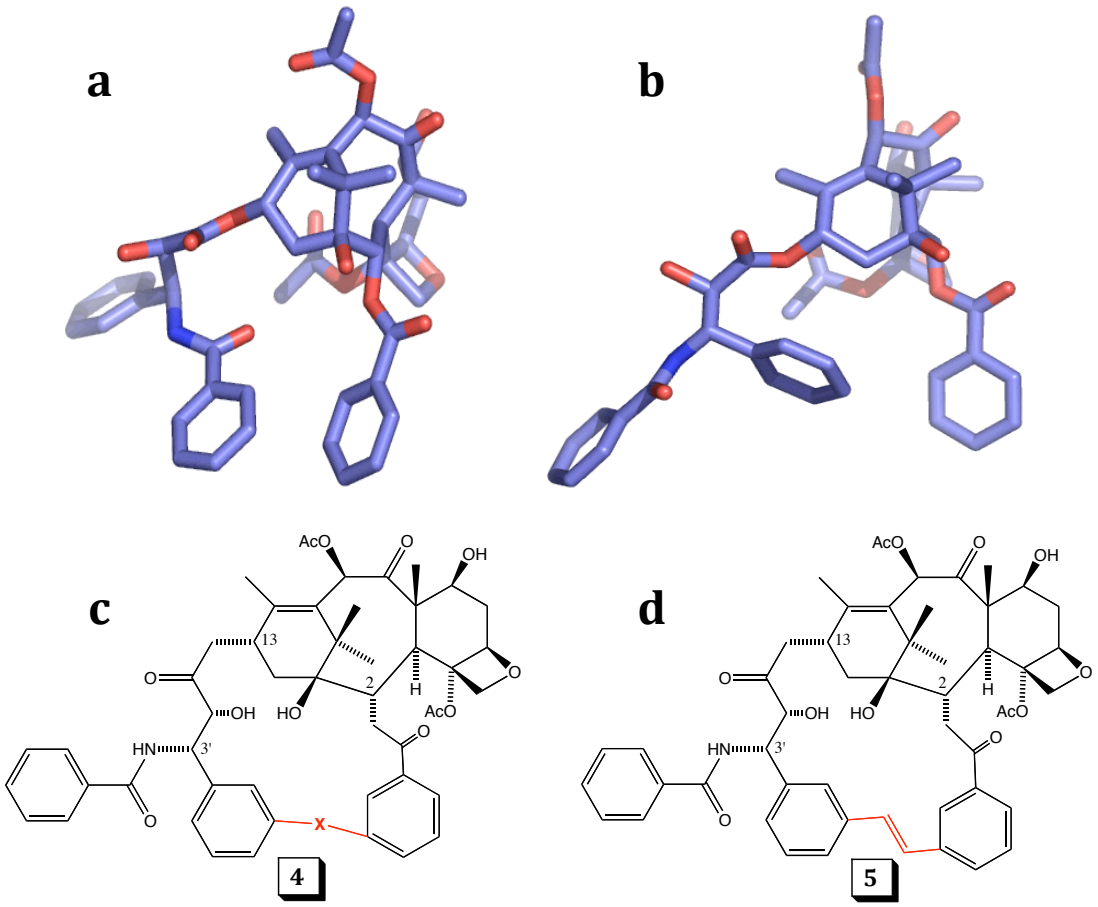

Figure 7. The two proposed bioactive conformations of PTX that present hydrophobic collapse: (a) Non-polar or apolar and (b) Polar. (c) A general representation (**4**) of conformationally resistricted analogs of the polar conformation and (d) a specific example (**5**) that does not compete with PTX for the binding site.

The design of bioactive taxane analogs based on the collapsed conformations was attempted with varying degrees of success. Conformationally restricted analogs of the polar conformation were built with 2-carbon tethers connecting the C-3' phenyl and C-2 benzoyl groups (Figure 7; **4**).[69] The presence of the conformation in solution was validated by NMR, with large H-2'/H-3' couplings, as

well as aromatic-aromatic and aromatic/C-4 acetyl NOEs observed, but none of the analogs presented any significant microtubule assembly. In addition, the E-configured macrocyclic olefin (Figure 7; **5**) does not compete with PTX for the binding site on tubulin. The results indicate that another conformation acts as the bioactive conformer of PTX. Also, taxanes were synthesized that replaced the C-2 benzoyl group, the one always involved in the hydrophobic collapse, with C-2–OC(O)-alkyl or -alkenyl groups.[70] These taxanes showed equivalent or higher *in vitro* activity as compared to the parent drug, suggesting that the active conformation of PTX does not require hydrophobic collapse.

A significant development towards the discovery of the bioactive conformation of PTX occurred when Nogales, Wolf and Downing solved the EC structure of the α,β-tubulin dimer by analyzing polymeric sheets of microtubules stabilized by zinc cations and the bound drug.[61] Unfortunately, while the 3.7 Å resolution structure (PDB id 1TUB)[71-73] presents the protein fold as a readily discernable collection of α-helices and β-sheets, it was insufficiently resolved to define the conformation of PTX. Consequently, the single-crystal X-ray structure of DTX (**3**)[38] was positioned in the ligand density as a placeholder. In this structure, DTX exhibits a conformation that folds the C-13 side chain to place the C-3' *tert*-butoxy amide group close to the C-2 benzoyl phenyl ring, reminiscent of the apolar[64-66] conformation (Figure 7a). This important but tantalizing result led to a number of efforts to define the details of the ligand's conformation. A number of groups synthesized bridged analogs based on various principles that enforce the

collapsed conformation, but none of the early attempts proved to match PTX's profile against either the protein *in vitro* or cells.[74-76]

Deconvolution of Conformationally Averaged Structures

To summarize, up through the release of the EC structure of tubulin in 1998,[61] two conformations prevailed as competitors for the bioactive form (Figure 7). These conformations, differing mainly in the torsion angles around the flexible C-13 side chain, were proposed by NMR methods and are also found in the solid state. As mentioned above, crystallography only yields one or two conformations and cannot provide information about the dynamics of small molecules. As for NMR, spectra of flexible molecules are time averaged. NOE's and coupling constants (*J*'s) reflect a weighted average from the rapidly exchanging individual conformations. NMR spectra, though, are commonly fitted to one structure, with the assumption that only one conformation exists in solution or strongly dominates an equilibrium mixture. If the assumption does not hold, then a "virtual" conformation is obtained by over-fitting the NMR data to a single form that is not present in solution.[77]

PTX (**1**) possesses at least nine easily rotated single bonds in addition to three C-OH bonds. The existence of a low population conformer different from the two described above was considered to be highly likely. In order to identify any such conformers, members in this laboratory pursued an empirically based conformational search of the molecule.[78] The NAMFIS methodology (NMR analysis of molecular flexibility in solution)[79] was applied to the PTX system. NAMFIS is a hybrid experimental/computational technique that uses the NOEs and *J*'s obtained by NMR in combination with a conformer pool obtained by Monte Carlo (MC)

conformational searches[80] to select an ensemble of structures that best satisfy the data. In this way, the different conformations obtained by a flexible molecule in solution can be established instead of settling on a "virtual" conformation[77] that will never be observed.

The authors made use of the ROESY data set carefully obtained by Hilton[81] in $CDCl_3$ and the AMBER*/GBSA/$CHCl_3$ conformational search protocol as implemented in Schrödinger's MacroModel (v2).[82,83] A 30,000 step MC search produced 2995 conformers that were clustered into 509 families and subjected to a NAMFIS fit of 42 NOE-derived H---H distances and a H-2'/H-3' coupling constant of 2.7 Hz. The analysis resulted in eight PTX conformations (Table 2) with solution populations ranging between 1 and 35%, corresponding to a maximum free energy difference ($\Delta\Delta G(CDCl_3)$) of 2.1 kcal/mol based on a Boltzmann distribution of the mole fractions at 298 K.[78]

Table 2. PTX conformers derived from NAMFIS analysis:[78] Mole fractions (MF), $\Delta G(CDCl_3)$, Ph—Ph centroid distances and conformer family.

		C-2 Ph to C-3' Ph centroid distances, Å			
	MF, %	C-3' Ph	C-3' Bza	$\Delta G(CDCl_3)$, kcal/mol	Family
1	35	9.65	5.41	0.0	Apolar
2	26	11.06	4.68	0.2	Apolar
3	19	10.52	11.32	0.4	Open
4	10	8.63	10.78	0.7	Open
5	4	5.66	12.03	1.3	Polar
6	3	9.87	10.92	1.5	Open
7	2	10.87	4.72	1.7	Apolar
8	1	11.66	12.87	2.1	Open

The eight conformers fall into three families. Conformers 1, 2 and 7, representing a total of 63% of the population, represent the non-polar form of the molecule with the C-2 benzoyl and C-3' benzamide phenyl groups clustered together and the C-3' phenyl out in solvent. The fifth most populated conformer (4%) is the only representative of the polar conformation with clustering of the C-2 benzoyl, C-3' phenyl and C-4 acetyl groups as observed in DMSO-d_6/D_2O mixtures, in CD_3OD, and in the crystal structure of PTX.[58] Conformers 3, 4, 6 and 8 comprise the third and second largest subset (33%) of the NAMFIS results. They are all "open" conformers, lacking any phenyl—phenyl hydrophobic collapse. At the time the authors did not conclude that a non-hydrophobically collapsed conformer of PTX binds to β-tubulin, but only that the single conformation hypothesis of the compound in solution was incomplete.[78] Later work, though, demonstrates that the former is the case.

The T-Taxol Conformation

Snyder, et al. utilized the results from the NAMFIS analysis in integration with the EC density of the α,β-tubulin/PTX complex (PTX-TB) in an effort to define the binding conformation of the ligand.[84] The individual conformers,[78] along with conformers derived from X-ray crystal structures[85,86] and other NMR analyses,[64,66-68,78,87,88] were docked into the EC density map of the complex. The results depicted most of the conformations with the terminal C-13 phenyl rings in regions devoid of density, except for three very similar conformations, two from the solid state[85,86] and one from the NAMFIS solution results,[78] that fit reasonably well in the density. One of the later was chosen to undergo restricted low-temperature dynamics and

force-field optimization within the experimental density. The PTX conformer was then removed from the protein complex, conformationally altered, and flexibly redocked into the binding pocket to demonstrate that the obtained conformation was both unique and reproducible. Of the results, the protein encased only two conformers and the lower energy form was identical in shape and location to that obtained from the optimization within the experimental density. The authors named this conformation the T- or butterfly-binding motif (Figure 8).[84]

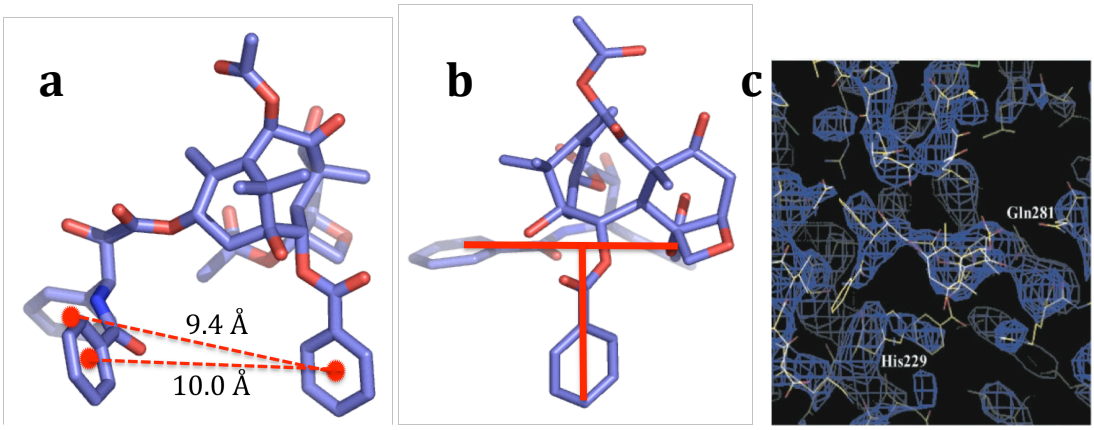

Figure 8. (a) The T-Taxol designation describes the almost equidistant placement of the C-3' Ph rings from the C-2 benzoyl group and (b) is readily visualized when looking across the molecule from C-2 to C-3'. (c) This conformation was found to be the best fit for the EC density.[78]

The T-Taxol conformation is characterized by the approximately equidistant position of the C-2 benzoyl phenyl from the C-3' phenyl rings and represents one of the "open" conformations resulting from the NAMFIS analysis of PTX. Nestled in the EC density of the PTX-TB complex as shown in Figure 8c, the C-2 and C-3' phenyl rings encase His229,[89] preventing their hydrophobic collapse, and all three hydrophobic centers of the molecule engage in complementary interactions with the

protein rather than self, as in the polar and non-polar conformations. This model predicts that taxoids designed on a hydrophobically collapsed motif would be inactive, as is the case with the linked compound mentioned above.[26,69,74-76]

Concurrent to the above work, refinement of the original 3.7 Å resolution structure of the α,β-tubulin dimer[61] to 3.5 Å defined the bioactive conformer as a structure very similar to T-Taxol.[90] This refined structure, named 1JFF in reference to the PDB code, also lacks the clustering of distant phenyl rings in order to allow His227 to reside between the C-3' benzamido and C-2 benzoyl phenyl groups.

Although doubts have been raised that the tubulin sheet model housing the T-Taxol conformation is representative of genuine microtubules,[91,92] several observations reinforce the proposition that the taxane binding site is shared between them. First, the T-Taxol tubulin model explains the capacity of epothilones A and B to assemble and stabilize purified yeast microtubules (*Saccharomyces cerevisiae*) by contrast with PTX's inability to do so.[93] The same model accurately predicted the mutation of five yeast tubulin binding site residues that restored PTX's tubulin assembly activity.[94] Second, it is completely consistent with all known acquired tubulin mutations in resistant human cell lines in response to persistent taxane drug exposure.[41,95] Third and most compelling, unlike all other previous bridging strategies, the design of bridged taxanes based on the T-Taxol conformation has achieved *both* tubulin polymerization capacities *and* cytotoxicities in several cell lines superior to PTX.[96,97] Since the T-Taxol geometry is predictive of activity in this context and both types of experiments involve genuine microtubules,

it implies that the microtubule and tubulin sheet binding sites are sufficiently similar to serve as mutual mimics.

The REDOR Conformation

However, reservations about the validity of T-Taxol as the binding conformation of PTX continue to be expressed. A combined REDOR-NMR and fluorescence spectroscopy study by the groups of Schaefer, Bane and Kingston used the PTX derivative 2-(*p*-fluorobenzoyl)paclitaxel) (2-FB-PT, **6**, Figure 9) to determine two intramolecular distances of the ligand when bound to tubulin. They reported the distances between the fluorine at the *para*-position of the C-2 benzoyl group and ^{13}C-labeled C-5' amide carbonyl carbon (X, 9.8 Å) and the C-3' methine carbon (Y, 10.3 Å) with the uncertainty estimated to be ± 0.5 Å for both.[62] This work interpreted the REDOR distances in terms of the hydrophobically collapsed polar conformer of PTX.[58,67,68] However, the inactivity of bridged analogs that enforce the same 3-D form fails to support it as the binding conformer.[26,69,75]

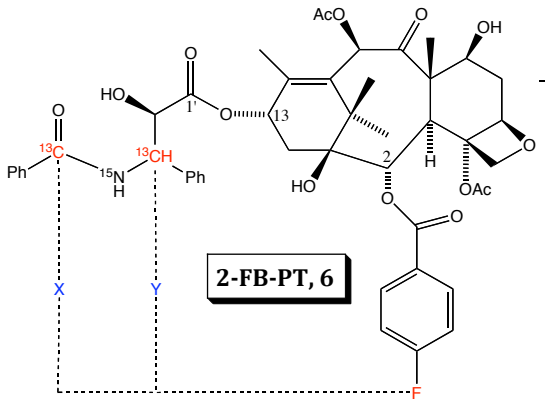

Conformer	R_X, Å (F---C-5')	R_Y, Å (F---C-3')	Degree ϕ_1	ϕ_2
REDOR	9.8	10.3		
Polar	10.4	9.6	-101	103
1JFF	8.1	9.3	-94	56
T-Taxol	9.1	9.9	-103	70
T-Taxol (i)	9.9	10.3	-89	70
T-Taxol (ii)	9.8	10.1	-103	82
T-Taxol (iii)	9.8	10.2	-97	76
PTX-NY	10.0	9.4	-160	-100

Figure 9. The distances between the fluorine and labeled carbons of 2-FB-PT (**6**) were determined by a REDOR experiment.[62] These distances are compared amongst a number of different proposals for the bioactive conformation of PTX. Dihedral angles ϕ_1 and ϕ_2 correspond to C12-C13-O-C1' and O-C1'-C2'-C3', respectively.

The T-Taxol form has been criticized for its inability to comply with the two intramolecular distances obtained by the solid-state experiments (Figure 9).[62] According to Geney, Ojima and coworkers[92] T-Taxol sustains values of 8.1 and 9.3 Å for X and Y, respectively, well outside the reported REDOR errors. Unfortunately, the authors used the numbers for the 1JFF structure[90] as opposed to T-Taxol.[84] As a result, these authors proposed a modified conformation with a reversed C-13 side chain orientation ("REDOR-Taxol") as an equally plausible bioactive shape. To obtain this conformation, they performed a MC conformational search on 2-FB-PT in vacuo, clustered the results into 16 families and performed a 2-step partial induced fit docking routine to obtain a binding model.[92] Covalent complexes were then formed between the C-7 benzodihydrocinnamyl derivative of the PTX conformers

and the protein on the basis of the observation that the compound labels the M-loop of β-tubulin exclusively at Arg282.[98] They then performed a second MC analysis, this time of the entire complex, resulting in a number of conformers. None of the representative structures strictly maintained the REDOR-NMR distances (Figure 9) but the authors picked the conformation with the closest values. This conformation is similar to T-Taxol in that the phenyl rings are similarly positioned in the pocket, but the C-13 side chain experiences a different position with the C-2' OH reoriented towards His227 and forming a hydrogen bond (Figure 10).

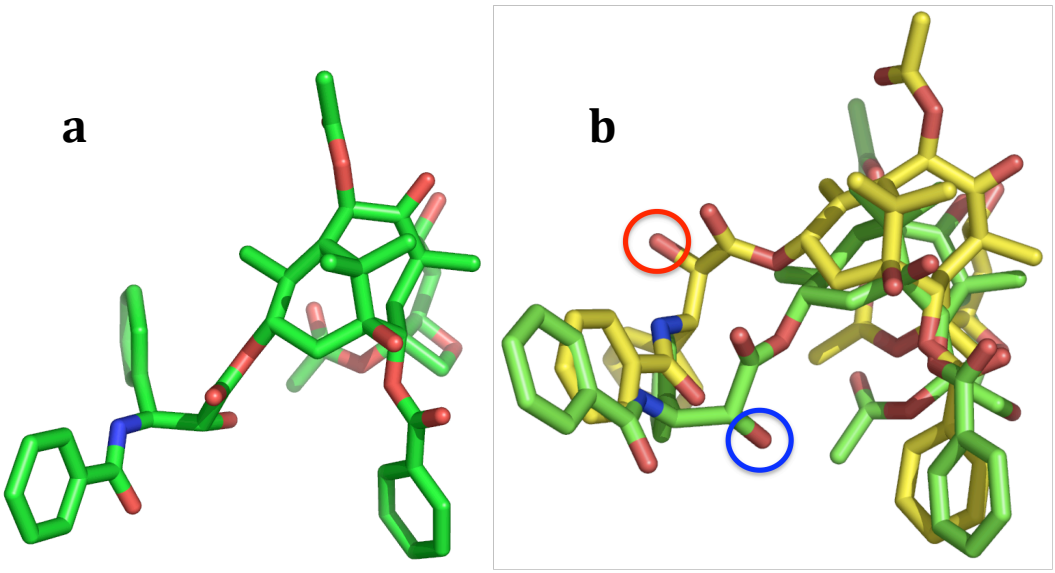

Figure 10. (a) The proposed NY conformation. (b) Superposition with T-Taxol as in the EC picture below demonstrates the difference in the C-13 side chin orientation. Red and blue circles highlight the C-2' hydroxyls.

As I mentioned, the internal interatomic distances Geney, et al. used for the T-Taxol comparison were unfortunately taken from the refined PTX-TB EC structure (1JFF-PTX)[90] and not from the derived T-Taxol model (Figure 9).[84] The latter sustains X and Y values of 9.1 and 9.9 Å, respectively (Figure 9), the lower value

falling outside the conservative ± 0.5 Å error bar by 0.2 Å. Interestingly, the model selected by the Geney-Ojima group for further work was recorded as having X/Y = 10.0/9.4 Å, the second of which is also outside the reported 0.5 Å error boundary by 0.4 Å (Figure 9).[92] The latter proposal cannot be considered *the* "REDOR" conformation while disregarding T-Taxol when neither match the reported distances within the error boundaries; as such, we put forth that T-Taxol must also be considered a "REDOR" conformation. Moreover, as explained in detail below, many different conformations actually fall into the REDOR-defined limits; therefore, to distinguish the proposal by the Geney-Ojima group[92] from other "REDOR" conformations, it shall be referred to as PTX-NY from here on in this document (Figure 10). The purpose of the present work is to examine the various proposals critically in light of the REDOR measurements, as well as an array of data encompassing biophysical measures, including the EC density, and biological outcomes, such as SAR.

Methods

All images were prepared using PyMOL.[99]

Preparation of PTX-NY. A conformation of PTX was modified by replacing the *para*-H of the C-2 benzoyl side chain phenyl with *para*-F to give 2-FB-PT. Then, four C-13 side chain angles obtained from Figure 5 of the Geney et al. paper[92] were incorporated to generate the New York conformation (PTX-NY): C12-C13-O13-C1' 155°, C13-O13-C1'-O1' 4°, O13-C1'-C2'-O2' 22°, and O2'-C2'-C3'-N3' 178°. The structure was then superimposed onto T-Taxol to provide the relative orientation of the two structures as depicted in Figure 3A of the Geney work (Figure 10).[92]

EC density maps. All the maps were prepared by Scott Johnson as published.[100,101] That procedure is replicated here for reference.

For all maps,[102,103] the 1JFF protein structure[90] and corresponding structure factors were employed with b-factors flattened to 30.0 during the map generation process. The T-Taxol structure was taken from the computationally refined PTX-TB complex,[84] while the New York conformation was obtained as described above. Both $2F_{obs}$-F_{calc} and difference maps were generated using CNS 1.1[104] and compared to maps generated from CCP4[105] for consistency. It should be noted that Fourier difference maps are capable of visualizing changes at low noise levels between two closely related ligands in a common binding site that correspond to only a few carbon atoms.[106] CNS topology and parameter files were obtained from the HIC-UP (Hetero-compound Information Centre - Uppsala) server hosted by Uppsala Universitet.[107] For easier visualization of the CNS $2F_{obs}$-F_{calc} omit map, a solvent mask was generated to hide solvent and protein density farther than 1.5 Å from either ligand's coordinates. The maps were compared in 'O'[108] and the publication images were generated with Pymol. Cut-off values for the difference maps were determined visually to maximize image quality and did not exceed a difference cut-off of +/- 2.50 sigma as determined by 'O'. Due to scaling inconsistencies between the masked $2F_{obs}$-F_{calc} omit map and the original map, the two maps were visually compared in 'O' at 1.00 sigma and the masked cut-off was adjusted accordingly.

Conformational Searches. Two 15,000 step Low Mode Monte Carlo (LMMC) conformational searches[109] using the MMFF[110-112] and MM3*[113-115] force fields and an aqueous continuum solvation model[82] were performed for 2-FB-PT(**6**) using

MacroModel version 8.6.[83] The F—C-5' and F—C-3' distances were constrained to the REDOR values (9.8 and 10.3 Å, respectively),[62] and an energy cutoff of 7.0 kcal/mol was used. The search provided 602 and 598 fully optimized MMFF and MM3* conformations, respectively. Distance constraints were removed, and the two sets of conformations fully optimized in their respective force fields. This resulted in 47 and 33 structures from MMFF and MM3*, respectively, that matched both REDOR distances within ± 0.3 Å.

A 10,000 step LMMC conformational search using the MMFF force field in MacroModel and a 10.0 kcal/mol cutoff was performed for bridged T-Taxol analog **9** (C-2 *para*-X = H). In total, 93 optimized conformations were obtained, and the global minimum was found 62 times. Twelve of these structures fall into the T-Taxol family on basis of the observation that the centroids of the C-3' phenyl rings fit the T-form within 20% of the distances found for the centroids of the corresponding T-Taxol phenyl rings. That is, the ranges for the 12 conformers are C-2 benzoyl to benzamide phenyl, 7.9—11.2 Å (T-Taxol 9.4 Å) and C-2 benzoyl to C-3' phenyl, 8.9—9.4 Å (T-Taxol 10.0 Å).[84] Not a single example of the PTX-NY conformation was located among the conformers of the optimized dataset.

Finally, a 5,000 step LMMC conformational search with an energy cutoff of 7.0 kcal/mol was performed for the New York construct **11** using the MMFF force field in MacroModel. A total of 105 optimized conformations was obtained, 28 of which conform to the T-Taxol conformation. The global minimum was located 40 times. Again, no conformation corresponds to the New York variation. A single MMFF conformer showed a C-3' side chain orientation similar to that in the latter

and C-3' phenyl centroid distances within 20% of the T-form (as that above). However, the torsion angles around C-2' direct the C-2' OH away from the bridge and, therefore, away from His227 as well, when the molecule is docked into the protein. This observation is consistent with the behavior of unbridged PTX-NY when subjected to MD within the taxane binding pocket (see following section).

Molecular Dynamics. The PTX-TB complex[84] was subjected to molecular dynamics for 5 ps at 300 K using the Tripos force field in Sybyl version 7.0.[116] The imidazole ring of His227 was treated both in the neutral and protonated states during the separate simulations.

Docetaxel (DTX, **3**) and nonataxel (NTX, **7**) were modified from T-Taxol and docked into the PTX-tubulin complex by superimposing the baccatin cores using Sybyl version 7.0.[116] Each model was subjected to MD at 20 K for 5 ps with the protein backbone held as a fixed aggregate. During this treatment, the energy gradually fell until it leveled off during the final picosecond. Because the DTX and NTX complexes were so similar to the starting PTX complex, no further MD was warranted. With the backbone still held fixed, the ligand and the tubulin side chains were then optimized with the Tripos force field.

2-FB-PT, as prepared in the PTX-NY conformation above, was manually docked into the 1JFF protein binding site.[90] MD simulations were performed with the MMFF94 force field in Sybyl version 7.0[116] by allowing movement of the ligand and all side chains surrounding it within a 10 Å sphere at 20 K with a time step of 0.5 fs and dielectric constant of 4.5 for 5 ps. Prior to molecular dynamics (MD) treatment, the C-C(O)-NH_2 bond of Asp26 was rotated to give the benzamide phenyl

room to reside in the pocket without severe steric conflict. Three constraints were enforced to maintain the PTX-NY conformation throughout the MD simulations: X (F—C-5') = 10.0 ± 0.2 Å; Y (F—C-3') = 9.4 ± 0.2 Å; and C2'-OH—His227-N = 2.5—3.5 Å. The model was regarded as stable because the last 3 ps of the simulation resulted in an overall RMS deviation of 0.35 Å for the ligand and an energy variation of less than 3 kcal/mol. At this point the constraints were removed, and a full optimization of the site was performed using MMFF. The optimized complex was then subjected to higher temperature MD to determine if the hydrogen bond distance would be maintained without the constraints. The same parameters were used, but the temperature was increased from 20 K to 300 K during a 4 ps MD run.

Throughout the simulations, the C2'-OH---N-His227 distance was constrained to 2.5-3.5 Å in accord with the observation that PTX-NY enjoys a hydrogen bond between these centers. As the MD simulations proceeded, the binding pocket of tubulin expanded slightly to better accommodate the ligand, although the only significant change observed was the position of the His227 side chain. Since, the unprotonated nitrogen of the imidazole ring attempted to form a hydrogen bond with the C2'-OH of the ligand (~3.0 Å), the plane of the ring rotated relative to its position in 1JFF to accommodate the interaction. The hydrogen bond length varied between 2.5 and 3.4 Å throughout the entire simulation, although for 90% of the trajectory it oscillated evenly between 2.5 and 3.0 Å. When the constraints were released and the model allowed to follow dynamic pathway at slightly higher temperatures, the electrostatic interaction between the C-2' OH and His227 was not maintained. Although the ligand stayed within the pocket for the

most part, the C-13 side chain, especially the phenyl rings, slowly drifted outward and starts to lose the PTX-NY conformation.

Our purpose here was not to perform a complete MD study but to generate a reasonable model of the New York conformer for comparison with the EC structure of tubulin bound to T-Taxol. Examination of Figure 10 in the main text and Figure 3a in the Geney-Ojima investigation[92] makes it clear we have accomplished this goal. A more vigorous treatment would most likely not do so.

Results and Discussion

Ojima and colleagues have proposed a new conformation as the bioactive form of PTX (PTX-NY)[92] in preference to T-Taxol.[84] The essential difference between the New York and the Emory models resides in the conformation of the C-13 side chain from C-1' to C-3'. In the latter conformer, the C-2' OH group experiences a hydrogen bond with the backbone NH of Gly370 on the loop that spans β-sheet strands B9 and B10 (Figure 10, red circle).[84]. The new proposal involves a conformational reorientation that directs the same group toward the hydrophobic basin but within hydrogen bonding distance of His227 on Helix 7 (Figure 10, blue circle).[92]

Electron Crystallographic Density Compatibility

The authors comment that the low resolution of the PTX-TB complex density map eliminates the possibility of distinguishing between T-Taxol and the New York variation.[92] It is accurate to state that during the initial structure-building,[61] the EC density alone was not sufficient to provide an unambiguous solution to the PTX

binding problem. Follow-up refinement that delivered 1JFF came close,[90] but it has been a combination of modeling and NMR with the EC density that has yielded a well-defined structure with predictive power.[84,96] While the density in question is incomplete and weak in some ligand regions (e.g. between C-2 and the terminal benzoyl phenyl), it is strong and discriminatory as it concerns the conformation of the C-13 side chain. Comparing T-Taxol and 1JFF-PTX against the New York conformer constructed from published torsion angles[92] is illustrative.

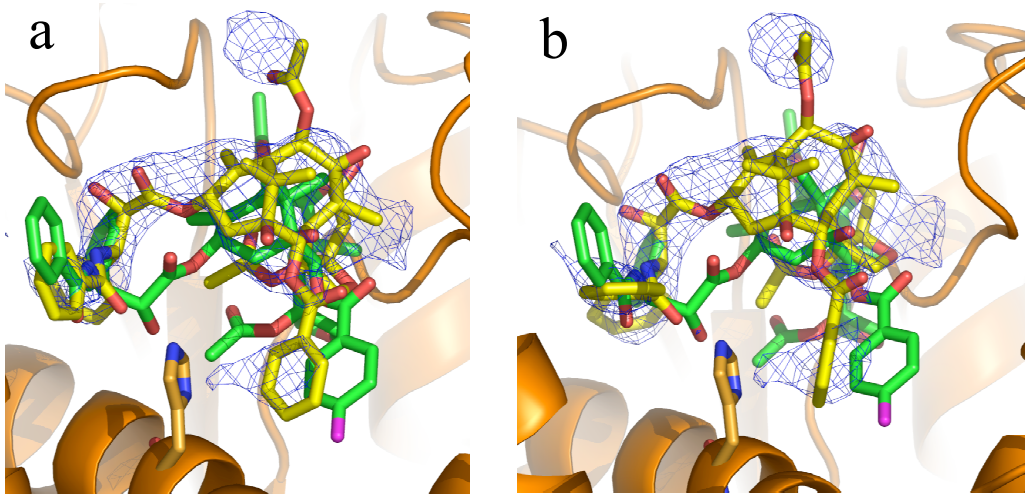

Figure 11. The structures of (a) T-Taxol[84] and (b) 1JFF-PTX[90] (yellow) superimposed with the NY-PTX conformation[92] of 2-FB-PT (green) in the β-tubulin binding site. The $2F_{obs}$-F_{calc} density maps for the former two are shown as blue 3-D contours.

A student in our lab, Scott Johnson, used the models I provided to develop omit and different maps that readily differentiate between the two conformations. Figure 11a depicts the T-Taxol and PTX-NY structures superimposed in the tubulin binding site simultaneously displayed with the $2F_{obs}$-F_{calc} omit map[102,103] as derived

from the original measurements.[61] The 3.7 Å resolution occasions missing density around C-2 and C-10. However, strong density displayed as a blue grid along the C-13 side chain from C-1' to C-3' illustrates that T-Taxol (yellow) matches the experimental data perfectly. Manual superposition of T-Taxol and PTX-NY within β-tubulin according to visual inspection of Figure 3A in the Geney, et al. report illustrates that the baccatin cores and the three terminal phenyl groups occupy similar regions of space (Figure 11a). However, while the PTX-NY conformation is a reasonable mimic of the T-Taxol binding rotamer at its extremities, the conformationally inverted C-2' center in the modified T-Taxol (green) falls well outside the EC density associated with C-13 to C-3'. Comparison of the New York conformer with 1JFF-PTX delivers the same result (Figure 11b). As mentioned above, while T-Taxol and the 1JFF variation sustain somewhat different C-13 torsions and internal distances (Figure 9), the structures occupy fundamentally the same space in the β-tubulin taxane binding pocket.

Another test of the New York conformation's ability to fit the density was carried out by performing low temperature MD on the tubulin—PTX-NY complex using the structure depicted in Figure 11 (green). The MD assured that these results were not compromised by the manual docking guided by Ojima's recent report.[92] The C2'-OH---N-His227 distance was constrained to a 2.5-3.5 Å window throughout the simulation, with the His227 side chain reorienting itself toward the C-2' OH group. Once the MD simulations provided a stable model, the constraints were removed and full optimization of the PTX-NY—TB complex was performed holding the protein backbone fixed. The resulting X and Y distances were measured at 11.0

and 10.4 Å, respectively, each 1 Å longer than those reported by the authors for the PTX-NY proposal. Slight movements of the ligand in the pocket were observed, but it retained essentially the same conformation and binding pocket orientation. The corresponding $2F_{obs}$-F_{calc} omit map (Figure 12) is qualitatively and quantitatively similar to those pictured above.

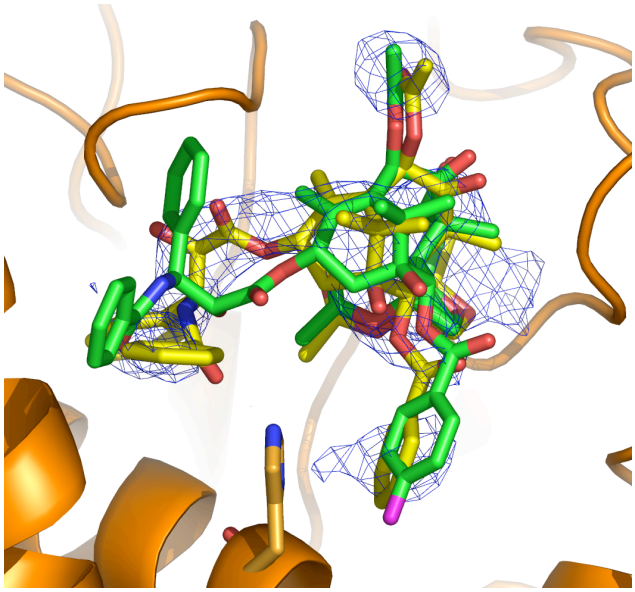

Figure 12. The structures of T-Taxol (yellow) and the NY-PTX conformation of 2-FB-PT (green) superimposed in the β-tubulin binding site. In contrast to the graphically constructed 2-FB-PT NY-PTX form in **Figure 11**, the tubulin—2-FB-PT complex pictured here has undergone low temperature MD as described in the **Methods *Molecular Dynamics*** section. By contrast with the green conformer pictured before, the C-13 phenyl rings have drifted outward and moved somewhat away from the NY-PTX conformation.

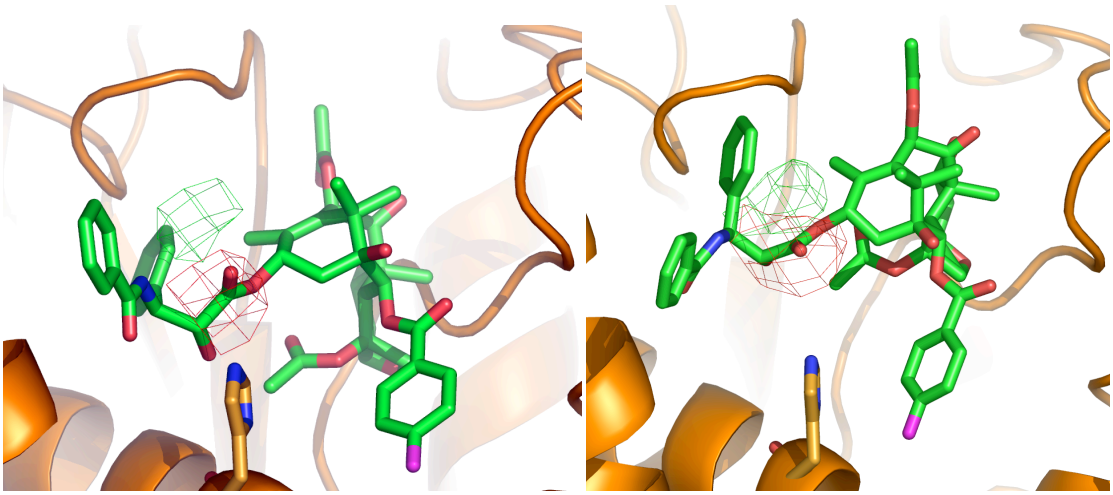

Figure 13. Difference maps (F_{obs}-F_{calc}) for the PTX-NY conformation (a) built from published torsions[92] and (b) after the MD simulation and optimization protocol described in the **Methods *Molecular Dynamics*** section. Green corresponds to unfilled density and red to incorrectly filled density. The latter structure shows the same qualitative behavior after MD as seen before.

Another means of evaluating the fit of a protein-ligand model is to generate F_{obs}-F_{calc} difference Fourier maps,[102,103] as depicted in Figure 13a for PTX-NY as positioned in Figure 11. In order to focus specifically on the C-13 side chain, the maps have been truncated to this region alone. Where model atoms lie outside $2F_{obs}$-F_{calc} contours, the F_{obs}-F_{calc} map portrays them within negative (red) contours. Positive (green) contours highlight the correct locations for the same atoms. Thus, the green grid represents density derived from experiment, but unfilled by the ligand model, while the red density corresponds to a region of the binding pocket that has been incorrectly filled by the taxane conformation. A similar exercise for the MD relaxed form of the PTX-NY—tubulin complex yields the same qualitative result (Figure 13b). They are virtually identical in their representation that the C-13

side chain is most likely misplaced. Taken together, the maps clearly distinguish the two conformations, suggest that the C-13 side chain of the PTX-NY structure has been improperly positioned in the binding site, and affirm that T-Taxol is the conformer that best fits the EC density.

REDOR Experiment Limitations

Ojima and colleagues contest T-Taxol's validity[92] as the bioactive conformation of PTX on account of one piece of data: the two distances reported by Li, et al. from their REDOR analysis of 2-FB-PT (**6**) bound to tubulin (Figure 9).[62] The Schaefer group's double REDOR solid state NMR measurement of F—^{13}C distances for quadruply labeled **6** bound to tubulin polymerized *in vitro* encompassed eight million scans and required three months of acquisition time. The experiment involved continuous dephasing by ^{15}N (^{13}C{^{15}N}) and ^{19}F (^{13}C{^{19}F}) to generate the difference spectra S_0 and ΔS, respectively. The $\Delta S/S_0$ ratio measures the dipolar coupling between the ^{13}C and ^{19}F atoms; i.e. the stronger the peak in the ΔS spectrum, the shorter the ^{13}C—^{19}F distance. As the ratio depends only on the ^{13}C—^{19}F distance (r_{CF}), acquisition of the internuclear separations requires only determination of $\Delta S/S_0$ at a single dephasing time.

In the REDOR analysis of **6**, consideration of signal-to-noise in the $\Delta S/S_0$ ratio led to the estimate of a 6% uncertainty in the F—^{13}C distances; i.e. ± 0.5 Å.[62] In spite of the enormous resources expended to generate the distances, there are inherent limitations associated with fitting a single-parameter curve to a single data point, the latter being a necessity in the analysis of Li, et al. because each additional point would require at least three additional months of machine time. As a result, we

collaborated with Dr. Anil Mehta to reexamine the error calculations and certain assumptions underlying the REDOR measurements.

REDOR error recalculation. The dipolar coupling (D_{CF}), hence the $\Delta S/S_0$ ratio, between two NMR active nuclei is inversely proportional to the cube of the internuclear distance (r_{CF}) between them: $D_{CF} \sim 1/r^3$. Using standard error analysis for the 9.8 Å distance, the reported value of $\Delta S/S_0$ (0.14), and the 20% reported error, Dr. Mehta performed the error recalculation as follows

$$\pm\frac{r}{r_{CF}} = \pm\frac{\frac{1}{3}(0.2)(\Delta S/So)}{\Delta S/So} = \pm\frac{\frac{1}{3}(0.2)(0.14)}{0.14} = \pm 6.7\%$$

where $\pm r$ is the error in the calculated internuclear distance. Calculating the error in a similar manner for the 10.3 Å distance translates into 9.8 ± 0.7 Å and 10.3 ± 0.7 Å, providing a slightly expanded error window by comparison with the previously estimated one. In this context, the REDOR measurement accommodates the structures previously published for both the polar conformation and T-Taxol (Figure 9).

The REDOR dephasing curves corresponding to the reported distances[62] with the recalculated ± 0.7 Å error are displayed in Figure 14. Although the measured ratios accurately fall on the theoretical curves represented by the solid lines, a critical element inherent in the determined $^{13}C—^{19}F$ distances is that the distance measurement relies on fitting a single-parameter curve to a single data point. Although the ± 0.7 Å bracket represents the experimental error, there are a number

of reasons for believing that even this range of ^{13}C—^{19}F distances may be overly restrictive. The basis for this assertion follows.

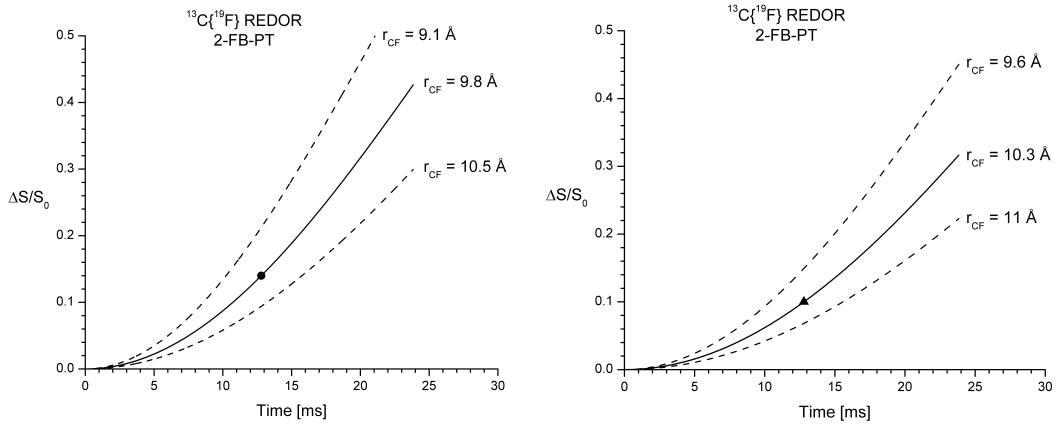

Figure 14. Experimental dephasing from reference 62 for ^{13}C-5'---^{19}F (circle) and ^{13}C-3'---^{19}F (triangle) and the calculated REDOR curves assuming a single ^{13}C---^{19}F distance to each ^{13}C center. Solid lines correspond to the ^{13}C---^{19}F distances[62] and the dotted lines represent the ± 0.7 Å error.

Conformer distribution of 6. The REDOR curves are calculated assuming a single ^{13}C—^{19}F distance and the lack of significant molecular motion. However, as implied by the MD simulations described below (Figure 17b), **6** appears to experience dynamic conformational equilibration when bound to the protein. Also, the solid-state baccatin III ^{13}C spectra[117] is consistent with the view that the molecule experiences dynamic conformational equilibration in the solid state. An alternative viewpoint arises from the observation that in the REDOR experiment the tubulin-microtubule samples stabilized by the labeled ligand (**6**) were rapidly frozen in liquid nitrogen (77 K) and lyophilized for 3-4 days.[62] It has been argued that such freeze drying traps all conformations present in solution prior to flash

freezing and thereby leads to microheterogeneity accompanied by the lack of equilibration.[118] However, raising the temperature from 77 to 268K (-5°C), where the REDOR experiment was conducted, can reestablish interconversion among a distribution of forms.[117,119,120] Accordingly, the C-2 and C-13 side chains furnishing the distance measurements may well oscillate around a cluster of interconverting structures characterized by both high amplitude torsional vibrations and interconverting conformations. As a result, the distributions depicted by the MD simulations (Figure 17b) may contribute to the observed REDOR dephasing.

In principle, REDOR can disentangle conformational effects in the solid lyophilized sample. However, to deconvolve internuclear distances for a possible range of trapped conformations, several dephasing times need to be collected. Multiple data points are required because dephasing for a distribution of distances depends on two parameters, the mean distance and the distribution.[121] In an attempt to estimate the effect of C-2 and C-3' side chain distributions on the shape of the REDOR dephasing lines in the absence of multiple measurements, we have modeled the dependence of the $\Delta S/S_0$ ratio in terms of Gaussian half-widths (Figure 15). For the 9.8 and 10.3 Å ^{13}C—^{19}F distances, Gaussian distributions of 0.8 and 1.6 Å give results essentially identical to that for no distribution. As there is only a single REDOR data point, all three models (no distribution, 0.8 and 1.6 Å distributions) are consistent with the distance data.

The Gaussian curves are properly interpreted as the distribution of conformations observed in the solid state with different ^{13}C—^{19}F separations. The larger the full-width half-maximum of the Gaussian distribution, the larger is the

disorder. The result of fitting the data to a distribution suggests that the $^{13}C—^{19}F$ distances would increase, at most, by 0.1 Å (Figure 15 table). However, for these distributions and distances, the raw distance error estimate is the same, ± 0.7 Å. For reasons expressed above, this analysis is also consistent with the view that a ± 0.7 Å error on the distance measurement resulting from fitting a single-parameter curve to a single data point is overly conservative.

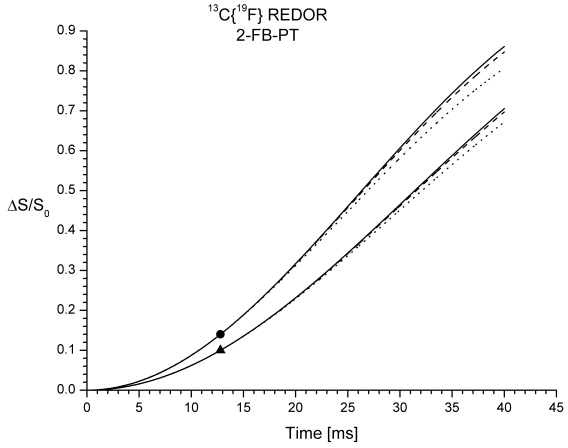

	Width of Gaussian Distribution (Å)	Distance (r_{CF}) (Å)
Carbonyl	0	9.8
	0.8	9.8
	1.6	9.9
Methine	0	10.3
	0.8	10.4
	1.6	10.5

Figure 15. *Left*: REDOR plots of ^{13}C-5'---^{19}F (circle) and ^{13}C-3'---^{19}F(triangle) dephasing with calculated curves for no distribution (solid lines) and Gaussian distributions with full-width and half maximum widths of 0.8 Å (dotted lines) and 1.6 Å (dashed lines). Distances from reference 62. *Right*: Full width at half-maximum of calculated Guassian distribution as a function of ^{13}C---^{19}F distances.

Lyophilization of the Tubulin-Ligand Complex. Another potential source of difference between the solid state and EC-refined distances arises from the 3-4 day lyophilization to which the tubulin—2-FB-PT NMR samples were subjected. The purpose of the process is to remove sufficient water to produce a solid but leave one or two aqueous solvation shells around the protein intact. In addition, to protect the

surface of the protein in the absence of bulk water, lyophilization is performed in the presence of a stabilization matrix. In the case of the tubulin—2-FB-PT complex, polyvinyl pyrrolydine was employed. Following the dehydration treatment, the presence of intact microtubules was detected in the reconstituted lyophilized sample by electron microscopy.[62]

Despite these precautions and controls, the actual number of water layers remaining after lyophilizaton is unknown. Likewise, the nature and extent of water structure near regions of relative hydrophobicity, for example, near the taxoid hydrophobic cleft, is undefined. Given that PTX is believed to bind either at the inner[61,122] or the outer[123] surface of the microtubule, one face of the molecule is exposed to the aqueous environment, whereas the other concave nonpolar one may share the binding pocket with a small number of water molecules.[124,125] Consequently, any disruption or reorganization of the first solvation shell could have an effect on how deep the ligand sits in the pocket, on features of conformation, or on ligand mobility.

Two interesting studies in this respect focus on a short peptide and a protein. The first evaluated the solid-state ^{13}C and ^{15}N NMR spectra of crystalline pentapeptide Leu- and Met-enkephalins experiencing different degrees of hydration.[120] Not only are the peptides' backbones and side chains dynamic in the 0 to –100 °C temperature range, but conformational disposition is influenced by dehydration. Significantly, REDOR distances were shown to change by as much as 25% as a result of partial dehydration. Although the hydrated crystalline enkephalin system is not a mimic of the PTX-TB complex in the solid state, the work

nonetheless teaches that modification of the solvation shells near the binding site carries the potential for alteration of both the static and dynamic structural features of the ligand. To evaluate motion in hydrated protein microcrystals, the second investigation compared the X-ray crystal structure and solution NMR analysis of ubiquitin with solid-state NMR measurements of the same protein labeled uniformly with ^{13}C and ^{15}N nuclei.[126] Reduced dipolar couplings were observed for residues with increased backbone motion, as measured both by solution-state NMR and increased crystallographic b-factors. The three measurements concur that sectors of hydrated proteins near room temperature (10 °C) experience significant motion. In summary, both the enkephalin and ubiquitin results provide an additional reason for not expecting perfect agreement between REDOR- and EC-determined internuclear distances.

The above analysis does not propose that uncertainties in the solvation properties of the protein binding pocket in any way invalidate the REDOR measurements. It does however suggest, that the error estimates of ± 0.5 and ± 0.7 Å are too narrow by this standard. Consideration of fitting the REDOR curve to a single point, conformer distribution, molecular motion, and variations in the nature of the binding site hydration relative to soluble or polymerized protein can easily explain the minor discrepancies between REDOR- and EC-determined intramolecular F—C distances. In summary, the ^{13}C—F REDOR distances are fully supportive of the T-Taxol and PTX-NY binding conformations as they are of the polar and numerous other energy minimum conformations.

Conformer Variability

As discussed thus far, two important pieces of biophysical experimental data support the T-Taxol pose as the bioactive conformation of PTX. One of these, the EC density, excludes the PTX-NY conformation, while the other, the REDOR distances, cannot distinguish between the two when evaluated with a ± 0.7 Å error range. One of the points discussed above involves the motion of the ligand during the solid-state experiment. PTX is a large, flexible molecule, as especially revealed in the NAMFIS study that deconvolved the conformations present in solution.[78] The REDOR data only provides two distances within the molecular volume of the compound. We hypothesized that many different PTX conformations could attain the reported distances, even when the ± 0.5 Å error range is strictly enforced.

Unbound PTX Structures that Conform to the REDOR Distances. To examine the possible range of structures strictly meeting the REDOR measures, two LMMC conformational searches[109] were performed for 2-FB-PT (**6**, Figure 9) using the MMFF[110-112] and MM3*[113,127,128] force fields and an aqueous continuum solvation model.[82] Throughout the searches, the F—C-5' and F—C-3' distances were constrained to the REDOR values (9.8 and 10.3 Å, respectively). A total of 602 and 598 structures were obtained with MMFF and MM3*, respectively, within an energy window of 7 kcal/mol from the global minimum. The distance constraints were removed, and the two sets of conformations were fully optimized with the respective force fields. Forty-seven structures with MMFF retained the REDOR distances within ± 0.3 Å, whereas 37 structures with MM3* did so.

Figure 16a displays a subset of the fully optimized conformations with retained REDOR distances for which the baccatin cores have been superimposed. With only two distances measured, the conformational profile of the system is not well defined. Within the boundaries of the search, the two phenyl groups emanating from C-3' are free to occupy a wide range of locations. Consequently, although the NMR-determined distances provide important intramolecular measures for two C-13 side chain atoms buried within the volume of the PTX molecule, they are silent with respect to the C-3' terminal hydrophobic contacts between ligand and protein. As a result, the REDOR outcome cannot distinguish between many of the proposed bioactive conformations, including T-Taxol, PTX-NY and the polar one (Figure 7-Figure 10).

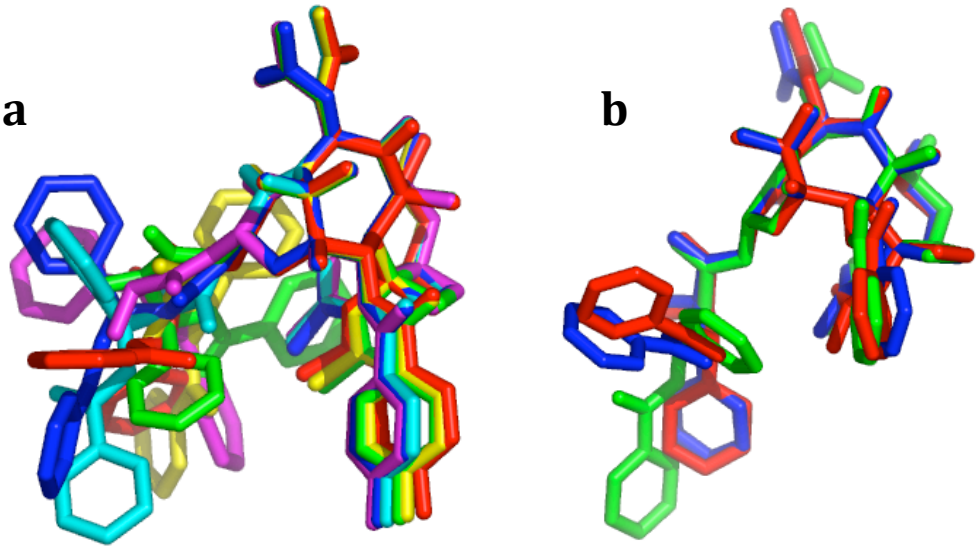

Figure 16. (a) A subset of the fully optimized conformations resulting from the MM3* LMMC conformational analyses of **6** with the F---C-5' and F---C-3' distances constrained to the REDOR values. (b) The spatial disposition of the C-3' terminal phenyl groups from superimposing the baccatin cores of T-Taxol (blue), 1JFF-PTX (red) and the polar conformation (green).

A subtler question concerns the spatial variability of the same two rings when the empirical structures for the bound conformation are superimposed. Figure 16b depicts the situation for T-Taxol (blue),[84] 1JFF-PTX (red)[90] and the polar conformation (green)[58,129] when the C-2, C-4, C-13 and C-15 baccatin core atoms are matched. The first two structures present fundamentally different orientations of the C-3' phenyl rings as compared to the polar conformation. 1JFF-PTX can be considered a T-type structure with its phenyl rings similarly positioned to those of T-Taxol and its C-13 side chain obtaining a comparable conformation. None of the structures, though, adhere strictly to the 9.3—10.3 and 9.8—10.8 Å ranges dictated by the ± 0.5 Å error boundaries derived from the REDOR data (Figure 9); T-Taxol

falls outside the error limit by 0.2 Å for the first distance, while the polar conformation does so by 0.1 Å and 0.2 Å, respectively. The large 1JFF-PTX differential of 0.5—1.7 Å is undoubtedly a consequence of the low-resolution data (3.5 Å) achieved during refinement.

T-Taxol and the C-13 Side Chain Dihedral Angles. Concerning T-Taxol itself, what are the origins of the observation that the F—^{13}C distances from the computationally refined structure fall near the lower boundaries of the error bars? This can be traced to small deviations in the C12-C13-O-C1' and O-C1'-C2'-C3' dihedral angles (ϕ_1 and ϕ_2) compared to those required for exactly meeting the REDOR constraints (Figure 9). In the published T-Taxol structure[84] these are –103 and 70°, respectively. A separate reduction of the first dihedral angle by 14 to –89° or enlargement of the second by 12 to 82° provides perfect agreement with the REDOR distances (T-Taxol (i) and (ii), respectively, in Figure 9). If both angles are simultaneously altered to –97° and 76°, respectively, a diminutive 6° change for each, the structure is once again brought into perfect alignment with the solid state distances (T-Taxol (iii) in Figure 9). One possible interpretation of the distance discrepancies is that the Kollman all-atom AMBER force field[130] used in the PTX-TB structure refinement utilized torsional parameters for the two angles in question that were not fully optimized. Nonetheless, the small 6—14° ϕ-angle variations do not alter the fundamental nature of the T-Taxol conformation. The differences are readily accommodated by the realization that small torsional angle variations correspond to ambient vibration about the corresponding energy minima. Figure 17a depicts the spatial consequences for the C-3' phenyl rings across the range of

angles with $\Delta\phi$ = 6—14°. Again, even the somewhat deviant 1JFF-PTX structure appears to be a closely related member of the T-taxoid family. A larger alteration in the later angle (ϕ_2) of 20°, with a slight change of 3° in the former (ϕ_1), results in the same dihedral angles as T-Taxol (iii), readily placing 1JFF-PTX in the T-Taxol shape.

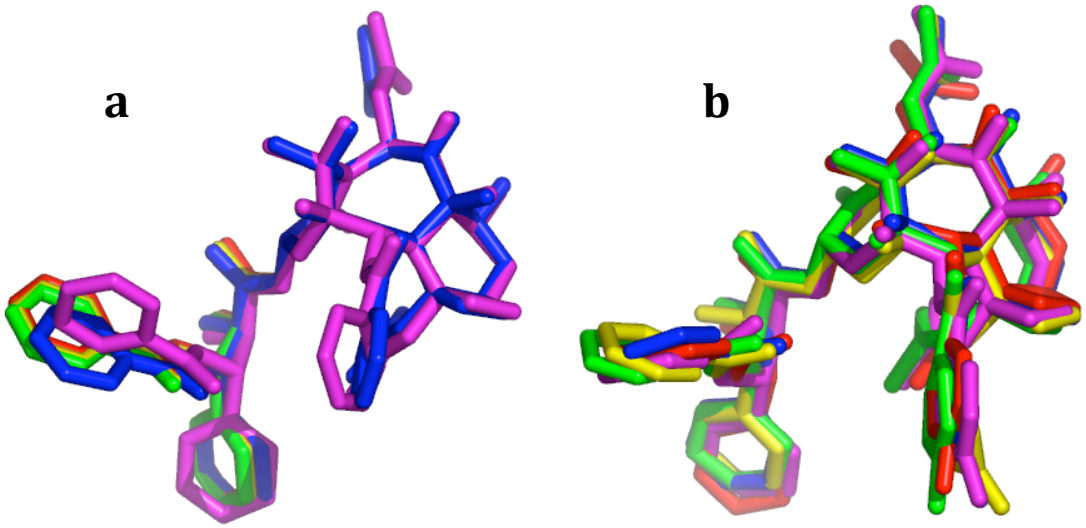

Figure 17. The spatial disposition of the C-3' terminal phenyl groups from superimposing the baccatin cores of various T-Taxol forms: (a) T-Taxol (blue), 1JFF-PTX (magenta) and the torsion angle variants (i)-(iii) (red, green and yellow) from **Figure 9**; (b) snapshots from the MD trajectory of **6** in the β-tubulin binding pocket.

Molecular Dynamics of T-Taxol in β-Tubulin. After a ligand has bound to its protein target, many degrees of freedom available to it in solution are lost and the structure becomes more static. This does not, however, mean that no movement is present within bound compounds. Thermal motion is always present, allowing for small changes in positions and torsion angles within the ligand, the protein and between the two. Therefore, we adopted a dynamic approach to learn how thermal

motion at room temperature might alter the F—C separations when 2-FB-PT (**6**) is bound to β-tubulin. Since His227 is believed to be in intimate association with the bound drug, we treated the imidazole ring in both its neutral and protonated states. The corresponding PTX-TB complexes were subjected to MD for 5 ps at 300 K with the Tripos force field,[131] during which time the F—C-5' and F—C-3' separations were constantly monitored. For neutral His227, the F—C distances fell in the 8.3—9.8 and 8.7—10.3 Å ranges, respectively. For the protonated side chain, the values oscillated more broadly between 6.8—10.2 and 7.5—10.2 Å. The Tripos force field, like AMBER, delivers values at the low end of the 268 K REDOR error boundaries. To illustrate the relationship with the static T-forms depicted in Figure 17a, the corresponding view for snapshots of **6** across the His227-neutral trajectory are shown in Figure 17b. Qualitatively, the conformational fluctuations are very similar.

Apart from the actual numerical values of the REDOR-determined distances, the present case is an illustration of the important fact that molecular structures above absolute zero are not static entities. Whether internal or external to a protein, small molecules are in constant motion, oscillating around the values measured by structural analyses. The degree to which they experience motion is related to both the temperature and medium employed for the measurements. An illustrative study in this respect examined a DMSO solvate of 10-deacetylbaccatin III (**2**) by ^{13}C NMR in the solid state.[117] Varying the temperature from 23 to –120 °C resulted in a strong chemical-shift dependence for the aromatic ring carbons of the C-2 benzoyl group. The changes were interpreted as a result of molecular motion causing the conjugated C=O and the phenyl groups to significantly deviate from

planarity. The baccatin III work suggests that movement within the C-2 center of **6**, which contains the fluorine label, may be significant. This is of interest because molecular motions of labeled atoms can reduce dipolar interactions resulting in apparent overestimation of internuclear distances.[132] Reduction of the reported REDOR distances by less than 0.5 Å would readily accommodate both T-Taxol and the polar conformation.

An important detail about the T-Taxol conformation is that it is *not* a static structure but a representation of the bound conformation of PTX. Slight variations in torsions may change certain physical properties, such as the distances between atoms or ring centroids, but still maintain the overall molecular shape and volume of the 3-D structure. This can be especially seen with 1JFF-PTX; it is not an ideal T-Taxol structure, but its overall shape accommodates the same spatial features in the protein and slight adjustments of different torsions brings it closer to the published values for the former.

Taxane Analogs

All bioactive proposals must be consistent with the biophysical properties of other taxane analogs. Each conformation must explain the significant PTX SAR data that is readily available.[27,48-56] To address this, we considered docetaxel, nonataxel and a number of bridged compounds to distinguish between the abilities of T-Taxol and PTX-NY to explain their activities.

Docetaxel and Nonataxel. Docetaxel (DTX, **3**), as discussed above, is an FDA-approved chemotherapeutic agent used in the treatment of advanced or metastatic breast cancer as well as others. Its X-ray structure[38] was used as a

placeholder in the original EC structure of PTX-TB (1TUB).[61,71-73] It is twice as effective as PTX at stabilizing microtubules and killing murine P388 leukemic cells.[133] Nonataxel (NTX, **7**) is a nonaromatic taxane derivative that is 2-7 fold more cytotoxic than PTX in a number of cell lines.[70] The collapsed form of this compound was very popular as a template[26] for an abandoned common pharmacaphore binding model for the taxane pocket. Both DTX and NTX differ structurally from PTX in replacing the benzamido side chain phenyl with the O-*tert*-butyl moiety. In addition, NTX employs isobutenyl instead of the phenyl functionality at C-2 and C-3' (Figure 18).

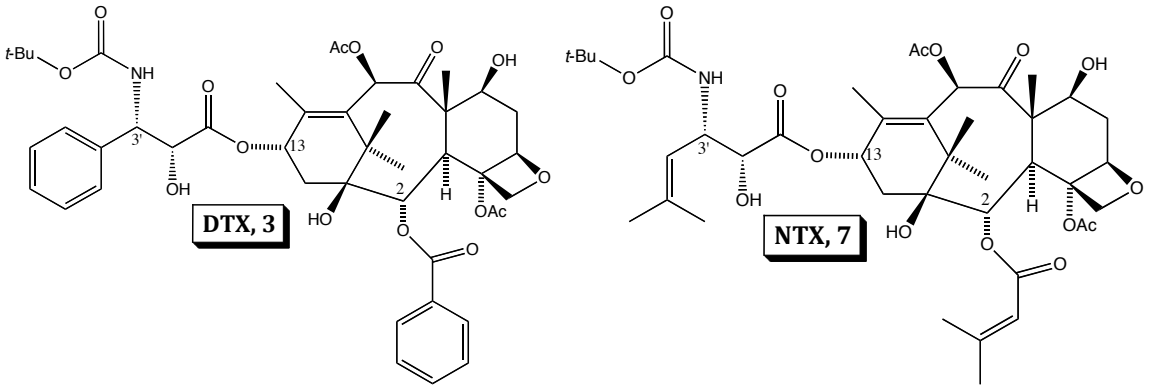

Figure 18. Docetaxel (DTX, **3**) and nonataxel (NTX, **7**) are both slightly more active than the parent PTX (**1**).

Given the different steric requirements for the hydrophobic termini at C-2 and C-3' for **1**, **3** and **7**, we decided to examine the relative disposition of the analogs in the binding site associated with T-Taxol (Figure 8).[84] The latter two structures were modified from the T-form of PTX and docked into tubulin by superimposing the baccatin cores. Each model was subjected to cold MD (20 K) with the backbone held in a fixed position to remove short ligand-protein contacts and optimized with

the Tripos force field.[100,131] Figure 19a illustrates overlap of the three structures in the T-conformation within the tubulin taxane binding pocket. Each structure resides comfortably in the site and shows no evidence of high-energy contacts with the protein. However, Figure 19b, depicting the overlapped NH—C(O)-R moieties for **1** and **3**, shows that both the phenyl and O-*t*-Bu groups, respectively, are in van der Waals contact with the CH_2 of the Asp26 side chain. The geometry around the carbamate oxygen atoms in both DTX and NTX positions the amide groups to permit a hydrogen bond between one of the Asp carboxylate oxygens and NH (1.8 Å). However, the shorter connector and less flexible C-3' benzamido group for Taxol leads to an AspCOO—HN distance of 4.2 Å, short enough to sustain a productive electrostatic interaction but too long to qualify as a hydrogen bond. The more favorable interaction could well be the source of the 2—7-fold increase in activity in DTX and NTX in comparison with that in PTX.

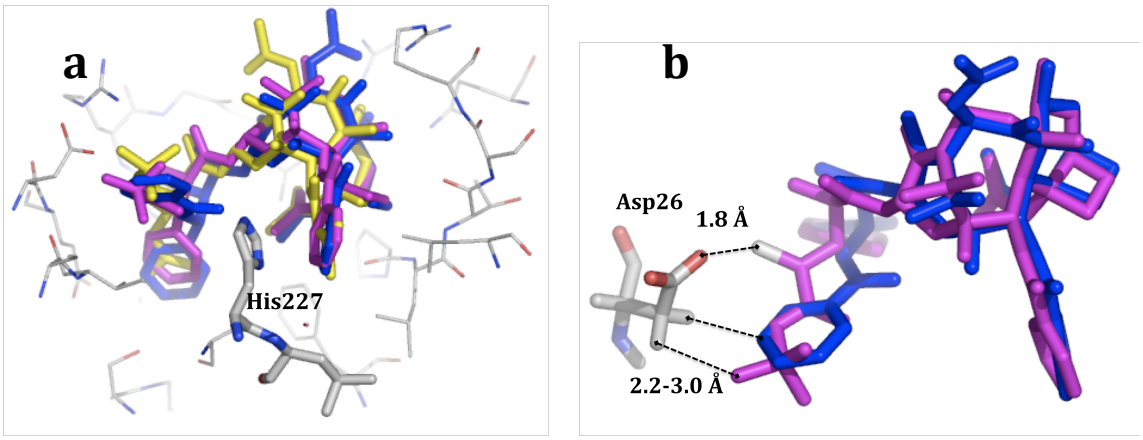

Figure 19. (a) Superposition of PTX (**1**, blue), DTX (**3**, magenta) and NTX (**7**, yellow) in the T-Taxol-tubulin binding site showing residue His227 sandwiched between the C-2 Ph and C-3' substituents. (b) The spatial relationship of PTX and DTX with Asp26: both C-3' side chains experience van der Waals contact with the residue with H---H distances ranging from 2.2 to 3.0 Å, but DTX makes a productive N-H---O hydrogen bond with the carboxylate (1.8 Å), whereas PTX does not (4.2 Å).

A related analysis in a Taxol-resistant epidermoid tumor line with the acquired Asp26Glu mutation likewise employs the T-Taxol model to explain the PTX versus DTX-resistance profile in the resistant cells.[95] Again, the DTX NH has been proposed to form a strong hydrogen bond to the Glu carboxylate, whereas PTX is prevented from doing so by steric congestion.

Bridged Taxanes. Four research teams have prepared a wide range of bridged PTX analogs based on several conformational themes in an attempt to lock the molecules into the actual binding conformation.[26,69,74-76,134-136] The only design approach that has been able to match and surpass the biological action of parent PTX **1** in both cytotoxicity and *in vitro* microtubule assembly assays is that based on

the T-Taxol conformation.[96,136] In this conformer, a short separation of 3—4 Å between the methyl of the C-4 acetyl group and the *ortho* position of the C-3' Ph (Figure 8) suggested that short bridges between these centers would constrain the molecule largely to the T-taxane shape. A generic representation of the bridged series is given by **8**, while **9** (C-2 *para*-X = H) exemplifies a structure with at least a 20-fold greater potency than PTX in the A2780 ovarian cancer cell line and a 2-fold greater effect in the microtubule assembly assay (Figure 20).[96]

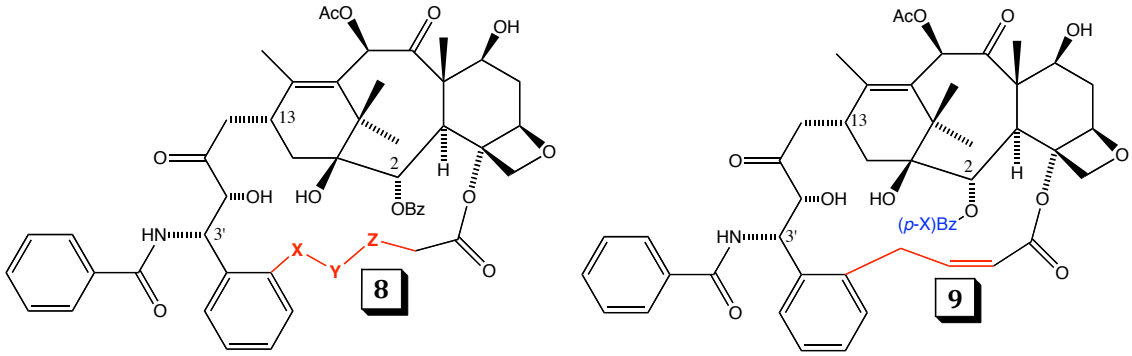

Figure 20. A generic representation (**8**) of a bridged series of analogs that enforce the T-shape and a specific example (**9**) with a 20-fold greater potency than PTX.

Conformational analysis for **9** (C-2 *para*-X = H), employing the MMFF94s force field[83,110-112] yielded 93 conformers, 12 of which fall into the T-family by the measure of the distances between the centroids of the C-2 and C-3' phenyl rings (see **Methods *Conformational Searches***). The C-2 benzoyl phenyl was supplemented with a *p*-F atom and the F—C-3' and F—C-5' distances that were measured ranged from 8.8 to 9.8 and 7.4 to 10.0 Å, respectively. These values average to approximately 1 Å lower than the REDOR distances (Figure 9).[62] A more specific measure for the T-form is the distances between the centroids of the C-2 benzoyl phenyl ring and the C-3' phenyl and C-3' benzamido phenyl rings. Unlike the C-3'

and C-5' centers with the potential to rotate within the van der Waals surface boundaries of the bound taxane ligand, these three rings are in direct contact with the protein amino acid side chains composing the binding pocket. Not a single example of PTX-NY was found among the 93 conformers of **9**.

As mentioned above in connection with Figure 16, the REDOR distances tolerate a wide variation in the positions of the two terminal C-3' phenyl groups. The reverse situation appears to be mutual. Namely, the terminal phenyl rings in taxane derivatives can be located in T-form locations although permitting a range of C—F distances. Four of the *p*-fluorinated C-2 Ph conformers of **9** (C-2 *para*-X = F) were docked into β-tubulin and, although displaying shorter C—F separations within the van der Waals volume of the molecule, they nonetheless sustain phenyl centroid—centroid distances very similar to those of T-Taxol (9.4 ± 0.1 and 10.0 ± 0.3).[84] Figure 21 illustrates one of the four conformations in the tubulin-taxane pocket following an extensive MD treatment superimposed on the EC structure of PTX[84] in the same pocket. This highly active and constrained T-taxoid PTX analog (**9**) (C-2 *para*-X = F) does not appear to place its C-3' phenyl rings precisely in the same locations as those of PTX. The rather broad hydrophobic cleft is tolerant of small phenyl displacements along this wall as suggested by the molecular dynamics portrait in Figure 17b and by the lack of significant side chain displacement from PTX to **9** (C-2 *para*-X = F) (Figure 21). The same does not appear to be true along the floor of the pocket when a longer bridge falls outside the parent Taxol molecular volume.[53]

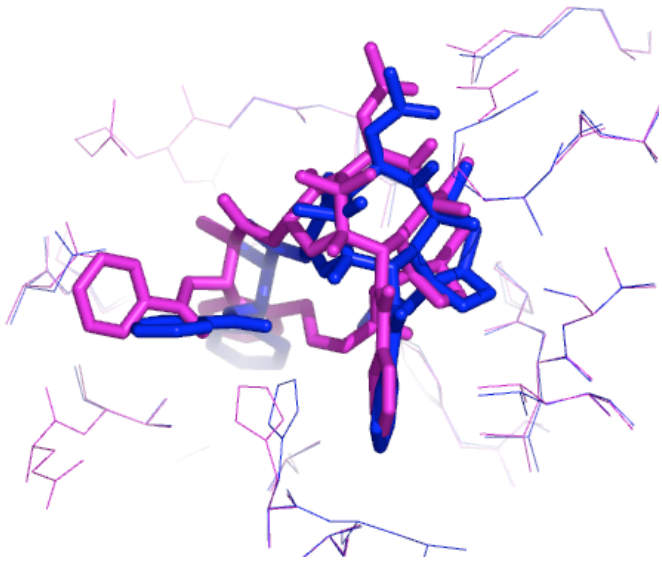

Figure 21. T-Taxol conformation of C-4 to C-3' bridged taxane (**9**, C-2 *para*-X = F) docked into the β-tubulin taxane binding site and subjected to MD (magenta). The EC structure of PTX is shown in blue. The surrounding side chains show little change between the structures.

In support of these ideas, a report by Dubois and co-workers implemented a taxoid design based on bridging between the C-2 benzoyl phenyl group and an alkyl replacement of the C-3' benzamido moiety.[135] Most of the compounds were found to be inactive, but the tubulin polymerization assay ranked one as effective as PTX, although the compound fell considerably short of PTX in the cytotoxicity assays. The authors interpreted the results as confirmatory of the T-conformer, demonstrating in their docking study that the analog obtains the T-form with the long bridge (n = 7) organized around His227.

In the spirit of the T-Taxol design study,[96] the Ojima group measured short distances between the C-4 acetyl methyl and the C-2' carbon and between the C-14 center and the C-3' benzamido phenyl. The analysis led reasonably to the design of

structures **10** and **11** (Figure 22), respectively, which bridge the model's contiguous centers. The compounds were prepared and tested against a variety of cell lines and subjected to the microtubule stabilization assay. Compound **10**, with a bridging point from the C-4 acetyl methyl similar to **8** and **9** (Figure 20) and the C-13 side chain of DTX (**3**), proved to be completely inactive. In contrast, the C-14 to C-3' analog **11** was shown to be as effective as PTX in inhibiting tubulin depolymerization, although in several breast and colon cancer cell lines it is 4—20-fold less cytotoxic than the parent drug.

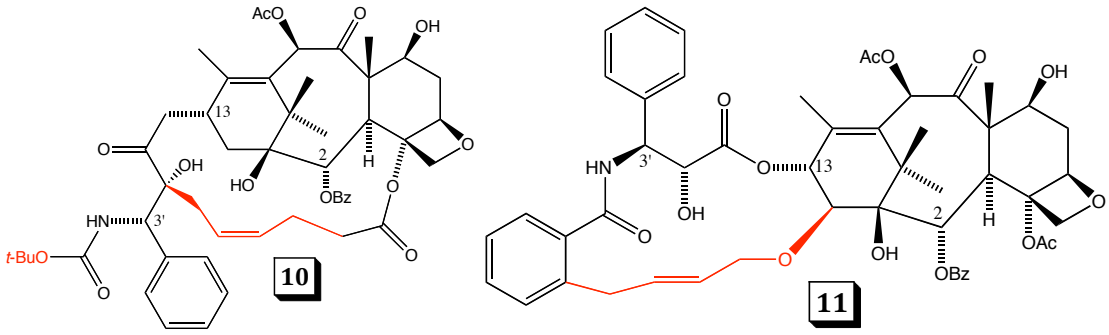

Figure 22. Ojima and co-workers designed macrocyclic taxanes **10** and **11** to constrain PTX in their proposed conformation.[92]

The authors submit the effective analog (**11**) as supportive of their bioactive proposal, PTX-NY (Figure 10), while at the same time dismissing T-Taxol, which has led to the design of highly active molecules (**8** and **9,** Figure 20).[96,136] In an effort to analyze the New York construct, we performed a 5000 step LMMC conformational search for the 15-membered ring of **11** that encompasses both the C-13 side chain and the C-14 to C-3' benzamido bridge. The resulting conformational pool contains 105 structures, 28 of which sustain the T-Taxol geometry. One of these was docked into the taxane site of β-tubulin and subjected to a series of MD steps at 20 K to

remove unfavorable steric contacts. The simulation was continued at 350 K for 5 ps to model the behavior of compound **11** in the protein.[100]

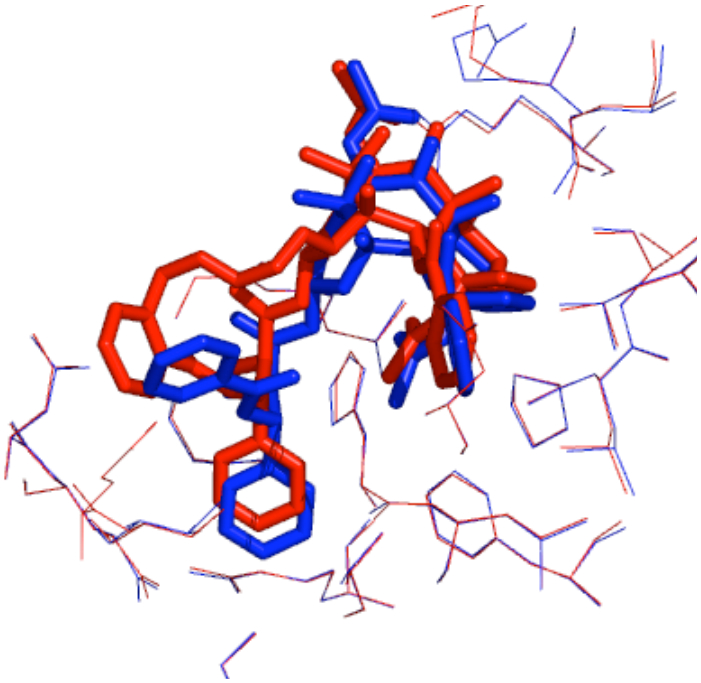

Figure 23. Superposition of β-tubulins from the optimized protein-ligand complexes containing T-Taxol (blue) and bridged **11** (red). The active-site side chains show little change, whereas **11** is seated a little higher than T-Taxol in the binding pocket.

As is evident from Figure 23, the side chains of the protein around the binding pocket, colored red and blue, change very little. Compound **11** is seated almost identically to T-Taxol with the exception that the linker relocates the C3' benzamide group somewhat less deep in the pocket. And as observed for bridged **9**, the C-3' phenyl rings are shifted somewhat from those of PTX. Nonetheless, **11** displays distances between the centroid of the C2 benzoyl phenyl and the C-13 terminal phenyls very similar to those found for T-Taxol in the EC-refined model (C-

3’ benzamido Ph: 10.0 vs 9.4 Å; C-3’ Ph: 9.6 vs 10.0 Å).[84] A characteristic feature of the complex is that the C-2’ OH group is associated with the backbone NH of Gly368 as it is in the EC model. This contrasts with a proposed reorientation of the OH functionality in PTX-NY.[92] Clearly, the distribution of forms represented by the structures in Figure 17 is accessible to bridged taxanes with very similar but non-identical spatial requirements.

Finally, we have addressed the idea of constrained analogs in a slightly different way.[100] As mentioned above, the T-Taxol conformer has been used to design highly active taxane analogs with short bridges as a result of H—H distances measured at 2.5—2.9 Å between the C-4 acetate methyl group and the *ortho* position of the C-3’ phenyl. For example, compound **12**, incorporating a two carbon tether between these centers, is 2—13-fold more cytotoxic than PTX depending on cell line and 5-fold as effective in the tubulin aggregation assay.[96] We wondered if the New York proposal was predictive of this taxane modification. The corresponding H—H separations in the MD-optimized structure (Figure 12) were measured to be 3.5—5.3 Å. Although these quantities might possibly motivate bridging between the two centers in question, an inspection of PTX-NY reveals that the location of C-2’ OH group would interfere with such a bridge. To test this idea, we converted the New York conformer shown in Figure 10 into **12** and optimized its geometry in both the unbound and bound state (see **Methods**). As expected, the structure experiences conformational reorganization around the C-13 side chain to avoid a steric clash with the built in bridge. Superposition of the PTX-NY conformation (green) and the corresponding tethered, optimized variant (magenta)

depicted in Figure 24a shows that both the C-3' OH's (red arrow) and the C-3' phenyl groups experience serious displacement.

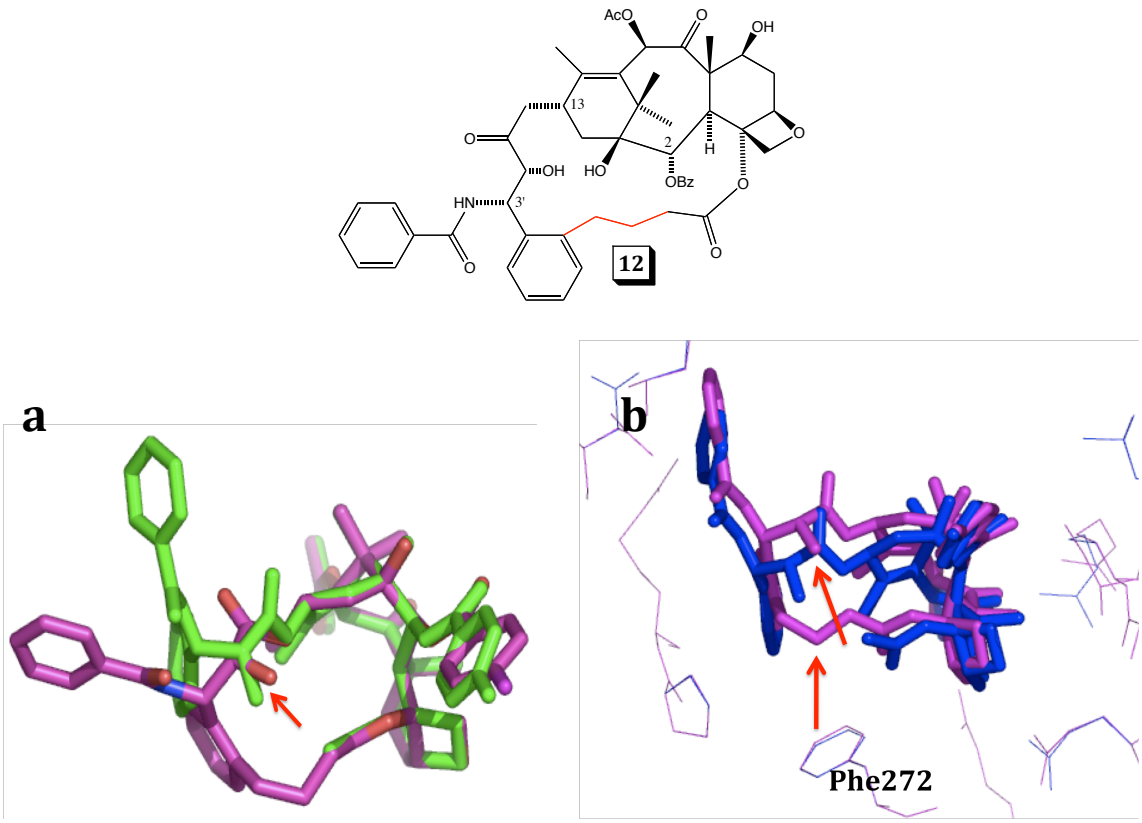

Figure 24. (a) Superposition of PTX-NY shown in **Figure 10** (green) and the same conformer enhanced with a two-carbon bridge as shown in **12** followed by optimization (magenta). The arrow marks the location of the two C-2' OH groups. (b) Superposition of the PTX-NY complex in **Figure 11** (blue) and the MD optimized structure of **12** in the PTX-NY conformation (magenta). Red arrows indicate the movement of the C-2' OH of the bridged analog and the displacement of the structure due to a clash of the bridge with Phe272.

Whereas protein-free optimization of the bridged species caused a major conformational reorganization, the rather tight binding site captures the structure in a less reorganized form (Figure 24b, magenta). Nonetheless, the ligand still attempts to relieve strain by uncoiling. The red arrows in Figure 24b illustrate the torquing of the C-2' C-OH group in response to the steric encumbrance. Equally important, the path of the bridge in the New York form runs beneath the baccatin core and is directed toward the deep hydrophobic cleft of the protein. Consequently, this conformation encounters an unfavorable steric contact with Phe272, pushing it further out of the pocket in comparison with the unbridged form. As was previously shown in a report from this lab, a bridge—Phe272 interaction of this type leads to reduced activity for the corresponding taxanes.[53] Accordingly, the New York conformation in complex with tubulin cannot account for the superior activity of the analogs of **8**.

T-Taxol Inspired REDOR Experiment

As with the use of T-Taxol to derive highly active bridged taxanes, the conformation was used to inspire a new REDOR experiment.[137] The previous study, with labeled PTX **6** did not provide information on the spatial separation of the C-4 acetate methyl group and atoms or groups located in the C-13 side chain. In collaboration with the Jake Schaefer group, this consideration led to the design of two labeled PTX analogs (**13** and **14**, Figure 25). Ligand **13** was particularly attractive, since in principle it allows the determination of two key distances; namely, between the C-4 acetate and the C-2 benzoate and between the C-2 benzoate and the C-3' Ph. Ligand **14** was designed to allow a direct measurement of

the distance between the C-4 acetate and the C-3' Ph. Both compounds were tested for their tubulin assembly activity: **13** was found to be about 2-fold less active than PTX, while **14** showed similar activity to the parent drug. When tested for cytotoxicity in the A2780 ovarian cancer line, **13** showed more than 2 orders of magnitude less cytotoxicity. Compound **14** was found to be comparable to PTX.

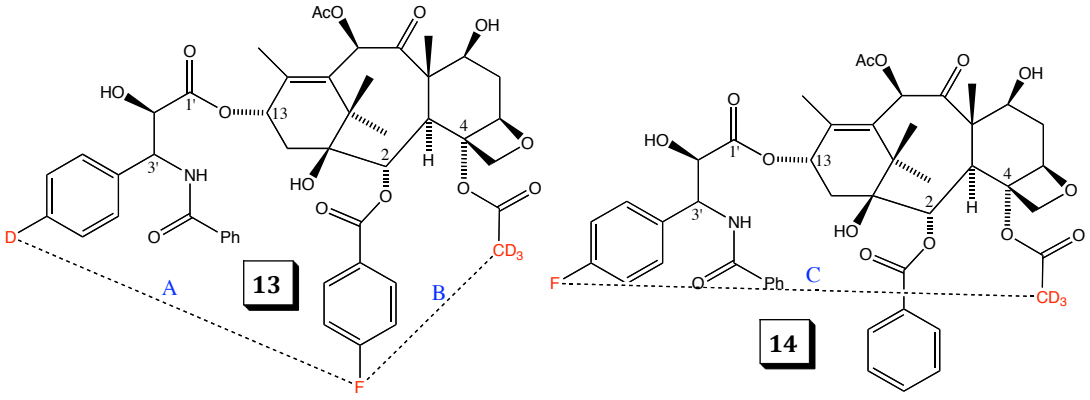

Conformer	R_A, Å (C2-F---Ph-D)	R_B, Å (C2-F---CD_3)	R_C, Å (C3'-F---CD_3)
REDOR	> 8	7.8	6.3
Polar	4.5	7.4	5.5
1JFF	11.6	6.5	7.2
T-Taxol	12.2	7.9	6.6
PTX-NY	13.1	7.3	6.4

Figure 25. PTX analogs **13** and **14** were designed to measure specific distances (A, B, and C) that distinguish between the T-Taxol conformation and other proposals.

Schaefer's group performed the REDOR experiment on both compounds for 64-rotor cycles. They accumulated 640,000 scans and determined the distances to be 7.8 Å and 6.3 Å between the C-4 deuterated acetate methyl and the two fluorinated groups: C-2 labeled benzoate and C-3' labeled phenyl (B and C in Figure 25, respectively. The error was again calculated to be ± 0.5 Å. Due to technical

reasons, the lower boundary of distance A could not be determined, but they confidently concluded that the C-2 F---C-4 CD_3 distance is greater than 8 Å.[137]

As can be seen in the table in Figure 25 the polar conformation lies 0.3 Å outside the error range of the C-3' F---C-4 CD_3 distance, but this does not fully disqualify it, for the reasons discussed above that detail the need for a broader error estimate. It is the C-2 F---Ph-D distance that truly excludes this conformation as a potential bioactive form. The greater than 8 Å gap corroborates the need for an extended conformation in the taxane binding pocket. The other three conformations discussed (T-Taxol, 1JFF-PTX and PTX-NY) present this requirement. 1JFF-PTX again fails to match the REDOR distances, falling outside the reported distances by 1.3 and 1.1 Å for B and C in Figure 25. Unfortunately, the new REDOR distances cannot distinguish between T-Taxol and PTX-NY. The former matches the measured distances more closely, 7.9 to 7.8 Å for B and 6.6 to 6.3 Å for C, but PTX-NY falls within the ± 0.5 Å error for both.

Our analysis of the PTX-NY conformation had, up to this point, been done with a model reconstructed from the published torsions[92]. Professor Ojima kindly provided the original coordinates after our original publications[100,101] and we compared the two structures to verify that our results were valid. Figure 26 shows the original PTX-NY (green) overlaid on the reconstructed version (rust) by a five-point atom—atom superposition (C-2, C-11, C-13, C-15 and C-3'). The terminal phenyl rings are offset somewhat, particularly at C-2, but the conformation of PTX-NY is faithfully reproduced from C-1' to C-3' as highlighted by the circled atoms in Figure 26. As a result, the previous comparisons of the conformations[100,101] detailed

above are completely valid, including the EC density omit and difference maps (Figure 11, Figure 12 and Figure 13) which eliminate the New York proposal as the bioactive conformation of PTX.

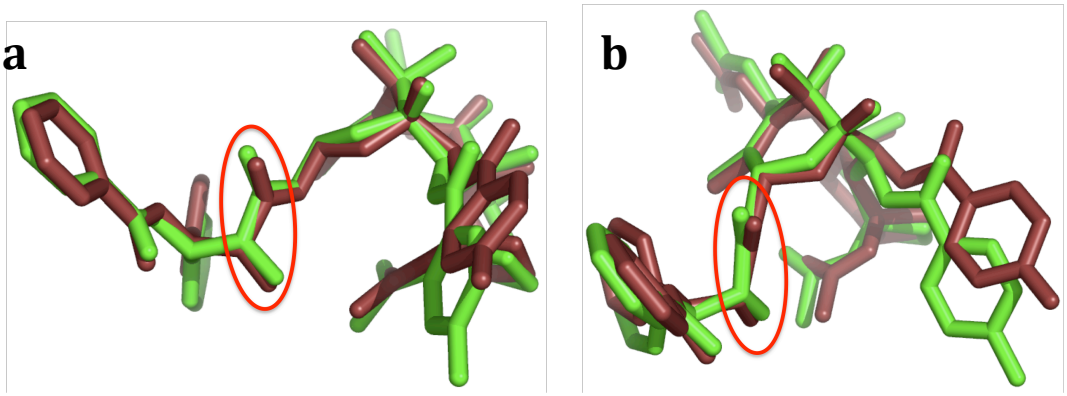

Figure 26. PTX-NY (green)[92] and our reconstructed version (rust) superposed and with key oxygens at C-1' and C-2' encircled in red.

In the comparison of our reconstructed version of PTX-NY to the one provided by Professor Ojima, a spatial discrepancy of the C-2 phenyl rings troubled us. The distances from the original REDOR experiment,[62] as well as two of the three from the more recent one,[137] involve measurement from a fluorine atom at the para position of the C-2 benzoyl phenyl to other atoms in the taxane structure. Accurate atomic separations in a given structure require that the fluorine is correctly located relative to other atoms in the molecule. We decided to examine which of the two structures in Figure 26 was responsible for the visual discrepancy and try to understand the origin of the difference. As standards, we selected the X-ray structures of PTX[58] and DTX.[38] These were supplemented with *para*-F atoms and superposed, along with T-Taxol, by aligning the baccatin cores (i.e., atoms C-2, C-11, C-13 and C-15). Figure 27a shows that, in all three cases, the C-2 ester group and

the pendent phenyl rings overlap well; the three fluorines cluster within the red sphere with a radius of 1.1 Å.

The identical superposition of PTX-NY is shown in Figure 27b. It would appear that, while the remainder of the PTX molecule is reasonably optimized, the C-2 side chain in PTX-NY is at odds with the experimental structures. The origin of the displacement is captured in Figure 28. While the T-Taxol geometry around C-2 is very similar to the experimental structures, PTX-NY exhibits a distortion characterized by a flattening of the C-2 tetrahedral geometry (d = 0.41 Å) and by an expansion of all three measured bond angles, but especially of θ_3 to 131°. These distortions all work together to displace the C-2 side chain toward the concave face of the baccatin core, as illustrated by Figure 26 and Figure 27b. The implication is that, while the PTX-NY structure closely matches the REDOR distances from the second experiment (Figure 25), the match is fortuitous and dependent on an incorrectly optimized C-2 geometry that deviates significantly from experiment.

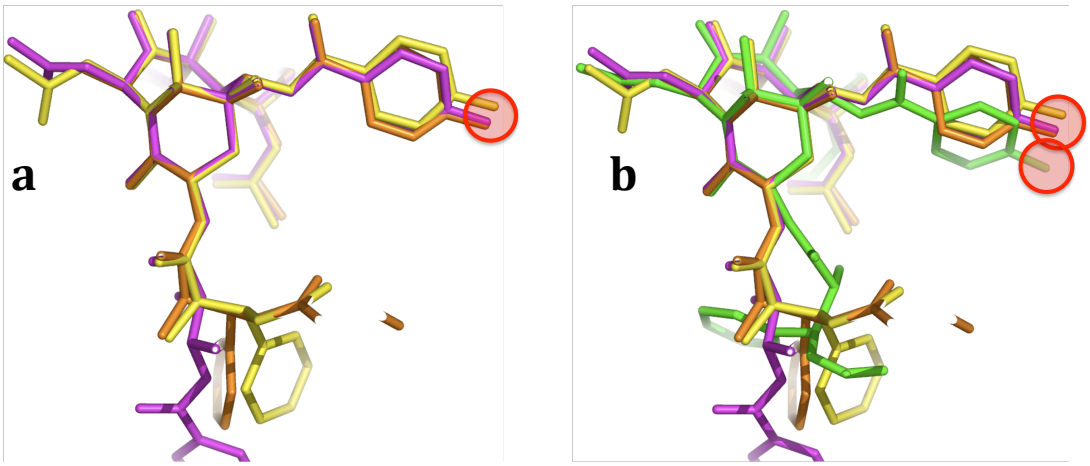

Figure 27. Superposition of the baccatin cores of (a) PTX crystal structure (magenta), DTX (orange) and T-Taxol (yellow), as well as (b) PTX-NY (green). The fluorines are encased in red spheres to emphasize the spatial similarities and differences.

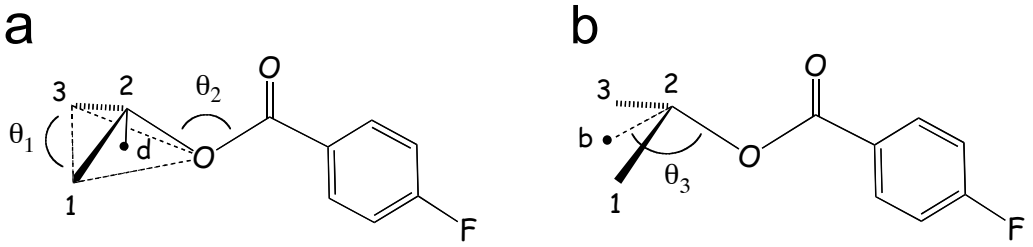

	θ_1 (°)	θ_2 (°)	θ_3 (°)	d (Å)
PTX X-ray	117.4	119.6	123.5	0.49
DTX X-ray	117.3	119.6	121.7	0.50
T-Taxol	119.1	119.1	123.9	0.48
PTX-NY	125.3	123.1	130.6	0.41

Figure 28. Geometry around C-2 in the PTX baccatin core: bond angles θ_1 (C-1—C-2—C-3), θ_2 (C-2—O—C(O)) and θ_3. The latter measures from the bisector (b) of C-1 and C-3 to the ester O (i.e., (b—C-2—O)). Variable d corresponds to the distance from C-2 to the centroid of C-1, C-3 and O.

Summary and Conclusions

A number of biophysical techniques have been used to understand the 3-D shape of PTX in the taxane binding pocket of tubulin. Two important and highly cited studies are those using REDOR solid-state NMR[62,137] and electron crystallography (EC). The latter initially resulted in an insufficiently resolved structure[61] that could not define the conformation of PTX, but further refinement led to 1JFF-PTX (Figure 11b, yellow).[90] It was the combination of the EC density with solution NMR data that resulted in T-Taxol (Figure 8),[84] a conformation that agrees with the available experimental data and has predicted highly active analogs.[96]

The earlier REDOR study[62] provided two intramolecular ^{13}C—^{19}F ligand distances of 9.8 and 10.3 Å for PTX (Figure 9). They were initially associated with an uncertainty of ± 0.5 Å and are characterized by several noteworthy features as they pertain to PTX conformation. First, the corresponding T-Taxol conformer values differ by 0.7 and 0.4 Å, respectively, the first difference falling outside the original error estimate by 0.2 Å. One interpretation of the discrepancy can be traced to two torsions in the C-13 side chain. Alteration of both by a diminutive 6° restores perfect agreement with the measurement (T-Taxol (iii), Figure 9). Second, a reconsideration of the signal-to-noise in the $\Delta S/S_0$ ratio yields a 6.7% uncertainty in the distances leading to a ± 0.7 Å rather than an error value of ± 0.5 Å. This places the published distances of both T-Taxol and the polar PTX conformation within the expanded error boundaries. Third, in view of the fact that data analysis of the

resource-expensive REDOR experiment relied on a single measurement, the ± 0.7 Å window would appear to be too conservative.

Of equal importance is the fact that the solid-state measurements monitor intramolecular atomic separations deep within the molecular volume of bound PTX. Conformational searches show that the REDOR distances can be maintained by a variety of conformations with a wide spatial dispersion of the C-3' phenyl rings (Figure 16a), which are groups that are in contact with the protein side chains when the molecule is bound. A better measure of the overall shape of the bioactive conformation of PTX would seem to be distances between the centroids of the terminal C-2 and C-3' aromatic rings (Figure 8), though even these are not absolute quantities. In the protein, MD suggests the presence of a distribution of forms near room temperature (Figure 17b) oscillating around the REDOR-measured distances. The single-point measurements (Figure 14 and Figure 15)[62] cannot differentiate between them. Although the taxane binding site is reasonably well defined, it nonetheless accommodates certain small variations in the placement of the ligand's hydrophobic groups at the molecular periphery. Thus, variations in the location of C-3' phenyl rings along the wall of the taxane binding pocked are tolerated for both super active and moderately active bridged PTX analogs (e.g. **9** and **11**, respectively) by comparison with PTX (Figure 21 and Figure 23). These observations are also consistent with the proposal that the biological properties of DTX (**3**) and NTX (**7**) are readily accommodated by the T-conformation (Figure 19). The T-Taxol model *cannot* be regarded as a structure characterized by an immutable set of intramolecular distance relationships.

Another important point is that any proposal of a bioactive conformation *must* strive, at a minimum, to be consistent with the array of data encompassing biophysical measures, biological outcomes and the constraints imposed by super-active bridged analogs. As detailed by our work, T-Taxol[84] is the only published conformation that attains all these constraints. T-Taxol is compatible with REDOR-derived intramolecular distances[62] (Figure 9) and fits the available EC density (Figure 11a);[61] 1JFF-PTX does not do the former and the polar and PTX-NY conformations do not do the latter. Crucially, the model has led to the design and synthesis of bridged PTX analogs that match and surpass the bioactivity of paclitaxel itself (**8** and **9**; Figure 20 and Figure 21).[96,135] Constrained analogs based on the polar conformation are inactive and sometimes do not even compete for the taxane binding pocket.[69] While the C-13 variant, PTX-NY, does have the power to suggest reasonably active alternative bridged structures (**11**; Figure 22),[92] the compounds readily obtain the T-Taxol form (Figure 23). Finally, T-Taxol was used to design a new REDOR experiment[137] that resulted in measured distances (Figure 25) fully compatible with the proposal.

In more recent work performed by a colleague in our laboratory, molecular mechanics and quantum chemical methods were used to reveal that PTX-NY is less stable than T-Taxol, on average by 10-11 kcal/mol.[138] Docking of various PTX conformers into the EC binding site of tubulin demonstrates that PTX-NY cannot be accommodated unless the pocket is reorganized. In the structure provided by Professor Ojima, the short loop connecting strands B9 and B10 in tubulin has moved into the binding site, displacing the backbone residue atoms by 2 to 4 Å. This

pushes the ligand in the direction of the M loop on the opposite side of the binding site. In turn, the M-loop is remodeled by as much as 7.5 Å relative to the experimental structure (backbone atom displacements range from 2 to 7.5 Å). However, the most severe dislocation of tubulin in the structure is the unraveling of Helix 1. This reorganized pocket is not compatible with the original EC density of the protein.[61,90] Along with the distorted geometry around C-2 of PTX-NY (Figure 27 and Figure 28), this demonstrates the troubling lack of attention devoted to assuring that the structures are compatible with experimental values and data by the Stony Brook group. The proposed bioactive structure does not reside among low-energy conformers while T-Taxol was selected from two dozen experimental conformations within 2 to 3 kcal/mol of either solid-state or solution global minima.

Overall, T-Taxol has repeatedly proven to be consistent with experimental data of all forms and should not be excluded from contention for the bioactive form when other proposals are almost fully "virtual" in nature, 10 kcal/mol higher in energy and incompatible with the EC density. In the next chapter I discuss the use of the T-Taxol form to analyze and direct the research of new analogs.

CHAPTER THREE

Making predictions is difficult, especially about the future.

Neils Bohr

In the previous chapter I discussed the different proposals for the bioactive conformation of PTX (1, Figure 3) and demonstrated how T-Taxol is the only form that is compatible with all the available experimental data, including both biophysical properties and biological measures. I continue here by discussing how we have used the T-Taxol conformer to analyze new SAR data and direct research, especially in the generation of constrained and simplified analogs.

Design of Constrained Analogs

Before T-Taxol, the different proposals for the bioactive conformation of PTX inspired a number of elegant synthetic studies designed to generate constrained analogs that maintain these conformations (Figure 7).[69] However, none of the constrained analogs synthesized yielded analogs with both tubulin polymerization and cytotoxicity activities equal to or greater than those of PTX itself.[26,69,74-76,134,135]

After determination of T-Taxol as the bioactive form of PTX,[84] a similar study to those described above ensued through an on-going collaboration between our group and those of David G. I. Kingston at Virginia Polytechnic Institute and State University and Susan L. Bane at SUNY Binghamton. Examination of the T-shape shows that the C-3' phenyl and C-4 acetate moieties are juxtaposed (Figure 29). The distances between the *o*- and *m*-phenyl hydrogens and the methyl hydrogens are only 2.5-2.9 Å and 4.3-4.9 Å, respectively. The co-authors hypothesized that if the T-Taxol model accurately reflects the PTX-TB interaction, conformationally constrained analogs which maintain this juxtaposition would yield PTX analogs with improved tubulin binding properties.[53,96,136,139] Constraining the molecule would

greatly reduce the entropic penalty resulting from binding, thus demonstrating higher bioactivity than the parent compound PTX.

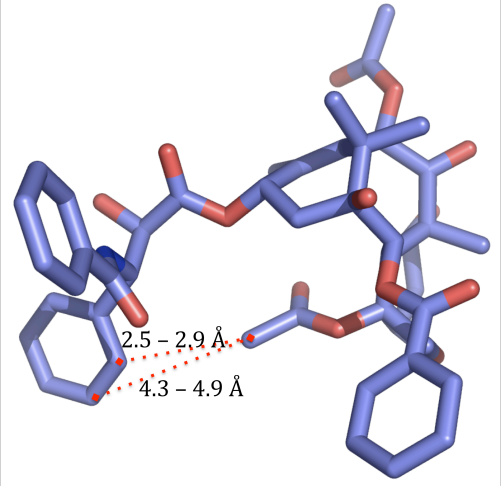

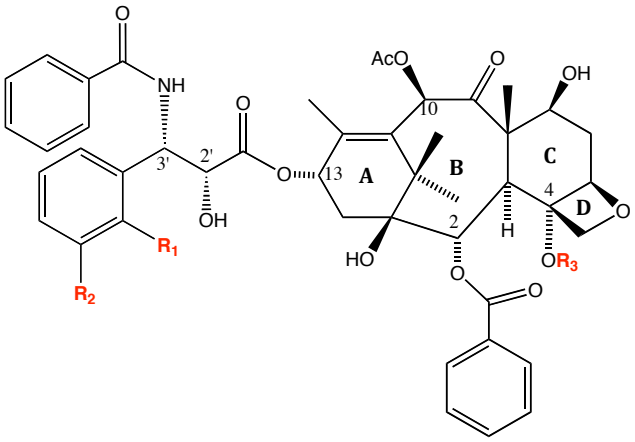

Derivatives	R_1	R_2—R_3
15	H	*Z*-CH=CH$(CH_2)_2$CO
16	H	*Z*-OCH_2CH=CH$(CH_2)_2$CO

Derivatives	R_1—R_3	R_2
9	*Z*-CH_2CH=CHCO	H
12	$(CH_2)_3$CO	H
17	*E*-CH=CHCH_2CO	H
18	*E*-OCH_2CH=CHCO	H
19	O$(CH_2)_3$CO	H

Figure 29. Depiction of T-Taxol with emphasis on the distances between the C-4 methyl hydrogens and the *ortho* and *meta* hydrogens of the C-3' phenyl, as well as, some of the structures developed to take advantage of this juxtaposition.

The initial strategy resulted in the design of compounds **15** and **16** with 3 and 5 atom linkers, respectively, connecting the C-4 methyl acetate to the *meta* position on the C-3' phenyl.[53] These analogs exhibited modest cytotoxicity against

the A2780 ovarian cancer cell line and significant tubulin polymerization activity, but the activities were considerably less than those of PTX.

In order to understand the reduced activities of these two PTX analogs, members of our group at the time, Ami Lakdawala and Ben Cornett, performed thorough conformational searches of both molecules with a number of different force fields.[53] A number of torsional isomers with excellent superposition of both the diterpenoid core and the C-2, C-4 and C-13 side chains on the same moieties of T-Taxol resulted. To determine if the T-forms were simply too high in energy to be available in solution, they proceeded with a NAMFIS deconvolution analysis for **16** that resulted in eight conformations with predicted populations ranging from 2 to 35%. Among these they found an unambiguous 3-D mimic of the T-form in 5%, along with two nonpolar forms and a number of other extended conformers. Since the compound in the T-form is clearly energetically available, the authors docked these T-conformers into the PTX binding pocket of the refined EC structure[90] resulting in poses for both molecules that do not fit nearly as snugly within the hydrophobic taxane pocket as PTX. Examination of the floor of the cleft reveals both a kink in the C-4—C-3' tether and close contacts between Ala233 and Phe272 of the protein and the propene fragment of the linker. Since the docking procedure held both bodies rigid, the authors attempted to introduce a degree of induced fit to the system by performing MD on the complex under different conditions and at several temperatures for 20 ps. The Phe272—tether interaction is not abated. Thus, while the results demonstrated compatibility with the T-Taxol binding motif, they concluded that a flexible and extended bridge can be deleterious to full expression

of taxoid activity.[53] The bridge does not remain within the PTX molecular volume, a necessity emphasized by my work detailed in Chapter 2. Other *meta*-linked taxanes were prepared, but they were inactive or demonstrated up to 125-fold less activity than PTX, seemingly for the same reasons as for **15** and **16**.[139]

Work continued into this area, resulting in a second attempt at obtaining constrained analogs that mimic the T-Taxol form and demonstrate increased bioactivity over PTX. To this end, the same groups continued their collaboration to seek experimental verification of the T-shape bioactive form from constrained analogs.[96] Since, the previous work resulted in less active compounds due to the close contact between the propene moiety of the *meta*-phenol linked tether and Phe270 of the protein, the authors theorized that a tether linked to the *ortho* position of the C-3' phenyl would be pulled closer to the baccatin core, remain within the molecular volume of the parent compound, and thereby, minimize the ligand-protein interaction. Thus, compounds **9**, **12**, **18** and **19** were synthesized and analyzed in tubulin-binding studies and by NMR to verify the hypothesis. The first three compounds (**9**, **12** and **18**) proved to be as potent as or more so than PTX in two cell lines while **19** was slightly less potent when compared with the same standard. Compound **9** proved to be highly active, approximately 50 times more potent than PTX in the A2780 ovarian cancer cell line. The analogs' capability to promote tubulin assembly was roughly parallel to their cytotoxicities (Table 3).

A NAMFIS analysis of compound **18**, as performed by Ami Lakdawala, resulted in 83% of the population demonstrating the T-form, clearly demonstrating that decreasing the torsional freedom and reducing the molecular volume of the

bridged taxane **16** to those of the *ortho*-bridged **18** contributes to the increase in potency. Compound **18** seats itself in the binding site in a manner almost identical with that of PTX, escaping a steric clash with hydrophobic residues at the bottom of the ligand pocket.[96]

At this point, the students working on the computational aspects of this on-going project graduated and it was passed on to me. Though other *ortho*-linked analogs were prepared, only one other achieved the potency of **9** and **12**, also with a 2-carbon linker.[139] I continued the investigation into these analogs using NAMFIS, docking and molecular dynamics (MD).

Methods

NAMFIS Analysis for 9 and 17. 2D NMR-ROESY Spectra: The 1D ^{1}H assignments of **9** and **17** were accomplished by interpretation of the corresponding COSY, HMBC and HSQC spectra by our collaborators. The 2D NMR ROESY analysis for both compounds was performed on an INOVA 400 MHz NMR spectrometer with 70, 100, 125, 150, 180 ms mixing times to check linearity of the cross-relaxation buildup rates. Interproton distances were calculated from the integrated cross peak volumes using the initial rate approximation and an internal calibration distance between H-16a and H-16b of 1.77 Å. This provided 19 and 15 ROE-based interproton distances for **9** and **17**, respectively.

Solution conformation deconvolution for **9** and **17**: A 10,000 step conformational search was performed on both molecules with the MMFF[110-112] force field and the GBSA/H_20 solvation model in MacroModel v7.2.[82,83] An energy cutoff of 12 kcal/mol resulted in a pool of 93 and 374 unique conformations for **9** and **17**,

respectively, with the global minimum found 62 and 29 times, respectively. The NAMFIS methodology[78,79] integrated the 19 ROE-determined distances measured in $CDCl_3$ and the 93 conformers of **9** to deconvolute the NMR data into four conformations with populations of 59, 33, 5 and 3% (SSD=54). The top populated conformer is in the T-form; the second most populated one is a slightly collapsed form of the T-conformation in which the C3'-phenyl to C2-phenyl centroid distance is 3 Å shorter. The third conformer is a non-polar collapsed conformation, and the last one is a fully collapsed conformation in which all three phenyl ring centroids are within 5-7 Å of each other. For **17**, NAMFIS deconvolution of the 374 conformer pool employed 15 ROE-determined distances. Three conformations resulted with populations of 52, 46 and 2% (SSD=82). The first one is an extended conformer, while the later two are T-like forms.

Glide docking. The structures used for docking are the following: PTX is the optimized T-Taxol structure;[84] **9** and **17** are the highest populated T-like conformers derived from the NAMFIS analysis; and **12** was modeled by hydrating **17** and optimizing it with MMFF in Maestro.[110-112,140] All four structures were docked into the 1JFF tubulin pocket using Glide in Maestro.[141] The protein structure was initially prepared and refined with the Protein Preparation tool in Glide, adding hydrogen atoms and optimizing the side chain positions to avoid vdW contacts; then the grid was generated. Extra precision (XP) flexible docking of the ligands followed. The vdW radii of the ligand atoms with partial atomic charges of less than 0.15 were scaled by 0.80 Å, and the top 20 poses for each ligand were kept. For PTX, only the top pose maintained the T-Taxol shape, with the other 19 showing a variety

of conformations and binding modes. Eleven of the twenty poses obtained for **17** were T-shaped, with the other nine giving the C2-benzoyl side chain in different orientations. Only the top five poses for **9** were in the T-form; the rest covered a variety of binding modes that were up to 5 kcal/mol higher in energy. **12** resulted in 16 T- conformations. The remaining four exhibited similar binding modes, but the C-13 benzamide or C-2 benzoyl groups were located in different positions. All twenty poses were no more than 2.5 kcal/mol higher in energy than the top pose. The resulting top T-pose for each ligand was employed for subsequent MD simulations.

Molecular Dynamics. All molecular dynamics (MD) simulations were performed with GROMACS 3.2.1.[142-144] The taxane ligand structures were prepared for the GROMOS96.1 force field[145] using the Dundee PRODRG2.5 Server.[144] Each compound was solvated in a box of SPC water molecules;[146] 512 for PTX and approximately 750 for the three bridged analogs. The systems ran for one nanosecond, initially, to determine how they behaved and what changes in conformation could be detected. After minimal analysis, the systems were run for an additional 10 ns (11 ns total) at 300K with a time step of 1 fs under NPT conditions (see below). Two plots were made to summarize the results of the dynamics. In the first, the RMSD of the molecules were calculated with respect to their starting T-form geometries (Figure 32). The bridged analogs **9** and **12** remain in the T-form throughout the entire 11 ns simulation, although **17** experiences a conformational interconversion. The second plot (Figure 33) represents the RMS

deviation of each atom in each molecule from its starting position throughout the entire simulation.

The MD simulations of the protein-ligand complexes were performed by Matthew Geballe as published[97,147] and are reproduced here for reference. The structure of the α,β-tubulin dimer was converted to the GROMOS96 united atom force field;[145] GTP, GDP and the taxane ligands were parameterized with the PRODRG Server.[144] The structures of *apo* α,β-tubulin (GTP and GDP still present), PTX-bound α,β-tubulin (based on 1JFF)[90] and **9**- and **12**-bound α,β-tubulin (based on the docking described above) were prepared for MD simulation. Each α,β-tubulin-ligand complex was solvated in a box of 35,000 to 39,000 SPC water molecules[146] with two magnesium cations associated with the phosphates of the nucleotides and 36 sodium cations added to each system to neutralize the overall charge. After a steepest descents minimization, the systems were subjected to a restrained MD run of 20 ps where the water was allowed to equilibrate around and within the structures. The restraints were removed, and the system was simulated at 50K for 5 ps to alleviate high energy interactions without large displacements. The systems were then treated with reverse annealing where the temperature was raised from 20K to 300K over a period of 25 ps. The simulations at 300K were then allowed to run for over 5 ns. *Apo* and PTX-bound α,β-tubulin were simulated for 10 ns. Trajectories were analyzed and visualized using VMD.[148] All simulations made use of PME electrostatics[149,150] with a 9 Å cutoff, were performed under NPT conditions utilizing the Berendsen thermostat,[151] and employed a time step of 2 fs except during the 5 ps simulation at 50K where a timestep of 1 fs was adopted.

Results and Discussion

At the outset of these bridging studies, it was hypothesized that linking the methyl of the C-4 acetate group to the C-3' phenyl would result in active constrained T-analogs. Though at first the strategy resulted in less than desired activities,[53] the creation of short bridges between the *ortho*-position of the C-3' phenyl and the C-4 acetate have resulted in highly active taxane analogs (Table 3).[96] The apex of these is demonstrated by **9** and **12**. Gratifyingly, the bridged taxoid **9** exhibited excellent bioactivity. It is at least 50 times more potent than PTX against A2780, while its dihydro derivative **12** shows about 30 times more activity than PTX against the same cell line. Both bridged taxoids also show slightly increased cytotoxicity compared with PTX against the PC3 cell line. An attempt to synthesize the *E* bridged macrocyclic analog of **9** resulted exclusively in the isomerized *E* alkene **17**. The compound was tested and showed cytotoxicity almost equal to that of the *Z* bridged derivative **9**, indicating that the precise stereochemistry of the bridging alkene linker causes only a small difference in the activity. The length of the linker appears to be the most important quality, with 2-atom linkers providing the greatest increase in activity.

Table 3. Cytotoxcicity and Tubulin Polymerization activity of *ortho*-linked macrocyclic PTX analogs.

Compound	IC_{50}, nM		$IC_{50\ (PTX)} / IC_{50\ (cmpd)}$		ED_{50}, μM (TB polym)
	A2780	PC3	A2780	PC3	
PTX (**1**)	15	5	—	—	0.50
9	0.3	2.5	50	2	0.30
12	0.5	2.4	30	2.1	0.21
17	0.5	3.1	30	1.6	0.33
18	15	5	1.0	1.0	0.28
19	19	17	0.8	0.3	0.83

Though it appears that the T-Taxol form has been verified as the bioactive conformation, no experimental structure of a bridged-taxane/tubulin complex is available. Even if one existed, the resolution would probably be too low to determine the absolute conformation just from the EC structure, as with the PTX-TB structure,[61,90] and would require a combination of experiment and modeling to obtain the structure, as with T-Taxol.[84] For **9** and **17**, the two-carbon bridges between the C-3' and C-4 positions enforce a 17-membered ring with two lactones, two C=C units and seven bonds rigidified by the baccatin core. It is still possible, though, that the newly installed macrocyclic rings might sustain sufficient flexibility to require considerable conformational reorganization upon binding to tubulin. To examine this question, we performed empirical conformational analyses for these two highly active analogs.[139]

For both compounds, a quantitative NMR-ROESY determination was carried out. The corresponding cross-peaks were translated into intramolecular proton-proton separations based on internal distance standards. The corresponding

distances were combined with taxane conformers derived by MC conformational analyses within the NAMFIS framework.[79] As briefly described in Chapter 2 and in numerous studies by our lab,[78,152-154] this technique is able to deconvolve an averaged NMR spectrum into a description of the ensemble of contributing conformations along with an estimate of the individual conformer populations.

As applied to **9**, NAMFIS analysis using 19 NMR-ROE-derived intramolecular atomic distances delivered only four conformations with estimated populations of 59, 33, 5 and 3%. The top populated conformer is in the T-form; while the second most populated one is a slightly collapsed form of the T-conformation in which the C3'-phenyl to C2-phenyl centroid distance is 3 Å shorter. The 5% third structure is a non-polar collapsed conformation, and the 3% form is a fully collapsed conformation in which all three phenyl ring centroids are within 5-7 Å of each other. Compound **17** delivers a similar result, namely only three conformations from 15 ROE cross peaks. One is an extended conformation (52%); the other two, T-forms (46 and 2%). A similar analysis for parent PTX (**1**) delivered T-conformers with much reduced populations of 2-5%.[78] Short-bridge *ortho*-tethering for this compound class increases the concentrations of the apparent bioactive conformers by 20-50 fold and thereby contributes to their exceptional activity. Figure 30 illustrates the superposition of PTX and **9** in the β-tubulin binding cleft as the molecules both accommodate the locus of His227 and avoid steric interaction with Phe272.[139]

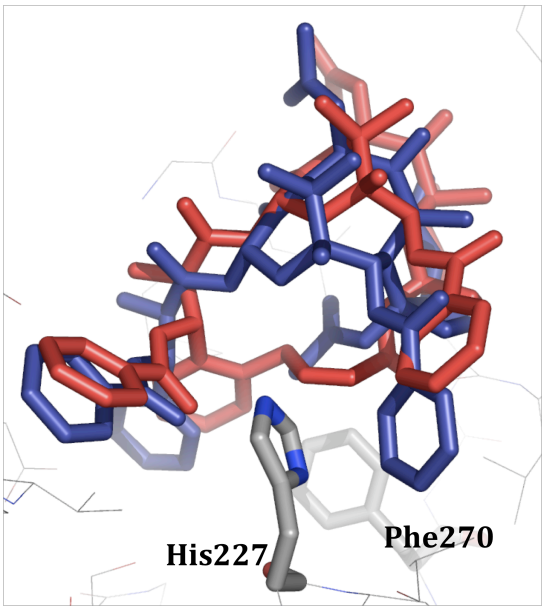

Figure 30. T-Conformations of PTX (blue) and **9** (red) in the β-tubulin binding site, the latter having been docked by the Glide software.[141] Both conformations were derived by NAMFIS analyses. His227 is shown in front of the structures, the **9** bridge behind, and Phe270 further behind.

As the work was being performed, an important discovery about some of the bridged PTX analogs was made. They display promising activity against PTX-resistant and epothilone A-resistant cell lines. These cell lines were developed by long-term exposure of 1A9 human ovarian carcinoma cells to PTX or epothilone A in order to generate cells with drug resistant clones. Molecular characterization of these clones revealed that distinct acquired β-tubulin mutations at the taxane binding site were providing the resistance.[24,155] The mutations impair PTX's ability to interact with tubulin, resulting in a significant lack of drug-induced microtubule-stabilizing activity and G2/M arrest.[156] Testing our analogs against the parental and drug-resistant cell lines demonstrates that many of them exhibit similar or slightly

improved activities over PTX (Table 4).[139] However, two compounds stand out: the bridged taxoid **9** and its dihydro analog **12** exhibit a remarkable activity in that not only are they about 50-fold more active than PTX against the parental 1A9 cells, but they are also 1200- and 150-times more effective than PTX, respectively, towards the PTX-resistant cell lines PTX10.

Table 4. Bioactivity of bridged taxoids **9** and **12** against PTX and epothilone A resistant cell lines.

Compound	IC_{50}, nM		RR	IC_{50}, nM	RR
	1A9	1A9-PTX10 (Fβ270V)	PTX10/1A9	1A9-A8 (Tβ274I)	A8/1A9
PTX (**1**)	4.8	157	20	21.5	4.5
9	0.32	0.13	1.8	0.27	0.84
12	0.07	1.03	12	0.44	6.3

As shown by their relative resistance values, **9** completely overcomes PTX resistance while **12** does so by about 50%. Both compounds are also 50 to 100 times more active than PTX against the epothilone-resistant 1A9-A8 cells. The relative resistance values (RR) for 1A9-PTX10 cells across the compounds listed in range from 2 to 21 and those for 1A9-A8 from 3 to 82.[139] The same quantities for **9** and **12** are perfectly normal by comparison, similar to PTX, and found in the windows RR = 0.8-2 and 6.8-12, respectively. The implication is that the bridged compounds, from the point of view of acquired resistance, are normal taxanes. The remarkable improvements of the two compounds over PTX in apparently overcoming resistance owe their origin to an unusually high potency rather than to subtle structural features of the ridged molecules that enable them to bypass the mutated binding site residues.

Though some of the resulting compounds exhibit both higher cytotoxicity in A2780 and PC3 cell lines and increased potency as inducers of microtubule assembly in comparison to the parent compound PTX, these assays do not necessarily directly test the original hypothesis about the receptor site binding conformation. Polymerization assays are a function of both the intrinsic affinity of the taxane for its receptor site and the effect of ligand binding on assembly. The two are not necessarily related.[157] Cytotoxicity is affected by both these factors, as well as, relative cell permeability, cytoplasmic metabolism and other variables. Therefore, separate evaluations of the affinity of taxanes for microtubules and the efficacy of the bound ligand on microtubule assembly are necessary.[123]

To further test these analogs, our collaborators in the Susan Bane group quantitatively determined the apparent association constants of the ligand/receptor interaction by competition experiments and the effects of the different ligands on the critical concentration of tubulin (including the effects of low temperature and the influence of Mg^{2+}).[97]

Association Constants. The apparent affinities of PTX and a number of bridged analogs for assembled tubulin were assessed by a competition assay with N-AB-PT (C-3' benzamido phenyl replaced by *m*-anilino group), a fluorescent derivative of PTX that binds to the taxane site on microtubules with comparable affinity. PTX and the analogs cause a concentration dependent decrease in N-AB-PT emission with GMPCPP-microtubules, providing data that can be used to calculate the relative affinity of taxanes for GMPCPP-microtubules. The *ortho*-linked derivatives resulted in more stable complexes than the *meta*-linked taxanes

(apparent ΔΔG° = 1.0-1.5 kcal/mol). Among the former group, the relative affinity of the taxanes decreases with increasing number of atoms in the linker. Compounds with the shortest 2-atom tether (**9**, **12** and **17**) bind to GMPCPP-microtubules with a 2- to 3- fold greater apparent affinity than PTX. The latter enhancement is most likely due to an entropic effect resulting from the constraint of the drugs to a few conformations, most notably an increase of 10-30% of the T-Taxol form in solution as opposed to the parent compound.[78,139] This enhances an already favorable entropy change due to the burial of accessible surface area and the release of water.

Critical Concentration Measurements. The critical concentration of tubulin is the concentration below which no microtubule formation occurs. To a good approximation, it is the reciprocal of the elongation equilibrium constant, K_p, which is the measure of affinity of the end of a microtubule for the unassembled tubulin dimer.[158] The critical concentrations of GDP-tubulin with the *meta*-linked derivatives are about 3-fold higher than the critical concentration of GDP-tubulin with PTX. In the *ortho*-linked derivative series, critical concentration decreases with decreasing chain length. For example, a 4-atom tethered analog induces a tubulin critical concentration similar to that induced by PTX, while the 2-atom tethered compounds, **17** and **9**, decrease the critical concentration of GDP-tubulin by 2- to 4-fold, respectively, when compared to the parent compound. Thus, the taxanes with the shortest tether are most efficient in inducing GDP-tubulin assembly, with the K_p for GDP-tubulin assembly in the presence of **12** being 12-fold greater than that for PTX. Two points of interest for these highly active analogs are important to note. First, the microtubules formed in the presence of equimolar

concentrations of **9** and **12** were observed to be shorter than those formed in the presence of PTX, as determined from the length distributions performed on the electron micrographs of the formed microtubules. Second, the "lag time" for tubulin assembly as observed by apparent light scattering appears to be significantly reduced in the presence of these analogs in comparison to PTX-induced assembly. These observations suggest that the macrocyclic taxanes with the 2-atom tethers result in more efficient tubulin nucleation than PTX.

Low-Temperature GDP-tubulin Assembly. The critical concentrations for GDP-tubulin in the presence of the 2-atom tethered macrocyclic taxanes and PTX were determined at 12, 25 and 37 °C, and as expected, they increase with a decrease in temperature. In other words, microtubule formation decreases with decreasing temperature. Interestingly, **12** was found to promote GDP-tubulin assembly at 12 °C when no significant assembly was observed in the presence of PTX under the same conditions, with a 3-fold decrease in critical concentration observed for both **9** and **12** as compared to PTX.

Influence of Mg^{2+} Ions on GDP-tubulin Assembly. An interesting observation with the 2-atom bridged taxanes **9** and **12** is their ability to successfully induce robust microtubule assembly in Mg^{2+} free, 0.1 M PIPES buffer. No assembly of GDP-tubulin with PTX was observed under identical conditions. To further investigate the role of Mg^{2+} ions in **12**-induced GDP-tubulin assembly, critical concentrations of GDP-tubulin with **12** were determined in 0.1 M PIPES at different Mg^{2+} ion concentrations. Remarkably, the critical concentration of GDP-tubulin remains unchanged within experimental error for **12**-induced assembly, suggesting

that it is able to dispense the Mg^{2+} ion requirement for GDP-tubulin assembly in 0.1 M PIPES.

To summarize the data: first, the receptor binding data runs analogous to that for cytotoxicity. For example, *meta*-linked compounds such as **15** and **16** are 6-40-fold less cytotoxic than PTX, while their corresponding *ortho*-linked compounds are similar to PTX in cytotoxicity and induction of tubulin assembly. The 2-atom tethered macrocycles are more cytotoxic than PTX. These derivatives (**9**, **12** and **17**) also bind to microtubules with apparent affinities higher than PTX. *In vivo*, PTX and **12** both cause bundling of microtubules in PC3 and A2780 cells.[97] Also, the assembly of GDP-tubulin induced by these derivatives is more robust than that induced by PTX, as is evident from the low critical concentration values observed and their abilities to induce GDP-tubulin assembly in the absence of Mg^{2+} ions and at 12 °C.[97]

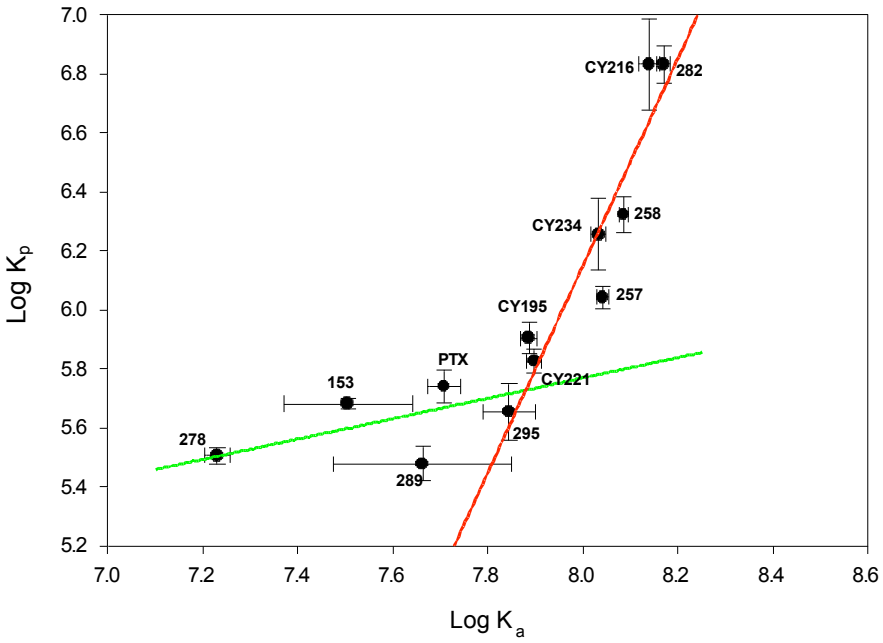

Figure 31. Correlation between ligand induced polymerization of GDP-tubulin (log K_p) and apparent affinity constant (log K_a) for the *ortho*-linked taxane derivatives. The relationship between affinity and efficacy changes when the size and flexibility of the C-3' phenyl to C-4 acetate bridge are decreased. The lines illustrate the trends in the data.

Correlating Apparent Affinity with Efficacy. The relationship between the affinity and efficacy (induced polymerization) of *ortho*-substituted C-3' analogs is plotted in Figure 31 as two separate trends. The dataset clustered about the green trend-line represents a classic SAR in which protein affinity increases as a function of reduced bridge length, introduction of unsaturation, and the replacement of the C-3' benzamido phenyl with O*t*Bu (as in DTX, **3**). The acyclic parent, PTX, clearly contributes to this correlation. At log $K_a \sim 8$, however, a second trend-line (red) materializes. At this point, the macrocyclic taxanes are more effective promoters of

tubulin assembly than would be predicted based on their apparent affinities for microtubules. Compounds **9** (258) and **12** (282) are extreme in this respect, as is 216, the C-3' O*t*Bu congener of **12**, and 234, the 216 construct with a methoxy group in the *para* position of the C-2 phenyl group. These compounds induce robust GDP-tubulin assembly at the low temperature of 12 °C and dispense with the Mg^{2+} ion requirement for tubulin assembly in 0.1 M PIPES. They appear to be tailored to form more stable microtubules than any other taxanes studied to date. Even at a 3-fold higher concentration than normal, PTX is not able to achieve such results.

One notable feature of the highly efficacious compounds is the steeper slope of the inhibition curves. The average slope of the sigmoidal curves for the four most extreme compounds (216, 282, 234, and 258) is 2.6 ± 0.4, indicating apparent cooperativity in ligand binding to the microtubules. In contrast, the average slope for the less-active taxanes, including PTX, is 1.1 ± 0.3. The association of these taxanes with microtubules can be properly described as an association of a ligand with identical and independent sites on the microtubule lattice. Cooperative ligand binding cannot be accurately described with the same analyses. The deviation from linearity for the K_a—K_p plot may be attributed to the presence of cooperativity in one set of ligands and the absence of cooperativity in others. Sorting out the various parameters involved in cooperative binding requires direct measurements of ligand binding to microtubules rather than competition experiments.[159] In the interim, the trends in the apparent affinity constant values reveal a fundamental difference in the ways that different classes of taxanes affect microtubule structure.[97]

Dynamicity of Uncomplexed Taxanes. To understand the dynamic properties that may contribute to the efficacy of these highly active taxanes, we used molecular dynamics (MD) to monitor any changes in both the individual unliganded compounds, as well as, liganded complexes of α,β-tubulin. In chapter 2 I discussed the variability of PTX and the use of conformational searching to obtain different static conformations that the molecule can obtain.[100] NAMFIS analysis of the compound[78] and a number of the bridged analogs,[96,139] as described above, also demonstrates the conformational variability of small molecules. Here, I have adopted a dynamic approach to study the behavior of these taxanes. PTX, **9**, **12**, and **17** were placed in boxes of water and subjected to MD simulations.[97] Figure 32 compares the overall RMSD for all the four compounds relative to T-Taxol over the 11 ns time course of the simulation. PTX assumes a number of conformations finding T-forms at least four times, while **17** samples at least two different conformations. By contrast, **9** and **12** are stable as T-Taxol conformers over the duration of their MD trajectories demonstrating a much reduced conformational flexibility. The latter is highlighted in terms of molecular fragments in Figure 33 by depicting the RMS fluctuation of each atom in the taxanes across the MD trajectories relative to the respective starting structures. PTX is most mobile with the C-4 acetate, the phenyl rings, and particularly the untethered C-3' phenyl group exhibiting the largest fluctuations. While molecular flexibility falls in the order PTX, **17**, **9**, and **12**, the C-4 acetate and the C-3' phenyl centers experience the greatest degree of motional damping from PTX/**17** to **9**/**12** (Figure 33) as expected for the termini of the short bridges connecting distal parts of the PTX framework.

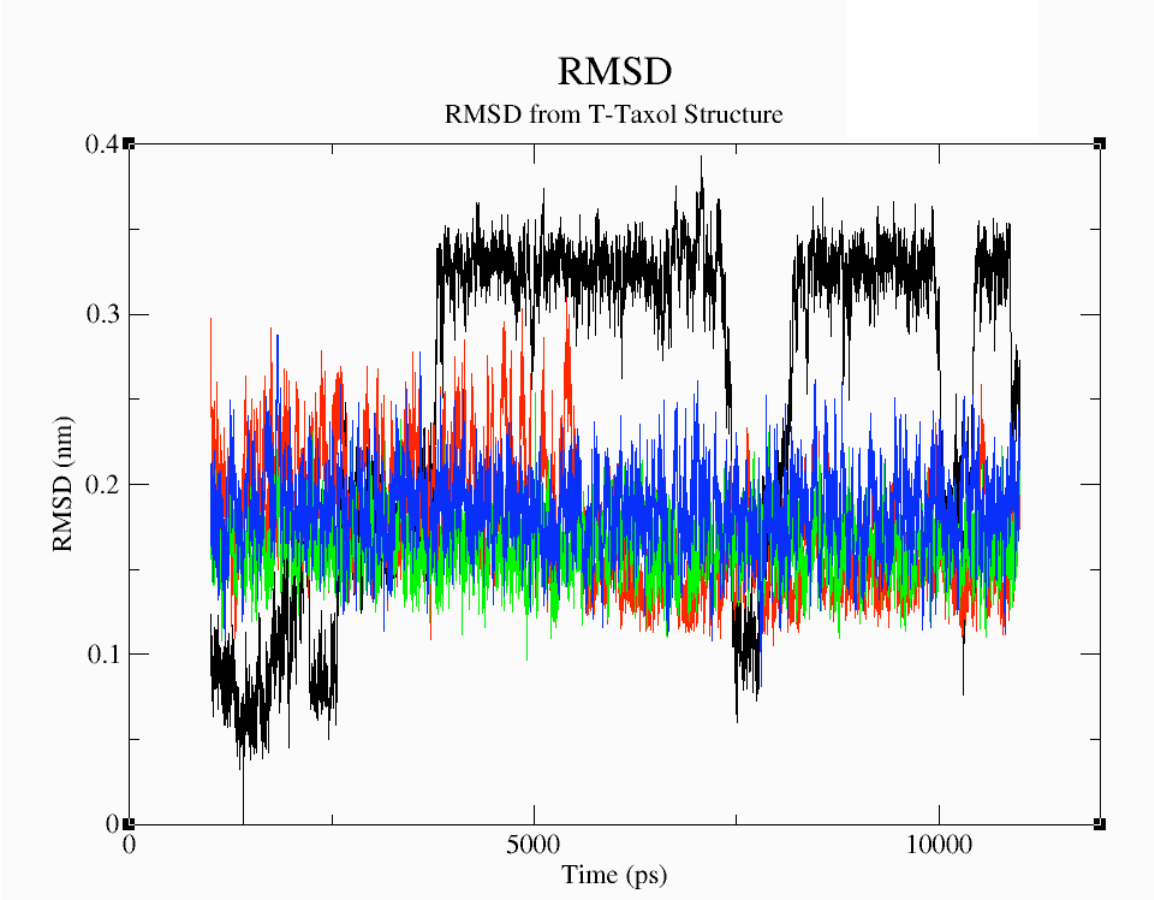

Figure 32. Relative molecular fluctuations throughout the MD for PTX and three bridged taxanes in a box of water at 300K for 11ns; PTX (black), **9** (green), **12** (blue), **17** (green). Movements are plotted as the average RMSD of the heavy atoms from the optimized T-form geometries of the individual molecules; T-Taxol is baseline at RMSD = 0. PTX can take a number of conformations, but finds the T-form at least four times. Structure **17** interconverts between two forms, while **9** and **12** are conformationally stable over the time course.

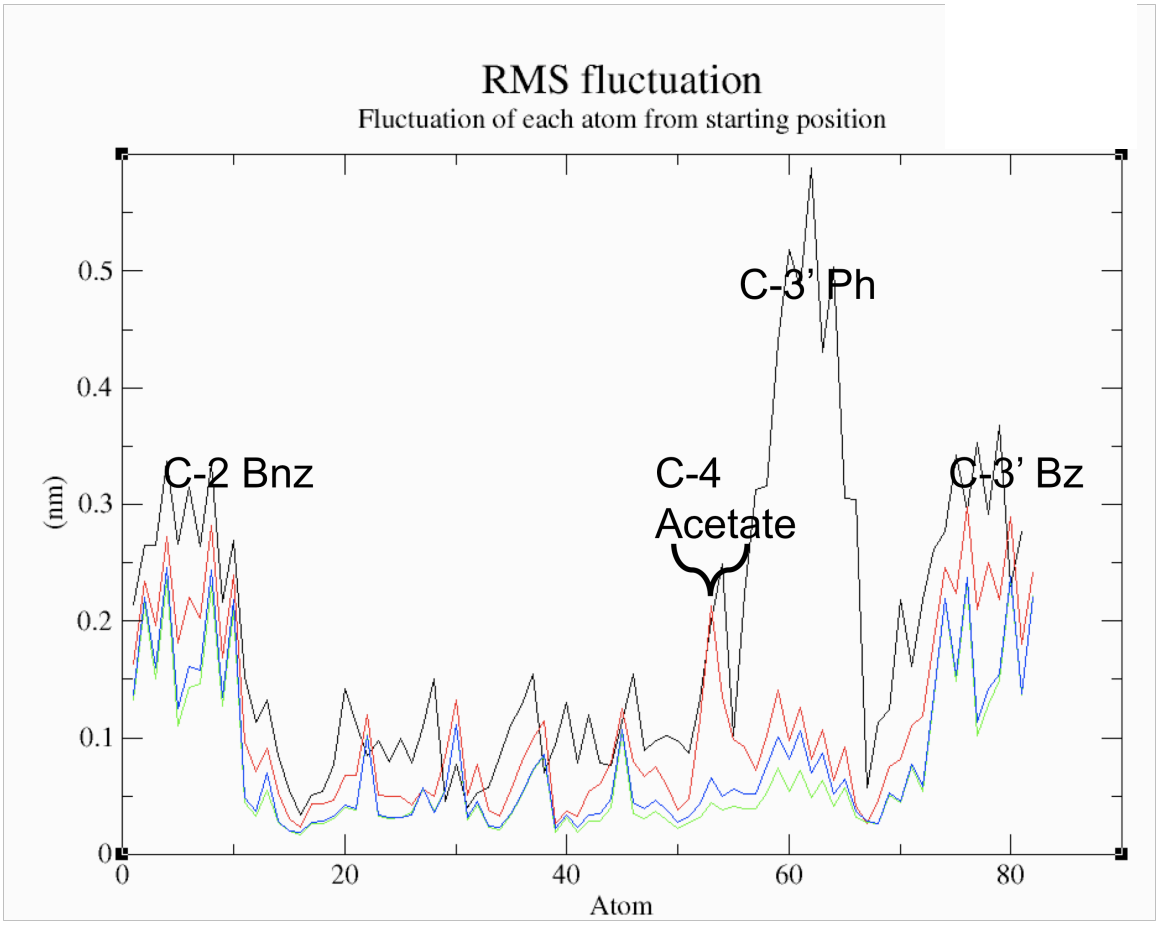

Figure 33. Relative atom fluctuations following MD for PTX and three bridged taxanes in a box of water at 300 K for 11 ns. Movements are plotted as the average RMSD from atomic positions in the optimized geometries of the individual molecules; important functional groups are identified; PTX (black), **9** (green), **12** (blue), **17** (red).

Dynamic Effects of Bridged Taxanes on β-tubulin. While I addressed the uncomplexed ligands, another student in our group, Matt Geballe, examined the dynamics of the individual complexes of PTX, **9**, and **12** with α,β-tubulin, as well as, the unliganded protein. The four systems were prepared for computation as described in the **Methods** section.[97,147] The key changes in the vicinity of the

binding site are associated with the location and conformation of the M-loop. Figure 34 summarizes the results for the complexes at 4 ns, the time point at which each has equilibrated and achieved stability. The M-loop of the ligand-free protein depicted in purple collapses onto the taxane binding site, and in this conformation presumably blocks ligand binding. In the presence of PTX, however, the loop (gray) adopts a less compact conformation and serves as one of the boundaries for the taxane binding pocket. With **9** as ligand, the M-loop (green) recedes further, reaching its most modulated conformation (brown) when interacting with **12**. Seen from this dynamic point of view, both PTX and the bridged ligands have a dramatic but differential effect on the conformation of the M-loop. It is precisely those compounds exhibiting a 3-fold decrease in the critical concentration of GDP-tubulin relative to PTX and inducing significant microtubule assembly in Mg^{2+} free buffer (**9** and **12**) that are predicted to alter the M-loop conformation of β-tubulin to the greatest extent.

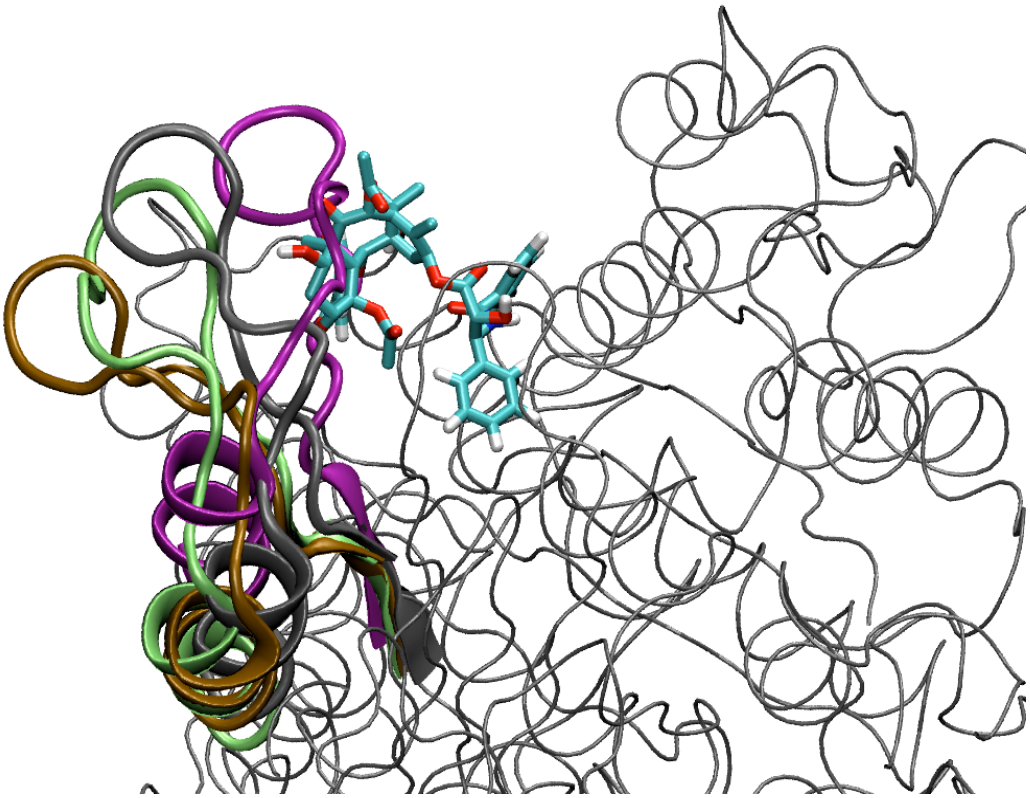

Figure 34. Four β-tubulin proteins overlapped following 4 ns MD treatment at 300K. M-loops at upper left; no ligand (purple); PTX (gray); **9** (green); **12** (brown). PTX is shown in the taxane binding site, the purple M-loop having moved in to fill the open pocket.

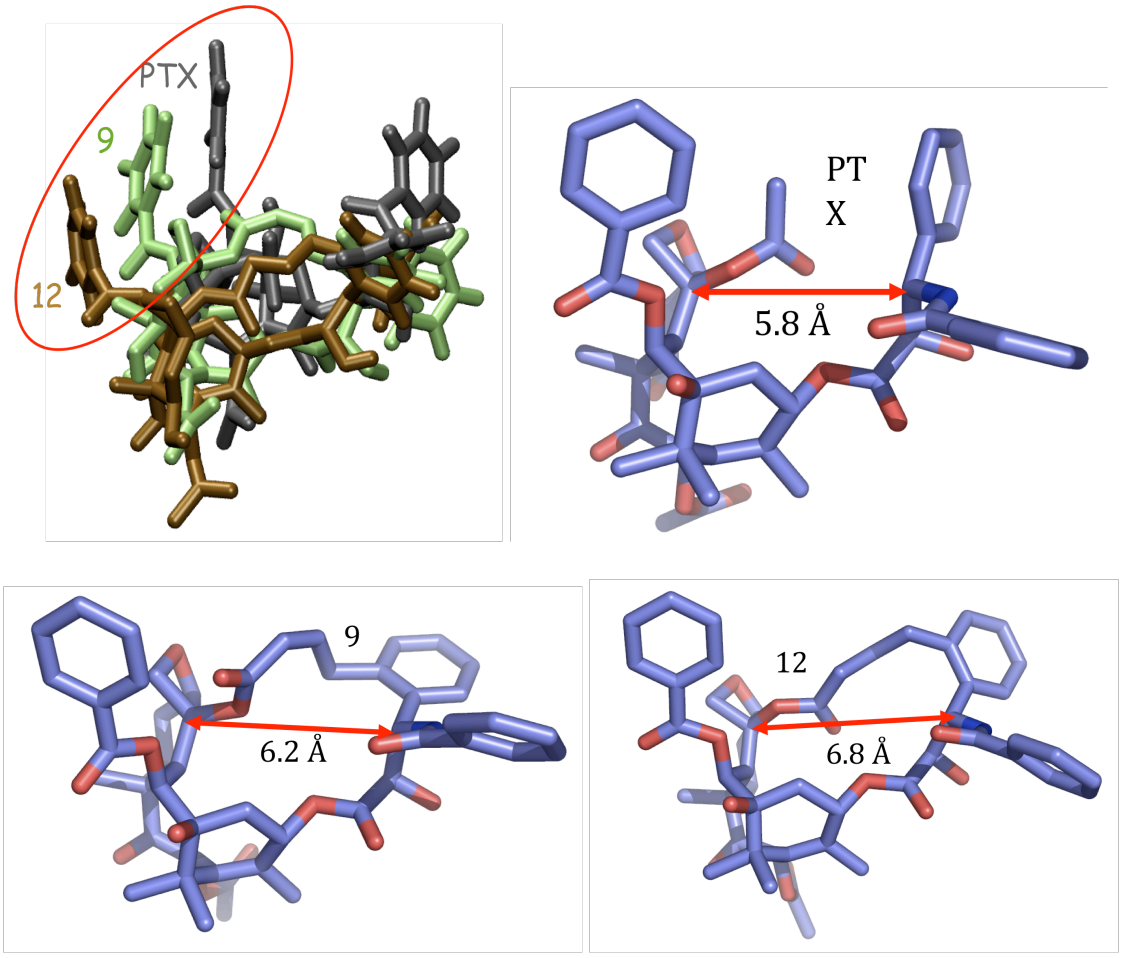

Figure 35. Geometric characteristics of PTX and bridged taxanes docked in β-tubulin and subjected to MD. (a) Relative orientation of C-2 benzoyl phenyl groups following superposition of the protein complexes depicted in **Figure 34**. (b) Distance between C-4 and C-13 in PTX. (c) The expanded C-4 to C-13 distance in bridged **9**. (d) Maximal C-4 to C-13 distance achieved by **12**.

The relative behavior of PTX, **9**, and **12** as depicted by Figure 34 and reflected by the SAR of Figure 31 suggests both static and dynamic aspects in the binding event rarely considered for ligands with such similar structures. A critical static element is registered by Figure 35a. In the latter, the R-carbon backbones of the taxane-tubulin complexes after 4 ns of MD were superposed and then the

protein structure hidden. The baccatin cores of the PTX, **9**, and **12** ligands occupy the same volume, but the C-2 benzoyl phenyl groups are displaced as shown by the red ellipse. It is noteworthy that the displacements are in the same direction as the M-loop translations of Figure 34. Measurement of the distances between C-4 and C-3' in the individual taxanes (Figure 35b-d) reveals another parallel; namely, the distances increase in the order PTX < **9** < **12**, stretching the molecules along the approximate long axis. This static effect alone suggests that overall molecular length may reposition the taxane ligands in the binding site and promote M-loop transposition. Along this analogue series, two molecular features reinforce one another. That is, the greater the molecular flexibility (Figure 32 and Figure 33), the more globular the taxane ligand (Figure 35). The least flexible structures are thus the more extended; namely, **9** and **12**. This observation correlates closely with the ability of these structures to enforce the greatest conformational change in the β-tubulin M-loop.

Bridged Taxanes, the M-Loop, and K_p. As outlined above, the taxane series PTX, **17**, **9**, and **12** increases in molecular length (Figure 35), decreases in molecular mobility (Figure 32 and Figure 33), and displaces the M-loop from its position in unliganded β-tubulin (Figure 34) in the order given. The operation of the ligands in the taxane binding cleft is best described by the panels of Figure 36, snapshots taken at the end of the protein ligand MD trajectories. Figure 36a shows that **12** resides near the luminal or interior surface of the microtubule. A 90° rotation of the protein (Figure 36b) illustrates that **12** spans the space between helix 1 (H1, at left in red) and the M-loop (at right in red). As pictured dramatically by the space-filling model

in Figure 36c, the benzamido phenyl is pushed up against H1, while the C-2 phenyl ring is pinioned against the M-loop. Hydrogen bonds between Asp26 in β-tubulin and both the benzamido NH and 2'-hydroxyl hydrogens facilitate this tight packing of the benzamido phenyl against H1. A similar hydrogen bond between the benzamido NH and the backbone of helix H1 was observed for **9**, but not for PTX. It should be recalled that **12** is the most rigid bridged T-taxane that forces the MD-positioned M-loop furthest from the body of the protein (Figure 34). This contrasts with the more flexible PTX, which binds in the more compact T-Taxol form. Also sandwiched between H1 and the M-loop, PTX sits somewhat deeper in the pocket and is less "right-shifted" toward the loop. The less pronounced molecular translation is partly the result of the conformational mobility of the unbridged molecule; it is able to place its C-2 phenyl group in a narrow subpocket orthogonal to the disposition of the *β*-tubulin M-loop (Figure 36d). As a consequence, this loop is folded around the PTX B, C, and D rings rather than being oriented outward toward the adjacent protofilament.

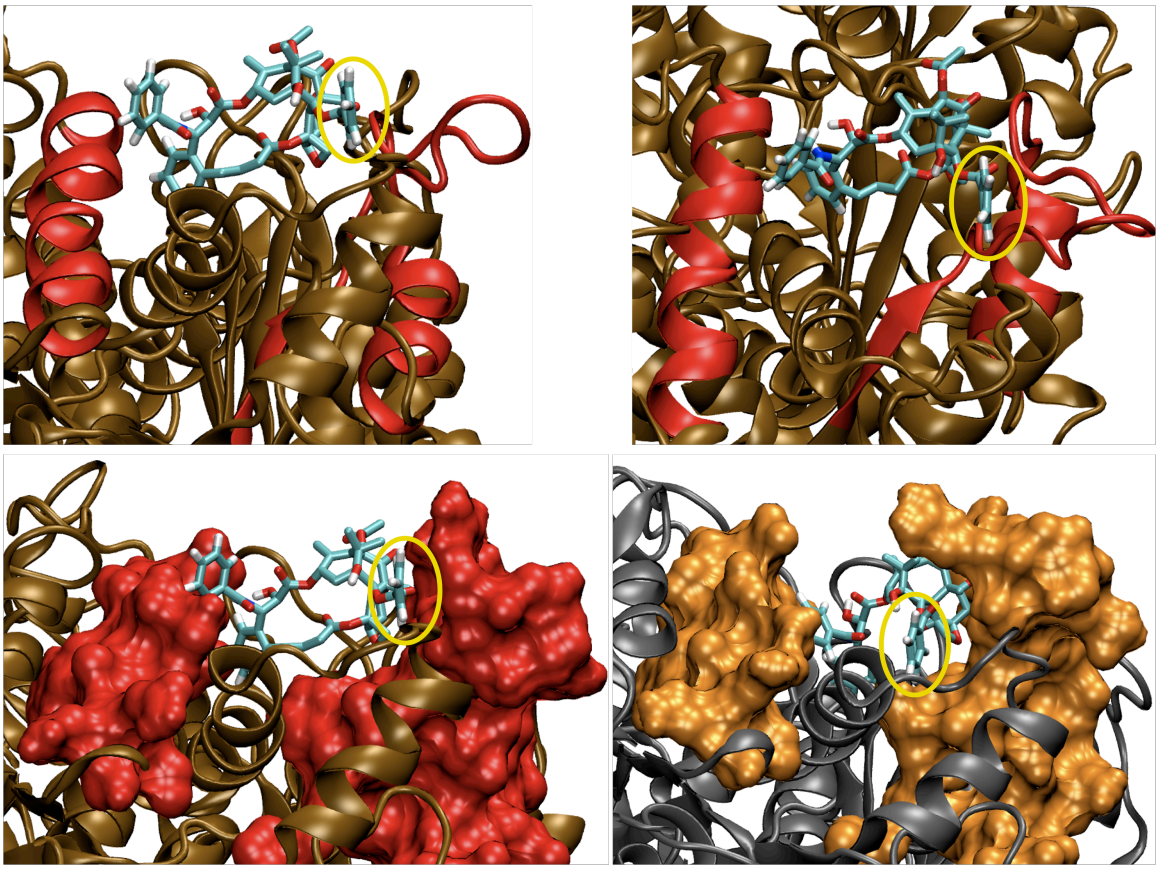

Figure 36. The binding sites of **12** and PTX in complex with β-tubulin following MD at 300 K for 4 ns in a box of water molecules. The C-2 benzoyl phenyl groups are identified within yellow ellipses. (a) **12** sandwiched between H-1 and the M-loop and exposed to the microtubule lumen. (b) Rotation of the latter by 90° to show the tight van der Waals interaction between the C-2 phenyl and the M-loop. (c) Representation of H-1 and the M-loop as space-filling boundaries for **12** in the binding pocket. (d) PTX sequestered between H-1 and the M-loop shown in space-filling format.

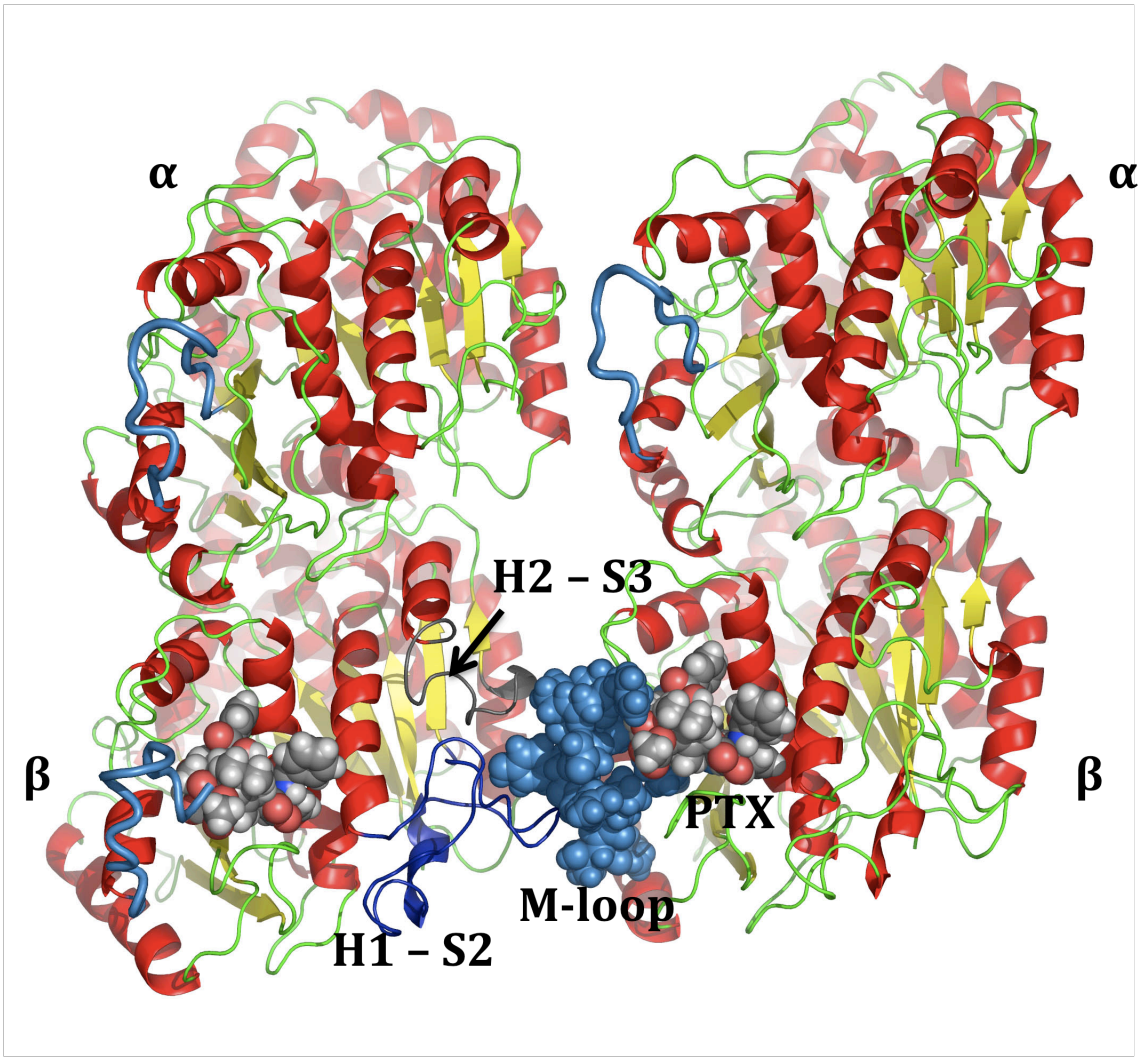

Figure 37. Four subunit component of a 13-protofilament microtubule illustrating the interaction between two vertically oriented protofilaments. In the β-subunits, two PTX molecules (space-filling) and two M-loops (blue) are highlighted. The space-filling M-loop associated with the β-subunit at lower right is in van der Waals contact with a PTX molecule to the right and the H1-S2 and H2-S3 loops to the left.

The latter underpins the remarkable observation that the cytotoxicity of certain bridged taxanes is dominated by microtubule elongation (K_p) rather than apparent affinity (K_a, Figure 31). It is well-known that protofilament-protofilament

interactions in microtubules are mediated by M-loops in contact with H1-S2 (the N-loop) and H2-S3 loops in a β-tubulin subunit within an adjacent protofilament[122,160] as modeled in Figure 37. It has also been suggested that PTX's microtubule stabilizing effect is likely to involve reshaping of the M-loop to induce a conformation that favors productive protofilament interaction.[84,122,161] In order to achieve strong lateral contact, the M-loop needs to be extended away from the β-tubulin subunit and into the space between protofilaments. In order to maintain this contact, a restraint on conformational refolding of the M-loop would be ideal. We suggest that the rigid structures of compounds **9** and **12** serve this purpose by directing the M-loop toward the adjacent protofilament and by hindering both the loop's mobility and the establishment of a pool of rapidly equilibrating conformers. Depleting the latter conformational ensemble of forms that place the M-loop near the surface of the home β-subunit eliminates torsional isomers that cannot furnish productive lateral interactions. Compounds such as **9** and **12**, once docked into microtubules, act as rigid rods to hold the M-loop away from β-tubulin and further facilitate persistent contact with the secondary structure on the neighbor protofilament. The space-filling representation of the blue M-loop in Figure 37 illustrates this idea for bound but flexible PTX. We presume that structure **12** translates the M-loop slightly further into the inter-protofilament space, while offering the loop no opportunity to escape by conformational redistribution. In this way, the lateral interface is stabilized and microtubule depolymerization is suppressed.

Reshaping of the M-loop by the most potent bridged taxanes may reverberate through the microtubule lattice, allowing these taxanes to associate with microtubules in a cooperative manner. The idea that taxanes with similar structures can affect the architecture of microtubules in distinctly different ways is not unprecedented. PTX (**1**) and DTX (**3**), which differ primarily in the substituent bonded to the C-3' nitrogen (benzoyl and O*t*Bu, respectively), promote the formation of different microtubule lattices.[162-164] Microtubules assembled in the presence of PTX have a significant population of 12-protofilament microtubules, while those assembled in the presence of DTX consist of mainly 13- and 14-protofilament microtubules, like those assembled in the presence of GTP. Microtubules assembled in the presence of DTX, however, can be reduced to 12-protofilament microtubules by addition of PTX to the solution.[165] The exchange of ligand in the taxane binding site is accompanied by a reorganization of the microtubule without disassembly of the polymer. In a similar fashion, the tubulin conformation change caused by compounds such as **9** and **12** may affect the conformation of adjacent tubulin dimers, reshaping the lattice in a manner that favors taxane binding.

Summary

Starting with the analysis of T-Taxol, we developed taxanes that contain bridges between the methyl group of the C-4 acetate and the *ortho*-position of the C-3' phenyl group, constraining the molecules to the bioactive molecular shape. A number of compounds were prepared, but three in particular are of great interest: **12** and **17** are about 30-fold more cytotoxic than PTX, while **9** shows a 50-fold

improvement. Also of consequence, **9** and **12** are 1200- and 160-fold more active than the parent compound in the PTX-resistant cell line PTX10. Application of the NAMFIS method to these two compounds resulted in four and three conformations, respectively, with 59% and 48% contributions from T-Taxol structures. While the significant activity increases measured for these substances cannot be attributed completely to conformational biasing, the results strongly suggest that this is a dominating factor. Direct measurement of the association constants and critical concentration of tubulin with the different analogs reveals that these highly active compounds are more effective promoters of tubulin assembly than would predicted (Figure 31). Molecular dynamics of the different tubulin-ligand complexes demonstrates a change in the protein conformation (Figure 34 and Figure 36) occurs that appears to depend on the ligand rigidity (Figure 35) and we propose that this translates throughout the microtubule, resulting in a decrease in the disassembly rate.

Simplified Taxanes

The T-Taxol[84] conformation has not only led to highly active constrained analogs (**9** and **12**),[96,97,139] but it has been used to develop a set of simplified taxanes.[166] One of the set-backs of taxanes is their difficulty of synthesis. Structurally simpler congeners of PTX would lead to a highly desirable future generation drugs that could be readily acquired, while retaining the full activity of the parent compound. Others have attempted such a feat, preparing various simplified PTX analogs. Some of these showed very weak cytotoxicities, but no tubulin polymerization activity.[167-171] Ojima and coworkers synthesized a simplified

macrocyclic PTX analog[170] based on the nonpolar conformation that exhibits no tubulin polymerization activity, but does have micromolar cytotoxicity in two cell lines.

After establishing the T-Taxol conformation as the bioactive form through the synthesis of highly active constrained compounds (**9** and **12**), we decided to pursue simplified taxanes that maintained the principal taxane pharmacophore, in addition to a short bridge. Namely the C-2 benzoate, C-3' phenyl and C-4 acetate groups would be maintained as they are in the parent compound, but the baccatin core replaced by a simplified bicyclic moiety. SAR studies indicate that modificiations to the northern hemisphere of PTX do not cause significant detriment to its bioactivity[27] so these groups were ignored in the simplified structure. This led to the simplified PTX analogs displayed in Figure 38 with a modified hydrophobic [3,3,1]-bicyclononane moiety replacing the baccatin core.

Methods

Structures **21** and **23** were constructed using T-Taxol[84] as the template in MacroModel 6.5.[83] Each was fully optimized using the MM3*[113-115] force field including the GBSA/H_2O solvation model.[82] The structures were manually docked into the β-tubulin binding site by superimposing them on bound PTX.[84] MD was then performed on a 10 Å sphere around the binding site of each model for 250 fs at 20K using the Tripos force field, followed by full optimization of the complex while holding the backbone of the protein aggregate fixed. The structure of **21** retains the essential features of the T-Taxol binding conformation by locating the bicyclononane core on the baccatin core and by superposing the C-13 phenyl rings

on those of PTX. The C-2 phenyl rings overlap, but that of **21** is offset and buried deeper in the pocket where it encounters a steric clash with the protein. When the T-Taxol model of **23** is docked into the β-tubulin protein coordinates, the C-13 terminal phenyl rings are positioned similar to those of paclitaxel. However, the diastereomerically relocated C-2 phenyl ring is positioned in the northern part of the binding site near Leu371, Pro274 and Phe272 (ligand—side-chain H---H separations from 2.2 to 2.7 Å). The resulting steric clash pushes the ligand out of the binding site during MD simulations.

Results and Discussion

Our collaborators in Virginia (D. G. I. Kingston group) proceeded with the design and synthesis of compounds **20**-**24**.[166] Susan Bane's group again obtained relevant biological data. All the compounds were cytotoxic, but significantly less so than PTX, against the A2780 ovarian cell line. They were, however, comparable to those prepared by Ojima.[170] These measurements were made very difficult by the very low solubility of the compounds in DMSO-H_2O mixtures, possibly leading to underestimated cytotoxicities. Interestingly, the cytotoxicities of all five compounds were all comparable within a factor of two, indicating that the relative regiochemistry of the benzoate group does not affect the activity significantly.

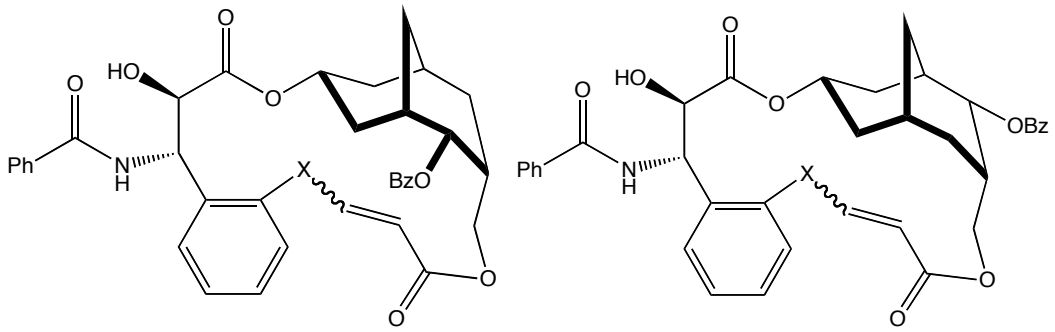

Cmpd	X	Bridge	IC_{50} (μM) A2780
20	OCH_2	Z	15.1
21	OCH_2CH_2	E	20

Cmpd	X	Bridge	IC_{50} (μM) A2780
22	OCH_2	Z	11.3
23	OCH_2CH_2	E	18
24	CH_2	E	10.9

Figure 38. The five simplified taxane analogs in which the baccatin core has been replaced with a modified hydrophobic [3.3.1]-bicyclononane moiety. The measured cytotoxicities in the A2780 cell line are also listed; PTX's IC_{50} is 0.02 μM.

Compounds **20**-**23** were also tested for microtubule assembly activity *in vitro*. All four molecules enhanced the rate and extent of DMSO-induced tubulin assembly at concentrations of 30 μM, which is near the limit of solubility for these molecules under the assay conditions. They also stabilize the microtubules to cold induced disassembly. In the absence of added ligand, DMSO-induced microtubules are completely depolymerized by dropping the temperature from 37 to 4° C. In the presence of the compounds, some polymer remains in the samples at 4° C. Compound **20** was the most active in stabilizing assembled microtubules, while compound **21** enhanced assembly to the greatest extent. These, of course, are nowhere near the numbers for the macrocyclic analogs of the PTX (Table 3),[96,139] but are interesting nonetheless. We hypothesize that a more soluble compound

with this simplified scaffold could produce better data and demonstrate greater activity.

We performed some modeling studies of **21** to determine if the molecule can obtain a T-like conformation. As seen in Figure 39 in the β-tubulin taxane site, the C-4 and C-13 side chains of the simplified analog match those of PTX closely. The C-2 phenyl overlaps that of PTX, but is forced deeper into the hydrophobic pocket as a result of a somewhat different positioning occasioned by the nonane core by comparison with the PTX baccatin core. This elicits steric congestion via short H---H contacts with the Leu230 and Leu275 tubulin side chains. Apart from insolubility, the reduced activity of **21** relative to PTX most likely derives from this source. Structure **23** does not dock into the taxane binding pocket in the T-form, but can assume a number of alternative conformations and binding modes. Considering the low potency of the compound, we regard none of these as predictive. The diminished activity of our diastereomers as well as that exhibited by the Ojima compounds[170] make it clear that neither class is sufficiently tailored to fully exploit the T-Taxol concept.

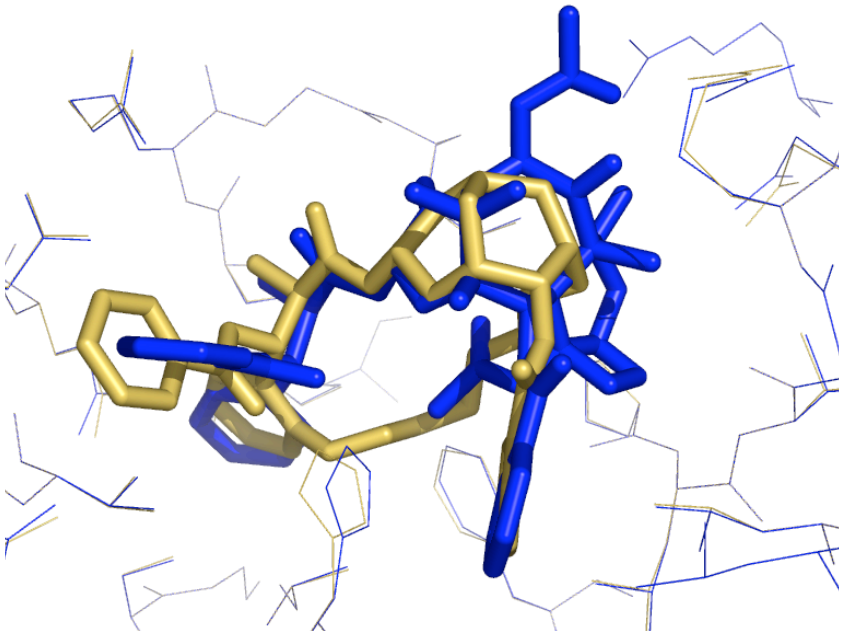

Figure 39. Overlay of structure **21** (yellow) on T-Taxol (blue) in β-tubulin; the C-4 and C-13 side chains match closely.

In summary, we designed a new class of cytotoxic PTX-like molecules that can approximate, but not precisely achieve the T-Taxol conformation. However, incorporation of polar functional groups in the structures to make them water-soluble may increase their bioactivity. Studies towards this end are in progress.

C-2 Sulfur Linked PTX Analogs

Some of the PTX SAR data was discussed in chapter 2, with specifics about DTX and NTX in our evaluations of bioactive conformation proposals. T-Taxol can explain the available data, taking into account modifications in all the side chains and to the baccatin core itself. The confirmation of this form as the bioactive conformation allows us to evaluate new SAR data and perhaps even make predictions about the activities of new ligands.

The extensive SAR studies over the past couple of decades have led to several generalizations, with a crucial one involving the three key side chains on the southern hemisphere of the PTX molecule: the C-13 N-benzoyl phenylisoserine, the C-2 benzoate and the C-4 acetate moieties. All are critical to taxane tubulin binding and cytotoxicity in terms of both atomic constitution and molecular conformation.[27,54,172] SAR studies at the C-2 position have shown that both the nature and stereochemistry of the 2-benzoyl group in PTX derivatives are determinants of activity. Removal of the 2-aroyl ester[173] (2-deoxy-PTX) or reorientation from α to β[174] (2-*epi*-PTX) causes either two-orders of magnitude reduction or complete abolition of cytotoxicity, respectively. On the other hand, many PTX analogs with aroyl[175,176] or alkyl[70] ester groups at the C-2 position have been reported with modest to highly potent bioactivity. In a continuing effort to probe the PTX C-2 structural requirements more deeply, Lei Wang, in Wei-Shuo Fang's lab at the Chinese Academy of Medical Sciences, undertook the preparation of a series of 2-N- and S-substituted taxanes.

When they approached us for collaboration, they had already reported on the synthesis of C-2 N-substituted taxoids,[177] the first transformation of the heteroatom on C-2 from oxygen reported to date. They used the methodology developed in that report to make other C-2 analogs, including 2-amido analogs, their C-10 modified analogs, and 2-debenzoyloxy-2α-phenylthio 10-acetyl docetaxel whose inactivity was attributed to its shorter chain length at C-2 compared with the benzoate.[178,179] They proceeded with the isosteric replacement of the C-2 ester of PTX with sulfur-linked substituents to further detail the structural requirements at this PTX side

chain. We performed some conformational analyses and used modeling to correlate their biological activities to the ability to bind to β-tubulin.[180]

Methods

Compounds **26** and **28** were analyzed in the binding pocket of α,β-tubulin using molecular dynamics (MD). Each one was built in MacroModel v.8.6[83] using T-Taxol[84] as a template and optimized with MMFF94/GBSA[82,110-112] to the nearest local minimum. The compounds were then manually and independently docked into the binding site of the α,β-tubulin model by superimposition of the baccatin cores of the molecules on bound PTX.[84] An extensive MD procedure was then followed to develop a stabile model for each complex. Sybyl 7.0[116] was used with the MMFF94 force field, a time step of 0.5 fs and a dialectric constant of 4.5 for each simulation.

An initial MD run was performed on each complex at 20K for 500 fs with the ligand and side chains in a 10Å sphere around the binding site allowed to move. This removed the bad steric contacts present from the docking placement of the new ligand. Another 500 fs of MD at 20K was performed with the 10Å sphere-binding site of the protein allowed to move and the ligand held fixed to allow the binding site to reorganize slightly if necessary. A 1 ps MD simulation at 20K followed with the ligand and side chains in a 10Å sphere around the binding site allowed to move. At this point, the energy of each complex had leveled off and no major fluctuations were observed so they were fully minimized with the backbone held fixed using the MMFF94 force field. The individual complexes were then each subjected to higher temperature MD by running 5 ps simulations at 50K, 100K, 200K and 300K to evaluate each ligand's behavior in the protein.

When minimized with MMFF94, compound **26** obtains a C2-S-C(O)-Ph torsion of 136°. Searching the Cambridge database[181] for C-S-C(O)-Ph containing compounds found 83 hits. While a few angles are in the 168-170° range, the vast majority fall in the 175-179° range. The 136° angle obtained using MMFF94 is an artifact; therefore, the C2-S-C(O)-Ph torsion was restrained to 178° $\pm$ 1° when performing the MD simulations. As the initial MD proceeded, the side chains in the binding site and the ligand rearranged slightly to better orient themselves, but no major changes in the pocket occurred. With longer and higher temperature MD, the C2-side chain attempted to obtain the same position as that of T-Taxol, i.e. encompassed in the pocket formed by His227, Asp224, Leu215 and Leu217. Due to the longer C-S bonds though, the side chain does not fit well, forcing the entire ligand to lift out of the pocket slightly (1.2 Å). The compound's inability to obtain the optimal binding conformation in the pocket may explain its lack of activity.

Compound **28** with a C2-S-CH_2 ether angle of 100° as compared to PTX's 180° C2-O-C(O) ester angle changes the shape of the C2 side chain. The phenyl ring sits flat and perpendicular to His227 and further out of the pocket than that of paclitaxel. As the initial MD proceeded, the binding site opened up slightly (0.20Å overall) with the largest variations occurring with Leu215 and 217. These two residues started out in direct contact with the C2 phenyl ring and moved slightly to avoid steric clashes. At the end of the simulations, the ring sits slightly further out of the pocket and more exposed to solvent, though the ligand remains in the pocket throughout the higher temperature MD simulations, sitting a little further out of the pocket than paclitaxel does throughout similar MD treatment. Again, the

compound's lack of activity seems to be due to its inability to obtain the proper conformation to fit into the pocket.

Results and Discussion

Lei Wang synthesized compounds **25**-**28** and their binding affinities to β-tubulin were determined by a fluorescent ligand displacement assay, as described above. Free energy changes for all four S-linked taxoids, calculated from binding constants at 35 °C, are -27 to -30 kJ/mol, corresponding to 65-72% of the affinity exhibited by PTX (*ca*. -42 kJ/mol).[182,183] The compounds' cytotoxicities were also measured against A2780 and the multidrug-resistant (MDR) counterpart that overexpresses P-glycoprotein (P-pg) (A2780/AD10). All members of the series were found to be 3-4 orders of magnitude less active than PTX in the former and 10 times less so in the latter cell line.[180]

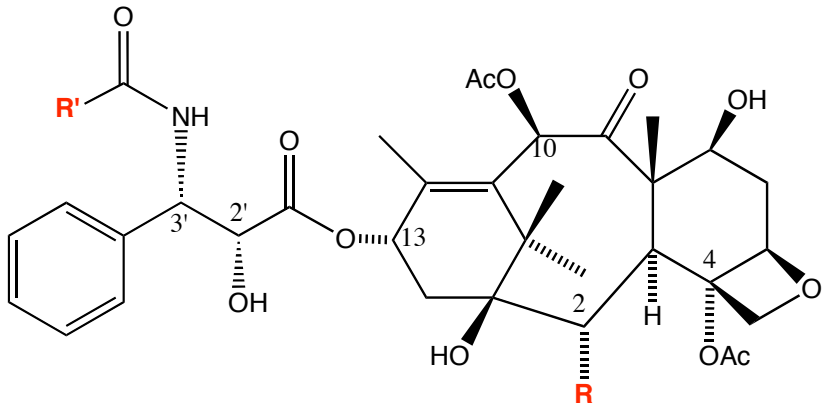

Compound	R	R'	IC_{50} (μM) A2780	IC_{50} (μM) A2780/AD	ΔG (kJ/mol)
PTX (**1**)	PhC(O)O	Ph	1.6 X 10^{-3}	0.92	-42.1
25	PhC(O)S	Boc	2.4	6.96	-30.1
26	PhC(O)S	Ph	11.7	27	-28.4
27	$PhCH_2S$	Boc	3.5	8.3	-29.9
28	$PhCH_2S$	Ph	9.9	9.4	-28.6

Figure 40. The four C-2 analogs with sulfur replacing the ester oxygen are listedn along with their cytotoxicities and calculated binding free energies.

In order to explain the low activity of these taxanes, the ligand-tubulin interaction was analyzed with molecular dynamics (MD) based on the T-conformation. The diminutive binding affinities and cytotoxicities of the series can be attributed to the alteration of the local geometry around the sulfur atoms by comparison with the classic C-2 benzoyl ester. In the latter case, the C-2 phenyl ring of PTX is encapsulated in a rather narrow pocket in the EC structure of tubulin.[84,90] The opposite faces of the ring are within van der Waals contact of His227 and Leu215, while the *para*-position is in equally short contact with the protein backbone at Asp224. Extension of the C-2 substituent either perpendicular to the faces of the ring or further from the baccatin core can be predicted to create one or

more steric clashes. To test the idea that the latter distance increment could cause a steric problem for series 10, thioester **26** was constructed by an O to S modification of T-Taxol, optimized with the MMFF/GBSA force field,[110-112] and docked into β-tubulin by superposing the taxane on the location of the original PTX ligand.[84] To relax the protein-ligand complex, MD was performed for the thio-PTX ligand and the side chains in a 10 Å sphere around the binding site at 20 K. Once any unfavorable steric contacts were removed, the temperature was slowly increased to 300 K and the system allowed to reach a stable state, as measured by energy equilibration. At this point, the entire taxane molecule had risen out of the binding site by 1–2 Å, and the terminal C-2 phenyl ring had slipped from the tight His/Leu/Asp sub-pocket to be repositioned in the first water shell around the protein. Figure 41a depicts these changes.

A similar set of calculations for thioether **28** causes a comparable extrusion of the molecule from the binding pocket. In this case, however, the saturated C-2 side chain deviates from planarity and causes a significant rearrangement of the surrounding residues. Of particular note, the terminal phenyl ring is now perpendicular to His227 and located in a pocket opened by the movement of the Leu217 and Leu215 residues. Figure 41b depicts the final conformation of the C-2–S–CH_2–Ph moiety and the displacement of the baccatin core by comparison with PTX.

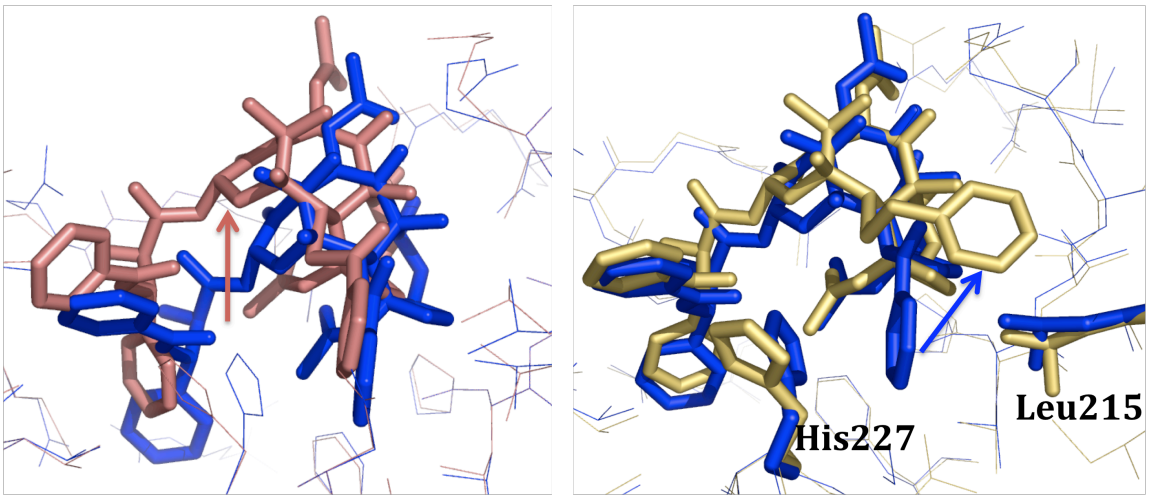

Figure 41. (a) Thioester **26** (peach) moves out of the pocket by 1-2 Å during the MD simulation; (b) Thioether **28** (cream) reorients the C-2 side chain out of the pocket formed by His227, Leu215 and Asp224; T-Taxol is in blue.

To summarize, C-2 S-linked PTX analogs were synthesized and analyzed. The compounds were found to be much less active in both tubulin binding ability and cytotoxicity, although for different reasons as revealed by molecular simulations. It is noteworthy that the T-Taxol conformation again explains the bioactivity of a new series of taxanes.

Conclusions

If a given compound adopts the bioactive form, does this guarantee amplified activity? In a review of bridged taxanes, the authors point out that enforcing the T-Taxol conformation is a necessary but not sufficient condition for eliciting high levels of drug potency.[136] In addition to the appropriate molecular conformation, the tubulin-taxane ligand must also adopt a compatible molecular volume, as discussed in the previous chapter. Compounds with longer bridges and those that

extend from the *meta*-position of the C-3' phenyl illustrate the molecular dilemma.[53] Compound **16**, like PTX, displays about 5% of the T-form in solution. Unlike PTX, however, the compound is 4-45-fold less cytotoxic depending on the cell line and 10-fold weaker as a tubulin polymerization agent. Modeling demonstrates that a section of the long, suboptimally substituted bridge falls outside the molecular volume of PTX and competes with tubulin's Phe272 for the same space within the binding pocket. Consequently, the ligand either rides higher in the pocket or is pushed out of it. By constrast, compound **18**, with a three atom *ortho*-bridge, likewise presents the T-from in solution, but the truncated bridge avoids a steric clash with the protein and results in activities equivalent to that of PTX.[96]

From the standpoint of microtubule assembly, taxanes synthetically bridged between the C-4 acetate methyl and the C-3' phenyl groups fall into two classes. The first class contains *meta*-bridged and long-linked *ortho*-bridged molecules, as well as the multitude of untethered analogs prepared over the years, PTX and DTX among them.[161] The compounds represented by this wealth of material exhibit significant conformational mobility particularly in the C-13 side chain, and the action of some of them can be traced to modest microtubule elongation capacities ($K_p < 10^6$) and affinities within a factor of two relative to PTX ($K_a < 10^8$; Table 3 and Figure 31). The second much smaller category encompasses four, maybe five, relatively elongated taxanes, including **9**, **12**, and **17** among them. These taxanes are characterized by the lack of significant dynamic behavior, little or no conformational freedom and high microtubule elongation constants ($K_p > 10^6$ and $K_a > 10^8$; Table 3, Figure 31 and Figure 33). They are also some of the most cytotoxic

taxanes known, with the ability to overcome taxane-resistant cell lines.[96,139] We propose that the substances operate within the β-tubulin taxane binding site by holding the M-loop in an open orientation with a conformation that strengthens the contact between adjacent microtubule protofilaments to an extend unachievable with the more flexible PTX ligand. Consequently, microtubules are locked into elongated states in which the rates of disassembly are significantly retarded.

An important consequence of this proposal is the potential for designing other highly active analogs with reduced resistance profiles. Such molecules would seem to need to incorporate three characteristics: 1) molecular geometries able to precisely span the space between helix-1 and the M-loop (Figure 37); 2) molecular rigidity to prevent the M-loop from folding out of the inter-protofilament regions (Figure 35); and 3) sufficient functionality to result in effective binding within the β-tubulin taxane cavity. We have begun to use these ideas to pursue further analogs in our respective groups. Some of these analogs may also use the knowledge we gained from the simplified PTX analogs. They need to be more water-soluble and perhaps obtain a longer and more rigid core that will enforce the tubulin conformation we observe with the highly active constrained analogs **9** and **12**.

The T-Taxol conformation is not only consistent with all the experimental data, as I discussed in Chapter 2, but is useful in both the analysis of SAR data, as with the C-2 S-linked PTX analogs, as well as an impetus for analog development.

PART II

ELUCIDATING INTERDEPENDENT BINDING SITES ON TUBULIN

The most exciting phrase to hear in science, the one that heralds new discoveries, is not 'Eureka!' but 'That's funny...'

Isaac Asimov

Trust that little voice in your head that says "Wouldn't it be interesting if..."; And then do it.

Duane Michals

Background

Colchicine (COL) is a small three-ring molecule first isolated from autumn crocus, or the meadow saffron, in 1820. It is one of the oldest identified anti-mitotic agents binding to tubulin and inhibiting microtubule polymerization. COL has the distinct privilege to be the compound used to initially isolate the protein. While COL has played a central role in the elucidation of the physical properties and biological function of tubulin and microtubules, its high toxicity has limited its therapeutic application. COL is used in the treatment of gout and other inflammatory diseases, but the maximum complete dose allowed for an individual is 4 mg for the entire treatment. This is the main reason it has never been developed as a chemotherapeutic.

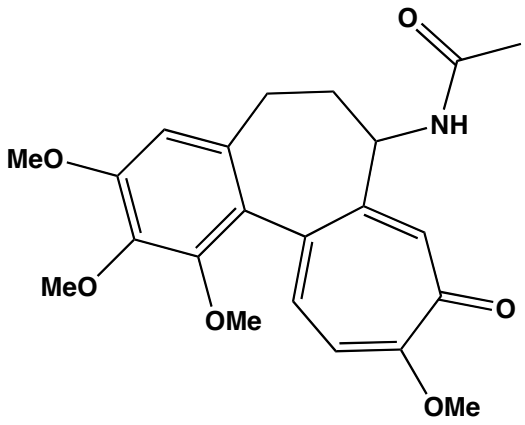

Figure 42. Depiction of colchicine (COL).

A lot of research proceeded on COL and tubulin after their identification. The compound was found to bind to tubulin stoichiometrically and with pseudo-irreversible kinetics, displaying a fast step followed by a slow step involving a conformational change in both the ligand and protein. The latter appears to promote fluorescence characteristic of the tropolone moiety of the molecule. Many

analogs of the compound have been prepared and studied, resulting in a varied SAR. It has been proposed that the A and C rings of COL both bind to specific loci of the protein, whereas the B ring is primarily a regulator of binding kinetics.[184]

From the beginning, many attempts were made to localize the binding site of COL in the tubulin dimer, but most led to conflicting results. Photolabeling experiments and NMR suggest what we will call binding site A.

Binding Site A

ANPAH-CLC, a photoaffinity derivative of COL, was used in photolysis experiments resulting in the α-subunit being identified. Covalent incorporation of the compound blocks binding of [^{3}H]COL.[185] The distance between the photoreactive aryl azido moiety and the nitrogen on the B-ring of COL is about 20 Å, however, so to reduce the distance between these two moieties, NAPDAC was synthesized, reducing the distance to 10 Å. This also allowed the examination of binding and photolabeling of tubulin by a COL analog with the carbonyl of the amide on the B-ring removed. This makes the compound more similar to colcemid than COL.[186] Limited proteolysis of photolabeled protein (with both ANPAH-CLC and NAPDAC) demonstrates that the two analogs interact with different sets of residues. The authors conclude that NAPDAC binds and photolabels two classes of COL sites on tubulin, one on α and one on β. They assume that the α-site is the high affinity one because the binding constants for three tested ligands are consistent with previous data; however, only one peptide from the α-subunit was labeled for both of the ligand-treated samples, though each one is different. Five labeled peptides were detected in β-tubulin of the NAPDAC-labeled tubulin.[186]

Ultraviolet irradiation of the [^{3}H]COL-TB complex leads to 70 to > 90% of labeling on β-tubulin early after irradiation, with α-monomer labeling occurring later, reducing the α/β labeling ration by prolonged incubation. The authors conclude that COL possibly binds at the interface or spans the interface of the dimer. Labeling of α-tubulin may result from structural modifications in the dimer coming from older, or "aged" tubulin. Labeling of β-tubulin is strongly favored, rendering unlikely any explanations based on filling a low-affinity site on this monomer, though one would be consistent with the α-subunit data.[187] The authors were later able to digest the labeled protein with chymotrypsin and trypsin, resulting in two labeled peptides corresponding to residues 1-46 (N-terminal) and 214-241 (C-terminal) of β-tubulin. These results show that at least two regions in this monomer are specifically involved in COL binding and that the span of the molecule, ≤ 11 Å, bridges these two regions in the native β-subunit. The findings are consistent with a model in which the two peptides, which are far removed from each other in the primary sequence, constitute a portion of the COL binding site in tubulin.[184] ^{13}C-NMR analysis of COL binding to tubulin demonstrates that the tropolone methoxy carbon undergoes a chemical shift of about 0.3 ppm (37.7 Hz) downfield, suggesting that the tropolone methoxy group binds near an aromatic group(s) in the protein.[188]

Comparison of the different β-tubulin sequences with the equilibrium constants for COL (K_a) and the K_i for inhibition by podophyllotoxin suggests that residue β-316 is directly involved in binding the common trimethoxyphenyl ring (A-ring). By contrast the analysis indicates that the local hydrophobicity affects the rate of one of the two conformational changes associated with COL binding, but does

not determine the affinity of the COL binding site. Analysis of the β-tubulin sequences strongly suggests that the relative affinities of the different tubulins depend upon residues in the immediate vicinity of β-316. Comparison of these residues with the experimental association constants indicates that tubulins with Iso^{316} must bind COL significantly more weakly than those with Val^{316} and/or Thr^{315}/Val^{316}, but more strongly than the Met^{316}, $Ala^{313}/Ser^{314}/Leu^{316}$, or Phe^{316}.[189]

The COL competitive inhibitor 3CTC binds to and covalently reacts with β-tubulin in a reaction inhibited by COL site drugs. As much as 90% of the covalent reaction between the [^{14}C]3CTC and β-tubulin occurs at Cys354 and the intramolecular distance between the C-3 oxygen and the chlorine atom of the 3-chloroacetyl group is 3 Å, indicating that the C-3 oxygen atom of colchicinoids is within 3 Å of the sulfur atom of the Cys354 residue. The authors also found minor reactivity at Cys239, which is within the sequence identified by Uppuluri *et al*. Examination of reactivity with 2CTC was hampered by a 2-4-fold lower covalent reactivity, but the authors found that the C-2 oxygen of COL is closer to Cys239 than is the C-3 oxygen and that the C-2 oxygen may be equidistant from both sulfur atoms of Cys239 and 354. This suggests that the COL A-ring lies between the two cysteines and the tropolone C-ring lies between the peptide region containing Cys239 and the amino-terminal β-tubulin sequence. This would agree with the failure of tropolonic compounds to inhibit formation of the Cys239-354 cross-link.[190]

Continuation of their work demonstrates that the adduct ratios for Cys239 to Cys254 are 77:23 and 27:73 for 2CTC and 3CTC, respectively.[191] The authors found two potential binding sites using docking to 1TUB.[61] One was entirely encompassed

within β-tubulin and the C-2 and C-3 oxygen atoms of 2CTC and 3CTC overlapped poorly with those of COL and thioCOL, but the distances from the reactive carbon atoms of the analogs to the sulfur atoms of the cysteins were qualitatively consistent with their reactivities. The other binding site was found at the α/β interface of the dimer with the oxygen atoms of the analogs overlapping well with those of COL, but the relative distances of the reactive carbons to the cysteine sulfur atoms did not correlate with the observed reactivities. The authors did note that several amino acid side chains form a 'significant' barrier between the sulfur atoms of both cysteines and COL for site A. For site B, these side chains form a barrier between the bound COL and the sulfur of Cys239 only. They conclude that site B is the most consistent with the data and that a significant conformational change must occur from this state of the tubulin dimer when COL binds or in the transition from the unpolymerized to the polymerized state.[191]

From the experimental data, we conclude that there is a binding site for COL most likely at the interface of the α,β-tubulin dimer. Bai, et al.'s second site may be the most reasonable representation to this point.

Binding Site B

In 2004 a crystal structure of tubulin in complex with COL was published by Ravelli, et al at 3.5 Å.[192] Because the compound depolymerizes microtubules, the dimer had to be stabilized with the stathmin-like domain (SLD) of protein RB3, a microtubule acting protein. Figure 43 shows the interaction of RB3-SLD with one of two tubulin heterodimers in a curved complex capped by the SLD amino-terminal domain. This domain prevents the incorporation of addition tubulin dimers to form

microtubules. When compared with the structure of tubulin in protofilaments (1TUB and 1JFF),[61,90] changes can be seen in the structure that correlate with the loss of lateral contacts and provide rationale for rapid microtubule depolymerization.

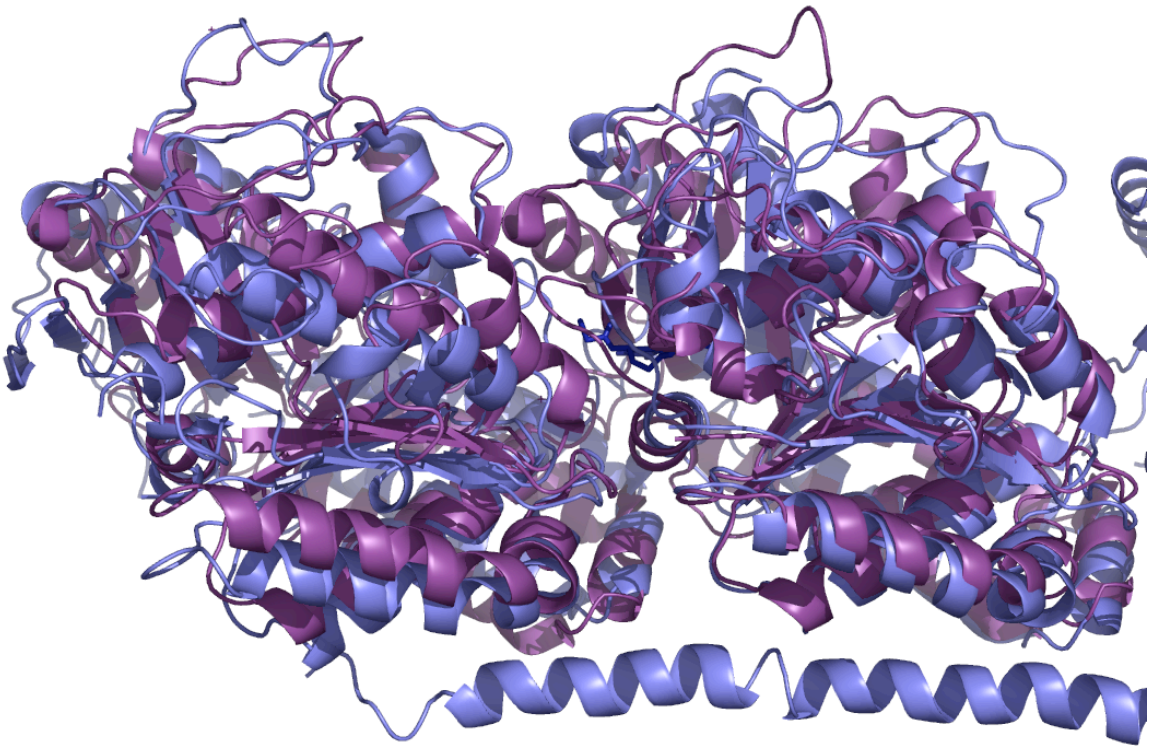

Figure 43. Overlay of Ravelli structure of COL binding (blue) on the 1JFF structure of straight tubulin (violet). RB3-SLD is the helix at the bottom of the picture. A pronounced can be observed from this view.

The authors put forth their structure as the complex that explains the mechanism of COL: it binds at a location where it prevents curved tubulin from adopting a straight structure, therefore inhibiting assembly. Comparison of the T2R structure to straight protofilaments shows three important differences: 1) rotation of 11.6 $\pm$ 1.0° is required to superimpose their α and β subunits in the T2R complex;

2) in both α and β, an 8° and 11° rotation, respectively, of their intermediate domains is required to superimpose them in the two structures (the N- and C-terminals superpose well); and 3) there are noticeable local differences comprised of conformational changes in the loops located at the longitudinal interfaces in protofilaments and also changes in the long, flexible, M and H1-S2 loops, mostly due to the influence of crystal packing. Changes at the intradimer α-β interface comprise of a movement of the β subunit T7 loop and H8 helix, which lie close to the COL binding site as well as differences in the conformations of the α subunit T5 and H6-H7 loops. Changes at the interdimer α-β interface comprise a different T5 loop conformation and a movement in one block of the H6-H7 loop following a 2.5 Å translation of the H7 helix along its axis, dragging along the C-terminal end of Helix 6 and interfering with the neighboring subunit positioned across a longitudinal straight protofilament interface.[192]

The problem with the Ravelli structure is that it does not meet some of the experimental criteria I described above. Most specifically, COL is located approximately 8 Å away from Cys239, one of the identified residues by the 3CTC photolabel. Many groups have attempted to develop predictive models based on this structure as well. Nguyen, et al. used a large number of synthetic and natural compounds with diverse structures to dock into the site and determine the binding modes. They then used these binding models and molecular dynamics to construct a comprehensive, structure-based pharmacophore.[193] Binding sites A and B are different. We set out to determine if we could properly identify site A based on the experimental data.

Methods

Colchicine Model. The model of α,β-tubulin with only GDP, GTP and Mg^{+2} that has undergone 10 ns molecular dynamics (MD)[97,147] was used as the starting point for all referred to modeling. The area encompassed by the H1—B2, H7—H8 and B9—B10 loops, the C-terminal ends of H1, H7, B8 and B9, and the N-terminal end of B10 was chosen as the primary investigative site for COL binding. Phe242 on the H7—H8 loop covers a small pocket containing Cys239 and Cys354, two residues known to be closely associated with COL.[190,191] In order to allow for opening and binding of this area, β-tubulin residues 237-246, part of the H7—H8 loop, were deleted from the structure and replaced with the previously proposed open conformation (unpublished). The referred to open conformation was obtained by performing MD on the loop with no protein as described: residues 239-251 of the H7—H8 loop were extracted from the optimized 1JJF tubulin-PTX structure and the terminal residues were defined as an aggregate. The rest of the peptide underwent MD at 300 K using a distance dependent dielectric of 4.5 in Sybyl.[116] A conformation that allows for opening of the binding site without steric conflicts with other protein residues was chosen to replace the original loop; the final low-energy loop model fit Ramachandran criteria. The area around the modified loop was optimized using MD. Simulations were run at low temperature and for short intervals, then manually analyzed to identify local atomic strain and adjusted to fit experimental data. This process continued until the model fit the data without manual intervention. At this point, using induced fit docking, a MMFFs minimized version of the X-ray conformation of COL[194] was inserted into the newly opened binding

pocket using the centroid of residues B42, B239, B318, B354 and B356 as the center of the enclosing box in Glide. B239 and B354 sulfurs were also chosen as receptor H-bond constraint atoms. In the initial docking step, protein prep constrained refinement was allowed, B242, B356, B42 and B43 residue side chains were removed, receptor vdW scaling of 0.70 and ligand vdW scaling of 0.50 were enforced and 20 poses were kept. During the second Prime induced fit phase, residues within 5.0 Ang of the ligand poses were refined, optimizing side chains, as well as all the residues of the H7—H8 loop (237-250). A final step of Glide redocking was then performed in which COL was redocked into the structures within 30 kcal/mol of the best structure and within the top 20 structures overall, using the SP setting.[140,141] Five poses of COL resulted, all with the B-ring amide facing α-tubulin and the A-ring methoxy groups pointing into the pocket. The major differences in the poses are the side chain placements and how deep COL is in the pocket. A MM-GBSA calculation was performed on all the results, but there are no large differences. In that respect, the top result was accepted as the new complex. The rotamers of Cys239 and Arg318 were then changed to the second most populated ones so that the cysteine could be in closer proximity to the COL methoxy group and the arginine would fit a better.

2ME2 Model. No crystal structure exists of 2ME2 bound to tubulin. The same MD model of tubulin used as the starting point for opening the COL site was used to open a site for 2ME2 to bind. The β-Val236Ile mutation causes a 30-fold resistance to 2ME2 binding in tubulin. The residue is located on Helix 7 and points towards a tiny hydrophobic pocket. To open this pocket enough to allow 2ME2 to

bind, residues 240 to 249, coinciding with the H7—H8 loop, were deleted from the protein. 2ME2 was then docked into the area, using Glide. In order to keep 2ME2 in the area of interest, the smallest grid available (8X8) was used and the ligand was forced to interact with Val236. A number of different poses resulted. The top one is located entirely within the protein molecular volume and forms a hydrogen bond between the A-ring –OH group and Thr237; it is also within vdW of Val236. Residues 240 to 249 were built back into the model with continuous minimization, allowing the loop to reorganize itself around 2ME2. The final complex was then subjected to at 300K for 50 ps with a 1.5 fs time step and 1.0 ps equilibration time using MMFFs/GBSA in Maestro.[82,110-112,140]

Results and Discussion

Examination of the protein around the Cys239 and 354 demonstrated a site blocked by another section of the protein (Figure 44a). Specifically, residue Phe244 covered the area. Phe244 is located on a 12 residue loop that spans a part of the β-tubulin subunit at the α,β-interface. A previous member of our group, Jim Nettles, hypothesized that this loop, and more specifically the triad, Phe-Pro-Gly, could act as a gate to control access to the binding site. He did some examination of the area, but I continued the project after he graduated. Molecular dynamics can be used to open the loop and allow for docking of COL as described in the **Methods**. Phe244 is repositioned from a location folded within a hydrophobic cleft of β-tubulin to an extended position against complementary residues on the adjacent alpha subunit (Figure 44b). It is as if Phe/Pro of the H7—H8 loop act as a lid to cover the COL site.

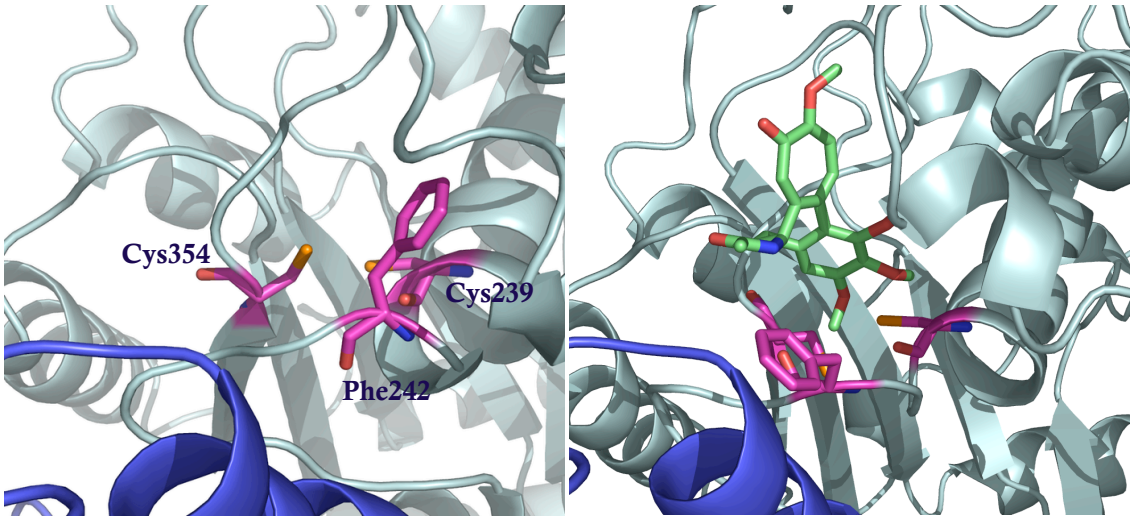

Figure 44. (a) Phe242 covers a hydrophobic cleft in which Cys239 and Cys354 are located. (b) MD of the area, and loop in particular, allows for a conformational change of Phe242 so that COL (green) can bind and interact with the cysteine residues.

Our interest in the COL binding site was augmented when some of our collaborators presented us with mutation data for 2-methoxyestradiol. 2ME2 is the major mammalian metabolite of estradiol. While studying the inhibitory effects of angiogenesis of 2-methoxyestradiol (2ME2), it became apparent that the compound has antimitotic properties. It is a relatively weak competitive inhibitor of the binding of [^{3}H]COL to tubulin (apparent K_i of 22 μM versus 0.5 μM for podophyllotoxin). Understanding the effects of the compound on tubulin assembly proved complicated. Under some conditions, it is incorporated into the microtubule polymer without any morphology change, but at high concentrations, it forces depolymerization of the protein. It has been hypothesized that 2ME2 is an

endogenous microtubule regulator and interest in developing antimitotic compounds based on the steroid is extensive.

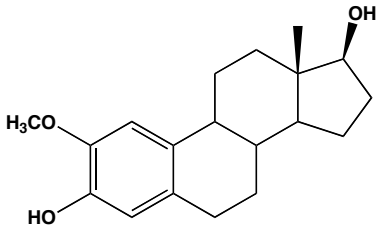

Figure 45. Depiction of 2ME2.

Due to its inhibitory effects, it has always been assumed that 2ME2 binds to the COL site. However, mutation of Val236 to Ile, which provides 30-fold resistance of cells to 2ME2, does not afford cross-resistance to COL. Investigation into the location of this residue demonstrates that it is located on the edge of what I have referred to as site B, the Ravelli COL binding site.[192] If COL truly binds here, some cross-resistance must be observed with the change into a bulkier residue. This residue, however, is not close to our proposed site for binding of the ligand.

We set out to determine if we could find a site for 2ME2 binding that demonstrates two equally important properties: resistance due to the Val-Ile mutation and inhibition of COL binding when 2ME2 is bound. To start, the mutant is located on Helix 7 and points into a very congested hydrophobic area. Interestingly the top part of that area is formed by the same H7—H8 loop involved in our model of COL binding. This encouraged us to investigate this area, as it could be integral in the competition between the two ligands.

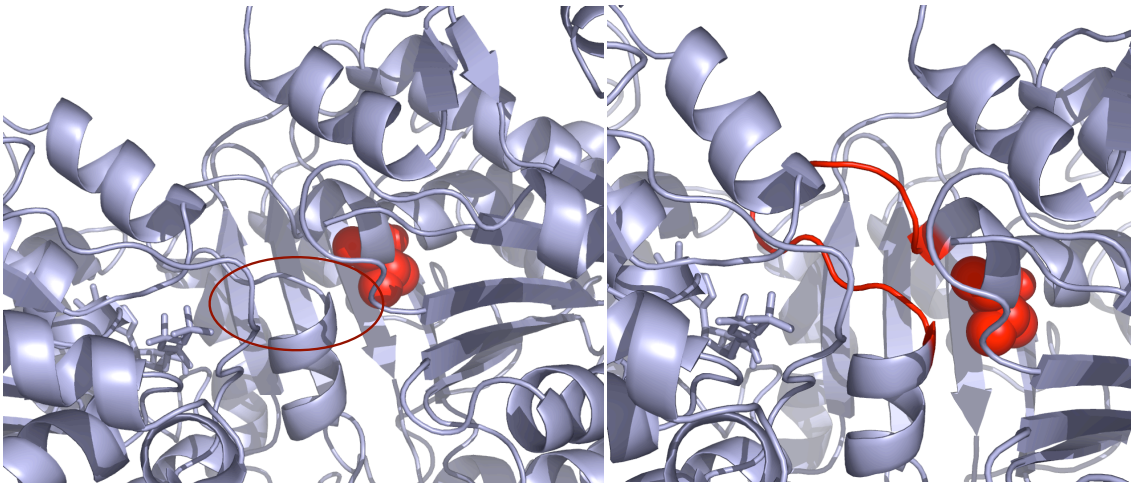

Figure 46. (a) Val236 (red space-fill) is located on Helix 7 and points into a congested hydrophobic pocket (red oval). (b) Loop H7—H8 (red) covers the area of interest.

As described in the methods, I removed the H7—H8 loop from the structure and docked 2ME2 into that site, forcing it to interact with the mutation. This resulted in a number of poses, though the only structurally significant ones are the ones that stay completely within the protein and form a specific interaction with the residue. The loop was then built back into the structure, residue by residue, allowing for optimization around the docked 2ME2. The final model was then allowed to relax fully, removing any bad contacts.

Conclusions

Examination of the final model shows that a conformational change of Ala250 is the only requirement to open up the site and allow 2ME2 to slip in. This new site is located right at the edge of Site B, overlapping with the Ravelli structure of COL. It, however, sits underneath COL Site A, with the loop in between. Comparing the

two structures, one notes that opposing conformational changes in the loop open one site as opposed to the other. The flip of Phe244 opens the site for COL, fully blocking any entrance for 2ME2, while the conformational change of Ala250 results in an opposite effect. With one ligand bound, the loop is locked and cannot open for the other compound. In this way, you can have competing ligands that do not necessarily bind to the same site and interact with the same residues, and therefore have no cross-resistance.

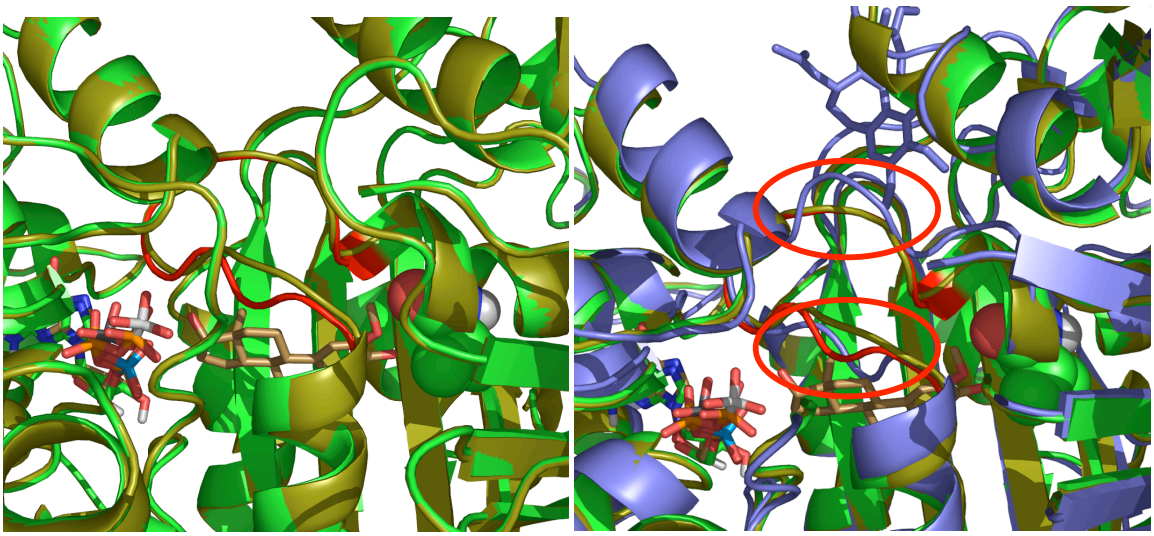

Figure 47. (a) Final model of 2ME2 binding site (brown) overlayed on the starting structure (green) with the original position of loop H7—H8 depicted in red. The conformational change of Ala250 can readily be observed. (b) As before with COL binding model (blue) also present. Red circles highlight the sections of loop H7—H8 (Phe244 above and Ala250 below) that undergo conformational changes to allow for interdependent binding of the compounds.

References

1. Verg, E.; Gottfried, P.; Scultheis, H. *Milestones: the Bayer story 1863-1988*; Bayer AG: Leverkusen, **1988**.

2. *Aspirin, the medicine of the century*; Alstaedter, R., Ed.; Bayer AG: Germany, **1984**.

3. The Asprin Foundation. Bayer HealthCare AG. www.aspirin-foundation.com (accessed Feb 10, 2009).

4. Ehrlich, P. In *Gesammelte Arbeiten*; Himmelweit, F., Ed.; Springer-Verlag: Berlin, **1957**.

5. Sneader, W. *Drug Discovery: A History*; John Wiley and Sons, Ltd.: West Sussex, England, **2005**.

6. Debré, P.; Debra(c), P.; Forster, E. *Louis Pasteur*; JHU Press: Baltimore, Maryland, **2000**.

7. Ehrlich, P. Chemo-therapy In *The Collected Papers of Paul Ehrlich*; Himmelweit, F., Marquardt, M., Dale, H. H., Eds.; Pergamon: London, **1913**; Vol. III, p 505-518.

8. Maehle, A.-H. *Med Hist.* **2004**, *48*, 153–174.

9. Robinson, R. *J. Chem. Soc., Trans.* **1917**, *111*, 762-768.

10. Kruif, P. D. *Microbe Hunters*; Houghton Mifflin Harcourt: Boston, MA, **2002**.

11. American Diabetes Association. www.diabetes.org (accessed Jan 15, 2009).

12. Fleming, A. *J. Pathol. Bacteriol.* **1932**, *35*, 831.

13. Waksman, S. A. *Science* **1953**, *118*, 259-266.

14. Drews, J. *Science* **2000**, *287*, 1960-1964.

15. Suffness, M. *Taxol: Science and Applications*; CRC Press: London, **1995**.

16. Drews, J.; Ryser, S. *Drug Inf. J.* **1996**, *30*, 97-108.

17. Weisbach, J. A.; Moos, W. H. *Drug Dev. Res.* **1995**, *34*, 243-259.

18. Roberts, N. A.; Martin, J. A.; Kinchington, D.; Broadhurst, A. V.; Craig, J. C.; Duncan, I. B.; Galpin, S. A.; Handa, B. K.; Kay, J.; Krohn, A.; Lambert, R. W.; Merrett, J. H.; Mills, J. S.; Parkes, K. E. B.; Redshaw, S.; Ritchie, A. J.; Taylor, D. L.; Thomas, G. J.; Machin, P. J. *Science* **1990**, *248*, 358-361.

19. Wlodawer, A.; Vondrasek, J. *Annu. Rev. Biophys. Biomol. Struct.* **1998**, *27*, 249-284.

20. Henry, C. M. *Chem. & Engineering News* **2001**, *79*, 69-74.

21. Jorgensen, W. L. *Science* **2004**.

22. Schlick, T. *Molecular Modeling and Simulation: An Interdisciplinary Guide*; Springer: New York, NY, **2002**.

23. Stahl, M.; Guba, W.; Kansy, M. *Drug Discovery Today* **2006**, *11*, 326-333.

24. Giannakakou, P.; Gussio, R.; Nogales, E.; Downing, K. H.; Zaharevitz, D.; Bollbuck, B.; Poy, G.; Sackett, D.; Nicolaou, K. C.; Fojo, T. *Proc. Natl. Acad. Sci.* **2000**, *97*, 2904-2909.

25. Wang, M. M.; Xia, X. Y.; Kim, Y.; Hwang, D.; Jansen, J. M.; Botta, M.; Liotta, D. C.; Snyder, J. P. *Org. Lett.* **1999**, *1*, 43-46.

26. Ojima, I.; Chakravarty, S.; Inoue, T.; Lin, S. N.; He, L. F.; Horwitz, S. B.; Kuduk, S. D.; Danishefsky, S. J. *Proc. Natl. Acad. Sci.* **1999**, *96*, 4256-4261.

27. Kingston, D. G. I. *J. Nat. Prod.* **2000**, *63*, 726-734.

28. Suffness, M.; Wall, M. E. In *Taxol: Science and Applications*; Suffness, M., Ed.; CRC Press: Boca Raton, FL, **1995**, p 3-25.

29. Taxol is the trade name used by Bristol-Myers Squibb while paclitaxel is the generic name (abbreviated PTX) and how it will be referred to throughout this dissertation.

30. Wani, M. C.; Taylor, H. L.; Wall, M. E.; Coggon, P.; Mcphail, A. T. *J. Am. Chem. Soc.* **1971**, *93*, 2325-&.

31. Schiff, P. B.; Fant, J.; Horwitz, S. B. *Nature* **1979**, *277*, 665-667.

32. Mcguire, W. P.; Rowinsky, E. K.; Rosenshein, N. B.; Grumbine, F. C.; Ettinger, D. S.; Armstrong, D. K.; Donehower, R. C. *Annals of Internal Medicine* **1989**, *111*, 273-279.

33. Holmes, F. A.; Walters, R. S.; Theriault, R. L.; Forman, A. D.; Newton, L. K.; Raber, M. N.; Buzdar, A. U.; Frye, D. K.; Hortobagyi, G. N. *Journal of the National Cancer Institute* **1991**, *83*, 1797-1805.

34. Eisenhauer, E. A.; Vermorken, J. B. *Drugs* **1998**, *55*, 5-30.

35. Bristol-Myers Squibb Company. www.bms.com (accessed Jan 15, 2009).

36. Denis, J. N.; Greene, A. E.; Guenard, D.; Guerittevoegelein, F.; Mangatal, L.; Potier, P. *J. Am. Chem. Soc.* **1988**, *110*, 5917-5919.

37. Bissery, M. C.; Guenard, D.; Gueritte-Voegelein, F.; Lavelle, F. *Cancer Research* **1991**, *51*, 4845-4852.

38. Gueritte-Voegelein, F.; Guenard, D.; Mangatal, L.; Potier, P.; Guilhem, J.; Cesario, M.; Pascard, C. *Acta Crystallographica Section C-Crystal Structure Communications* **1990**, *46*, 781-784.

39. Suffness, M. *Taxane Anticancer Agents* **1995**, *583*, 1-17.

40. DeVita, V. T. In *Cancer: Principles and Practice of Oncology*; 4th ed.; DeVita, V. T., Hellman, S., Rosenberg, S. A., Eds.; J. B. Lippincott Co.: Philadelphia, PA, **1993**, p 276-292.

41. Giannakakou, P.; Snyder, J. P. Resistance to Microtubule-Targeting Drugs In *The Role of Microtubules in Cell Biology, Neurobiology, and Oncology*; Fojo, A. T., Ed.; Springer: New York, NY, **2008**, p 357-394.

42. Dustin, P. *Microtubules*; 2nd ed.; Springer-Verlag: Berlin, **1984**.

43. Cooper, G. M. *The Cell: A Molecular Approach*; 2nd ed.; Sinauer Associates, Inc.: Sunderland, MA, **2000**, (accessed Feb 10, 2009).

44. Horwitz, S. B. *Trends in Pharmacological Sciences* **1992**, *13*, 134-136.

45. Jordan, M. A.; Toso, R. J.; Thrower, D.; Wilson, L. *Proc. Natl. Acad. Sci.* **1993**, *90*, 9552-9556.

46. American Cancer Society. www.cancer.org (accessed Jan 15, 2009).

47. Nelson, D. L.; Cox, M. M. *Lehninger Principles of Biochemistry*; 3rd ed.; Worth Publishers: New York, NY, **2000**.

48. Swindell, C. S.; Krauss, N. E.; Horwitz, S. B.; Ringel, I. *J. Med. Chem.* **1991**, *34*, 1176-1184.

49. Kingston, D. G. I. *Trends Biotechnol.* **1994**, *12*, 222-227.

50. Boge, T. C.; Himes, R. H.; Vander Velde, D. G.; Georg, G. I. *J. Med. Chem.* **1994**, *37*, 3337-3343.

51. Ojima, I.; Duclos, O.; Zucco, M.; Bissery, M. C.; Combeau, C.; Vrignaud, P.; Riou, J. F.; Lavelle, F. *J. Med. Chem.* **1994**, *37*, 2602-2608.

52. Chen, S. H.; Wei, J. M.; Long, B. H.; Fairchild, C. A.; Carboni, J.; Mamber, S. W.; Rose, W. C.; Johnston, K.; Casazza, A. M.; Kadow, J. F.; Farina, V.; Vyas, D. M.; Doyle, T. W. *Biorg. Med. Chem. Lett.* **1995**, *5*, 2741-2746.

53. Metaferia, B. B.; Hoch, J.; Glass, T. E.; Bane, S. L.; Chatterjee, S. K.; Snyder, J. P.; Lakdawala, A.; Cornett, B.; Kingston, D. G. I. *Org. Lett.* **2001**, *3*, 2461-2464.

54. Gueritte, F. *Current Pharmaceutical Design* **2001**, *7*, 1229-1249.

55. Wang, X.; Itokawa, H.; Lee, K.-H. Structure-activity relationships of taxoids In *Taxus: The Genus Taxus*; Itokawa, H., Lee, K.-H., Eds.; CRC Press: London, **2003**, p 298-389.

56. Kingston, D. G. I. Taxol and its Analogs In *Anticancer Agents from Natural Products*; Cragg, G. M. L., Kingston, D. G. I., Newman, D. J., Eds.; CRC Press: London, **2005**, p 89-122.

57. He, L. F.; Jagtap, P. G. F.; Kingston, D. G. I.; Shen, H. J.; Orr, G. A.; Horwitz, S. B. *Biochemistry* **2000**, *39*, 3972-3978.

58. Mastropaolo, D.; Camerman, A.; Luo, Y. G.; Brayer, G. D.; Camerman, N. *Proc. Natl. Acad. Sci.* **1995**, *92*, 6920-6924.

59. Miller, R. W. *J. Nat. Prod.* **1980**, *43*, 425-437.

60. Nogales, E.; Wolf, S. G.; Khan, I. A.; Luduena, R. F.; Downing, K. H. *Nature* **1995**, *375*, 424-427.

61. Nogales, E.; Wolf, S. G.; Downing, K. H. *Nature* **1998**, *391*, 199-203.

62. Li, Y. K.; Poliks, B.; Cegelski, L.; Poliks, M.; Gryczynski, Z.; Piszczek, G.; Jagtap, P. G.; Studelska, D. R.; Kingston, D. G. I.; Schaefer, J.; Bane, S. *Biochemistry* **2000**, *39*, 281-291.

63. Jiménez-Barbero, J.; Amat-Guerri, F.; Snyder, J. P. *Current medicinal chemistry Anti-cancer agents* **2002**, *2*, 91-122.

64. Dubois, J.; Guenard, D.; Gueritte-Voegelein, F.; Guedira, N.; Potier, P.; Gillet, B.; Beloeil, J. C. *Tetrahedron* **1993**, *49*, 6533-6544.

65. Williams, H. J.; Scott, A. I.; Dieden, R. A.; Swindell, C. S.; Chirlian, L. E.; Francl, M. M.; Heerding, J. M.; Krauss, N. E. *Canadian Journal of Chemistry-Revue Canadienne De Chimie* **1994**, *72*, 252-260.

66. Cachau, R. E.; Gussio, R.; Beutler, J. A.; Chmurny, G. N.; Hilton, B. D.; Muschik, G. M.; Erickson, J. W. *International Journal of Supercomputer Applications and High Performance Computing* **1994**, *8*, 24-34.

67. Vander Velde, D. G.; Georg, G. I.; Grunewald, G. L.; Gunn, G. W.; Mitscher, L. A. *J. Am. Chem. Soc.* **1993**, *115*, 11650-11651.

68. Ojima, I.; Kuduk, S. D.; Chakravarty, S.; Ourevitch, M.; Begue, J. P. *J. Am. Chem. Soc.* **1997**, *119*, 5519-5527.

69. Boge, T. C.; Wu, Z. J.; Himes, R. H.; Vander Velde, D. G.; Georg, G. I. *Biorg. Med. Chem. Lett.* **1999**, *9*, 3047-3052.

70. Ojima, I.; Kuduk, S. D.; Pera, P.; Veith, J. M.; Bernacki, R. J. *J. Med. Chem.* **1997**, *40*, 279-285.

71. Berman, H. M.; Westbrook, J.; Feng, Z.; Gilliland, G.; Bhat, T. N.; Weissig, H.; Shindyalov, I. N.; Bourne, P. E. *Nucleic Acids Res.* **2000**, *28*, 235-242.

72. Berman, H.; Henrick, K.; Nakamura, H. *Nature Structural Biology* **2003**, *10*, 980-980.

73. The RCSB Protein Data Bank. www.pdb.org

74. Ojima, I.; Lin, S. N.; Inoue, T.; Miller, M. L.; Borella, C. P.; Geng, X. D.; Walsh, J. J. *J. Am. Chem. Soc.* **2000**, *122*, 5343-5353.

75. Querolle, O.; Dubois, J.; Thoret, S.; Roussi, F.; Montiel-Smith, S.; Gueritte, F.; Guenard, D. *J. Med. Chem.* **2003**, *46*, 3623-3630.

76. Querolle, O.; Dubois, J.; Thoret, S.; Dupont, C.; Gueritte, F.; Guenard, D. *Eur. J. Org. Chem.* **2003**, 542-550.

77. Highsmith, S.; Jardetzky, O. *Biochemistry* **1981**, *20*, 780-783.

78. Snyder, J. P.; Nevins, N.; Cicero, D. O.; Jasen, J. *J. Am. Chem. Soc.* **2000**, *122*, 724-725.

79. Cicero, D. O.; Barbato, G.; Bazzo, R. *J. Am. Chem. Soc.* **1995**, *117*, 1027-1033.

80. Chang, G.; Guida, W. C.; Still, W. C. *J. Am. Chem. Soc.* **1989**, *111*, 4379-4386.

81. Hilton, B. D.; Chmurny, G. N.; Muschik, G. M. *J. Nat. Prod.* **1992**, *55*, 1157-1161.

82. Still, W. C.; Tempczyk, A.; Hawley, R. C.; Hendrickson, T. *J. Am. Chem. Soc.* **1990**, *112*, 6127-6129.

83. Schrodinger. www.schrodinger.com

84. Snyder, J. P.; Nettles, J. H.; Cornett, B.; Downing, K. H.; Nogales, E. *Proc. Natl. Acad. Sci.* **2001**, *98*, 5312-5316.

85. Gao, Q.; Wei, J. M.; Chen, S. H. *Pharm. Res.* **1995**, *12*, 337-341.

86. Gao, Q.; Chen, S. H. *Tetrahedron Lett.* **1996**, *37*, 3425-3428.

87. Williams, H. J.; Scott, A. I.; Dieden, R. A.; Swindell, C. S.; Chirlian, L. E.; Francl, M. M.; Heerding, J. M.; Krauss, N. E. *Tetrahedron* **1993**, *49*, 6545-6560.

88. Jimenez-Barbaro, J.; Souto, A. A.; Abal, M.; Barasoain, I.; Evangelio, J. A.; Acuna, A. U.; Andreu, J. M.; Amat-Guerri, F. *Biorg. Med. Chem.* **1998**, *6*, 1857-1863.

89. In the protein sequence, the residue is His227, but is labeled His229 in the 1TUB and 1JFF structures. It will be referred to as His227 throughout the rest of the document.

90. Lowe, J.; Li, H.; Downing, K. H.; Nogales, E. *J. Mol. Biol.* **2001**, *313*, 1045-1057.

91. Ivery, M. T. G.; Le, T. *Oncology Research* **2003**, *14*, 1-19.

92. Geney, R.; Sun, L.; Pera, P.; Bernacki, R. J.; Xia, S. J.; Horwitz, S. B.; Simmerling, C. L.; Ojima, I. *Chemistry & Biology* **2005**, *12*, 339-348.

93. Bode, C. J.; Gupta, M. L.; Reiff, E. A.; Suprenant, K. A.; Georg, G. I.; Himes, R. H. *Biochemistry* **2002**, *41*, 3870-3874.

94. Gupta, M. L.; Bode, C. J.; Georg, G. I.; Himes, R. H. *Proc. Natl. Acad. Sci.* **2003**, *100*, 6394-6397.

95. Hari, M.; Loganzo, F.; Annable, T.; Tan, X. Z.; Musto, S.; Morilla, D. B.; Nettles, J. H.; Snyder, J. P.; Greenberger, L. M. *Molecular Cancer Therapeutics* **2006**, *5*, 270-278.

96. Ganesh, T.; Guza, R. C.; Bane, S.; Ravindra, R.; Shanker, N.; Lakdawala, A. S.; Snyder, J. P.; Kingston, D. G. I. *Proc. Natl. Acad. Sci.* **2004**, *101*, 10006-10011.

97. Shanker, N.; Kingston, D. G. I.; Ganesh, T.; Yang, C.; Alcaraz, A. A.; Geballe, M. T.; Banerjee, A.; Mcgee, D.; Snyder, J. P.; Bane, S. *Biochemistry* **2007**, *46*, 11514-11527.

98. Rao, S.; He, L. F.; Chakravarty, S.; Ojima, I.; Orr, G. A.; Horwitz, S. B. *J. Biol. Chem.* **1999**, *274*, 37990-37994.

99. DeLano, W. L. *The PyMOL MOlecular Graphics System*. http://www.pymol.org, DeLano Scientific: San Carlos, CA, **2002**.

100. Alcaraz, A. A.; Mehta, A. K.; Johnson, S. A.; Snyder, J. P. *J. Med. Chem.* **2006**, *49*, 2478-2488.

101. Johnson, S. A.; Alcaraz, A. A.; Snyder, J. P. *Org. Lett.* **2005**, *7*, 5549-5552.

102. McRee, D. E.; David, P. R. *Practical protein crystallography*; 2nd ed.; Academic Press: San Diego, Calif., **1999**.

103. Rhodes, G. *Crystallography made crystal clear : a guide for users of macromolecular models*; 2nd. ed.; Academic Press: San Diego, **2000**.

104. Brunger, A. T.; Adams, P. D.; Clore, G. M.; DeLano, W. L.; Gros, P.; Grosse-Kunstleve, R. W.; Jiang, J. S.; Kuszewski, J.; Nilges, M.; Pannu, N. S.; Read, R. J.; Rice, L. M.; Simonson, T.; Warren, G. L. *Acta Crystallographica Section D-Biological Crystallography* **1998**, *54*, 905-921.

105. Bailey, S. *Acta Crystallographica Section D-Biological Crystallography* **1994**, *50*, 760-763.

106. Downing, K. H.; Li, H. L. *Microsc. Microanal.* **2001**, *7*, 407-417.

107. Kleywegt, G. J.; Jones, T. A. *Acta Crystallographica Section D-Biological Crystallography* **1998**, *54*, 1119-1131.

108. Jones, T. A.; Zou, J. Y.; Cowan, S. W.; Kjeldgaard, M. *Acta Crystallographica Section A* **1991**, *47*, 110-119.

109. Kolossvary, I.; Guida, W. C. *J. Am. Chem. Soc.* **1996**, *118*, 5011-5019.

110. Halgren, T. A. *J. Comput. Chem.* **1996**, *17*, 490-519.

111. Halgren, T. A. *J. Comput. Chem.* **1999**, *20*, 720-729.

112. Halgren, T. A. *J. Comput. Chem.* **1999**, *20*, 730-748.

113. Allinger, N. L.; Yuh, Y. H.; Lii, J. H. *J. Am. Chem. Soc.* **1989**, *111*, 8551-8566.

114. Lii, J. H.; Allinger, N. L. *J. Am. Chem. Soc.* **1989**, *111*, 8566-8575.

115. Lii, J. H.; Allinger, N. L. *J. Am. Chem. Soc.* **1989**, *111*, 8576-8582.

116. *Sybyl*. www.tripos.com/sybyl, Tripos, L. P.: St. Louis, MO

117. Harper, J. K.; Facelli, J. C.; Barich, D. H.; McGeorge, G.; Mulgrew, A. E.; Grant, D. M. *J. Am. Chem. Soc.* **2002**, *124*, 10589-10595.

118. Long, H. W.; Tycko, R. *J. Am. Chem. Soc.* **1998**, *120*, 7039-7048.

119. Anderson, J. E.; Casarini, D.; Lunazzi, L.; Mazzanti, A. *J. Org. Chem.* **2000**, *65*, 1729-1737.

120. Kamihira, M.; Naito, A.; Nishimura, K.; Tuzi, S.; Saito, H. *J. Phys. Chem. B* **1998**, *102*, 2826-2834.

121. Arshava, B.; Breslav, M.; Antohi, O.; Stark, R. E.; Garbow, J. R.; Becker, J. M.; Naider, F. *Solid State Nucl. Magn. Reson.* **1999**, *14*, 117-136.

122. Nogales, E.; Whittaker, M.; Milligan, R. A.; Downing, K. H. *Cell* **1999**, *96*, 79-88.

123. Diaz, J. F.; Strobe, R.; Engelborghs, Y.; Souto, A. A.; Andreu, J. M. *J. Biol. Chem.* **2000**, *275*, 26265-26276.

124. Epothilones, which reside in the same taxane pocket, are thought to sit on a small pool of water located between the ligand and protein.

125. Nettles, J. H.; Li, H. L.; Cornett, B.; Krahn, J. M.; Snyder, J. P.; Downing, K. H. *Science* **2004**, *305*, 866-869.

126. Igumenova, T. I.; McDermott, A. E.; Zilm, K. W.; Martin, R. W.; Paulson, E. K.; Wand, A. J. *J. Am. Chem. Soc.* **2004**, *126*, 6720-6727.

127. Allinger, N. L.; Rahman, M.; Lii, J. H. *J. Am. Chem. Soc.* **1990**, *112*, 8293-8307.

128. Allinger, N. L.; Li, F. B.; Yan, L. Q. *J. Comput. Chem.* **1990**, *11*, 848-867.

129. Although the coordiantes from the original PTX X-ray structure have never been deposited, the paper provides enough information to permit reconstruction of the conformation.

130. Cornell, W. D.; Cieplak, P.; Bayly, C. I.; Gould, I. R.; Merz, K. M.; Ferguson, D. M.; Spellmeyer, D. C.; Fox, T.; Caldwell, J. W.; Kollman, P. A. *J. Am. Chem. Soc.* **1995**, *117*, 5179-5197.

131. Clark, M.; Cramer, R. D.; Vanopdenbosch, N. *J. Comput. Chem.* **1989**, *10*, 982-1012.

132. Hing, A. W.; Schaefer, J. *Biochemistry* **1993**, *32*, 7593-7604.

133. Gueritte-Voegelein, F.; Guenard, D.; Lavelle, F.; Legoff, M. T.; Mangatal, L.; Potier, P. *J. Med. Chem.* **1991**, *34*, 992-998.

134. Geng, X. D.; Miller, M. L.; Lin, S. N.; Ojima, L. *Org. Lett.* **2003**, *5*, 3733-3736.

135. Querolle, O.; Dubois, J.; Thoret, S.; Roussi, F.; Gueritte, F.; Guenard, D. *J. Med. Chem.* **2004**, *47*, 5937-5944.

136. Kingston, D. G. I.; Bane, S.; Snyder, J. P. *Cell Cycle* **2005**, *4*, 279-289.

137. Paik, Y.; Yang, C.; Metaferia, B.; Tang, S. B.; Bane, S.; Ravindra, R.; Shanker, N.; Alcaraz, A. A.; Johnson, S. A.; Schaefer, J.; O'Connor, R. D.; Cegelski, L.; Snyder, J. P.; Kingston, D. G. I. *J. Am. Chem. Soc.* **2007**, *129*, 361-370.

138. Ms. Yutao Yang performed all the relevant calculations in work submitted to the Journal of Natural Products.

139. Ganesh, T.; Yang, C.; Norris, A.; Glass, T.; Bane, S.; Ravindra, R.; Banerjee, A.; Metaferia, B.; Thomas, S. L.; Giannakakou, P.; Alcaraz, A. A.; Lakdawala, A. S.; Snyder, J. P.; Kingston, D. G. I. *J. Med. Chem.* **2007**, *50*, 713-725.

140. *Maestro, version 7.5*. www.schrodinger.com, Schrodinger, LLC: New York, **2006**.

141. *Glide, version 4.0*. www.schrodinger.com, Schrodinger, LLC: New York, **2005**.

142. Lindahl, E.; Hess, B.; Van Der Spoel, D. *J. Mol. Model.* **2001**, *7*, 306-317.

143. Schuttelkopf, A. W.; van Aalten, D. M. F. *Acta Crystallographica Section D-Biological Crystallography* **2004**, *60*, 1355-1363.

144. *PRODRG*. http://davapc1.bioch.dundee.ac.uk/cgi-bin/prodrg_beta,

145. van Gunsteren, W. F.; Billeter, S. R.; Eising, A. A.; Hunenberger, P. H.; Kruger, P.; Mark, A. E.; Scott, W. R. P.; Tironi, I. G. *Biomolecular Simulations: The GROMOS96 manual and user guide*; Vdf Hochschulverlag: Zurich, Switzerland, **1996**.

146. Hermans, J.; Berendsen, H. J. C.; Vangunsteren, W. F.; Postma, J. P. M. *Biopolymers* **1984**, *23*, 1513-1518.

147. Geballe, M. T. Ph.D.,*Part I: Structure and Function in the NMDA Ligand Binding Domain Part II: Comparison of Paclitaxel Analogs through Molecular Dynamics Simulation; Solution Conformations of Cyclic Peptides*. Emory University, **2009**.

148. Humphrey, W.; Dalke, A.; Schulten, K. *Journal of Molecular Graphics* **1996**, *14*, 33-&.

149. Darden, T.; York, D.; Pedersen, L. *J. Chem. Phys.* **1993**, *98*, 10089-10092.

150. Essmann, U.; Perera, L.; Berkowitz, M. L.; Darden, T.; Lee, H.; Pedersen, L. G. *J. Chem. Phys.* **1995**, *103*, 8577-8593.

151. Berendsen, H. J. C.; Postma, J. P. M.; Vangunsteren, W. F.; Dinola, A.; Haak, J. R. *J. Chem. Phys.* **1984**, *81*, 3684-3690.

152. Nevins, N.; Cicero, D.; Snyder, J. P. *J. Org. Chem.* **1999**, *64*, 3979-3986.

153. Monteagudo, E.; Cicero, D. O.; Cornett, B.; Myles, D. C.; Snyder, J. P. *J. Am. Chem. Soc.* **2001**, *123*, 6929-6930.

154. Thepchatri, P.; Cicero, D. O.; Monteagudo, E.; Ghosh, A. K.; Cornett, B.; Weeks, E. R.; Snyder, J. P. *J. Am. Chem. Soc.* **2005**, *127*, 12838-12846.

155. Giannakakou, P.; Sackett, D. L.; Kang, Y. K.; Zhan, Z. R.; Buters, J. T. M.; Fojo, T.; Poruchynsky, M. S. *J. Biol. Chem.* **1997**, *272*, 17118-17125.

156. Zhou, J.; O'Brate, A.; Zelnak, A.; Giannakakou, P. *Cancer Research* **2004**, *64*, 8708-8714.

157. Diaz, J. F.; Menendez, M.; Andreu, J. M. *Biochemistry* **1993**, *32*, 10067-10077.

158. Lee, J. C.; Timasheff, S. N. *Biochemistry* **1977**, *16*, 1754-1764.

159. Sackett, D. L.; Saroff, H. A. *FEBS Lett.* **1996**, *397*, 1-6.

160. Li, H. L.; DeRosier, D. J.; Nicholson, W. V.; Nogales, E.; Downing, K. H. *Structure* **2002**, *10*, 1317-1328.

161. Amos, L. A.; Lowe, J. *Chemistry & Biology* **1999**, *6*, R65-R69.

162. Andreu, J. M.; Diaz, J. F.; Gil, R.; Depereda, J. M.; Delacoba, M. G.; Peyrot, V.; Briand, C.; Townsandrews, E.; Bordas, J. *J. Biol. Chem.* **1994**, *269*, 31785-31792.

163. Arnal, I.; Wade, R. H. *Current Biology* **1995**, *5*, 900-908.

164. Meurer-Grob, P.; Kasparian, J.; Wade, R. H. *Biochemistry* **2001**, *40*, 8000-8008.

165. Diaz, J. F.; Valpuesta, J. M.; Chacon, P.; Diakun, G.; Andreu, J. M. *J. Biol. Chem.* **1998**, *273*, 33803-33810.

166. Ganesh, T.; Norris, A.; Sharma, S.; Bane, S.; Alcaraz, A. A.; Snyder, J. P.; Kingston, D. G. I. *Biorg. Med. Chem.* **2006**, *14*, 3447-3454.

167. Blechert, S.; Kleineklausing, A. *Angewandte Chemie-International Edition in English* **1991**, *30*, 412-414.

168. Blechert, S.; Jansen, R.; Velder, J. *Tetrahedron* **1994**, *50*, 9649-9656.

169. Klar, U.; Graf, H.; Schenk, O.; Rohr, B.; Schulz, H. *Biorg. Med. Chem. Lett.* **1998**, *8*, 1397-1402.

170. Geng, X. D.; Geney, R.; Pera, P.; Bernacki, R. J.; Ojima, I. *Biorg. Med. Chem. Lett.* **2004**, *14*, 3491-3494.

171. Almqvist, F.; Manner, S.; Thornqvist, V.; Berg, U.; Wallin, M.; Frejd, T. *Organic & Biomolecular Chemistry* **2004**, *2*, 3085-3090.

172. Kingston, D. G. I. *Chem. Commun.* **2001**, 867-880.

173. Chen, S. H.; Wei, J. M.; Farina, V. *Tetrahedron Lett.* **1993**, *34*, 3205-3206.

174. Chordia, M. D.; Kingston, D. G. I. *J. Org. Chem.* **1996**, *61*, 799-801.

175. Chaudhary, A. G.; Gharpure, M. M.; Rimoldi, J. M.; Chordia, M. D.; Gunatilaka, A. A. L.; Kingston, D. G. I.; Grover, S.; Lin, C. M.; Hamel, E. *J. Am. Chem. Soc.* **1994**, *116*, 4097-4098.

176. Nicolaou, K. C.; Renaud, J.; Nantermet, P. G.; Couladouros, E. A.; Guy, R. K.; Wrasidlo, W. *J. Am. Chem. Soc.* **1995**, *117*, 2409-2420.

177. Fang, W. S.; Fang, Q. C.; Liang, X. T. *Tetrahedron Lett.* **2001**, *42*, 1331-1333.

178. Fang, W. S.; Liu, Y.; Liu, H. Y.; Xu, S. F.; Wang, L.; Fang, Q. C. *Biorg. Med. Chem. Lett.* **2002**, *12*, 1543-1546.

179. Fang, W. S.; Liu, H. Y.; Fang, Q. C. *Chin. Chem. Lett.* **2005**, *16*, 38-40.

180. Wang, L.; Alcaraz, A. A.; Matesanz, R.; Yang, C. G.; Barasoain, I.; Diaz, J. F.; Li, Y. Z.; Snyder, J. P.; Fang, W. S. *Biorg. Med. Chem. Lett.* **2007**, *17*, 3191-3194.

181. Allen, F. H. *Acta Crystallographica Section B-Structural Science* **2002**, *58*, 380-388.

182. Buey, R. M.; Diaz, J. F.; Andreu, J. M.; O'Brate, A.; Giannakakou, P.; Nicolaou, K. C.; Sasmal, P. K.; Ritzen, A.; Namoto, K. *Chemistry & Biology* **2004**, *11*, 225-236.

183. Yang, C. G.; Barasoain, I.; Li, X.; Matesanz, R.; Liu, R. H.; Sharom, F. J.; Yin, D. L.; Diaz, J. F.; Fang, W. S. *Chemmedchem* **2007**, *2*, 691-701.

184. Uppuluri, S.; Knipling, L.; Sackett, D. L.; Wolff, J. *Proc. Natl. Acad. Sci.* **1993**, *90*, 11598-11602.

185. Williams, R. F.; Mumford, C. L.; Williams, G. A.; Floyd, L. J.; Aivaliotis, M. J.; Martinez, R. A.; Robinson, A. K.; Barnes, L. D. *J. Biol. Chem.* **1985**, *260*, 3794-3802.

186. Floyd, L. J.; Barnes, L. D.; Williams, R. F. *Biochemistry* **1989**, *28*, 8515-8525.

187. Wolff, J.; Knipling, L.; Cahnmann, H. J.; Palumbo, G. *Proc. Natl. Acad. Sci.* **1991**, *88*, 2820-2824.

188. Osei, A. A.; Everett, G. W.; Ringel, I.; Himes, R. H. *Biochim. Biophys. Acta* **1991**, *1078*, 339-344.

189. Burns, R. G. *FEBS Lett.* **1992**, *297*, 205-208.

190. Bai, R. L.; Pei, X. F.; Boye, O.; Getahun, Z.; Grover, S.; Bekisz, J.; Nguyen, N. Y.; Brossi, A.; Hamel, E. *J. Biol. Chem.* **1996**, *271*, 12639-12645.

191. Bai, R. L.; Covell, D. G.; Pei, X. F.; Ewell, J. B.; Nguyen, N. Y.; Brossi, A.; Hamel, E. *J. Biol. Chem.* **2000**, *275*, 40443-40452.

192. Ravelli, R. B. G.; Gigant, B.; Curmi, P. A.; Jourdain, I.; Lachkar, S.; Sobel, A.; Knossow, M. *Nature* **2004**, *428*, 198-202.

193. Nguyen, T. L.; McGrath, C.; Hermone, A. R.; Burnett, J. C.; Zaharevitz, D. W.; Day, B. W.; Wipf, P.; Hamel, E.; Gussio, R. *J. Med. Chem.* **2005**, *48*, 6107-6116.

194. Lessinger, L.; Margulis, T. N. *Acta Crystallographica Section B-Structural Science* **1978**, *34*, 578-584.

When you have reached the end of all the light that you know, and you must step out into the darkness of the unknown, faith is knowing that one of two things will happen: either you will have something solid to stand on, or you will be taught how to fly!

Author Unknown